The influence of particle size and density on the combustion of Highveld coal.

George William van der Merwe,

B.Eng (Chemical Engineering) (North-West University)

Dissertation submitted in fulfilment of the requirements for the degree *Masters in Engineering in Chemical Engineering* at the North-West University, Potchefstroom Campus, South Africa.

Supervisor: Prof. R.C. Everson.

Co-supervisor: Prof. H.W.J.P. Neomagus.

Co-supervisor: Prof. J.R. Bunt.

DECLARATION

"I, George William van der Merwe, hereby declare that the dissertation entitled:

The influence of particle size and density on the combustion of Highveld coal.

Submitted to the North-West University in completion of the requirements set for the degree *Masters in Engineering in Chemical Engineering* is my own original work, except where acknowledged in the text and has not previously been submitted to any institution.

Signed at Potchefstroom

…….

G.W. van der Merwe.

ACKNOWLEDGEMENTS

I hereby wish to thank all of the persons and institutions who contributed to the completion of this research project. Your assistance and inputs are truly appreciated. The following persons deserve special thanks:

- Our heavenly Father for blessing me with the ability to learn and for giving me guidance and courage in everything I do.
- The work is dedicated in loving memory to Léon van der Merwe, a loving father who has always inspired me to pursue my greatest dreams.
- Professors Ray Everson, Hein Neomagus and John Bunt for their excellent guidance, assistance and willingness to help. Without their detailed evaluations and suggestion this dissertation would not have been a reality.
- Sasol for the financial support of this project.
- The coal research group at the North-West University for many valuable and insightful discussions.
- Jan Kroeze and Adrian Brock for assistance on the technical aspects.
- Eugene Coetzee for help regarding data acquisition
- My family for always believing in me and supporting me in every way possible.
- Susan du Preez for her love, support and understanding.

ABSTRACT

Coal from the Highveld seam 4 deposit was studied to determine and understand the influence of density and particle size on the high temperature combustion characteristics. All of the charring, as well as the combustion experiments were conducted in a high temperature horizontal tube furnace where charring was done at 1100 °C and combustion at 1000 °C. The furnace was equipped with carbon monoxide and carbon dioxide analysers to monitor carbon conversion during experimentation. The parent coal was characterised in terms of proximate analysis, ultimate analysis, calorific value analysis and FTIR analysis. The chars were investigated with FTIR analysis. The coals were categorized according to density from +1.4 $g.cm^{-3}$ to -2.0 $g.cm^{-3}$ using 0.2 $g.cm^{-3}$ intervals and the particle size effect was studied using particles of 20, 30 and 40 mm diameter.

The characterization results showed that the moisture content of the coal samples tended to decrease as the particle density increased and that the smaller particles tended to have a higher moisture content. The volatile matter and fixed carbon content decreased as the coal density increased, while both had a relatively even distribution across the size ranges. The ash content was found to significantly increase as the density increased.

Elemental analysis revealed that that carbon-, hydrogen- and nitrogen- content decreased as density increased with a relatively even distribution of the different size ranges. High sulphur values were observed in the high density particles. This was attributed to a higher pyrite content in this fraction. Smaller particles tended to have a higher oxygen content. Calorific value analysis showed that the high density fraction had a very low heating value and that the overall sample value would be improved by removing the high density fraction.

FTIR analysis showed that the properties of density separated fractions varied significantly; this was most prominent in the substitution structures occurring on the aromatic structures. It was found that the chemical composition of the size separated particles remained relatively constant. The properties of char particles with different densities tended to become more similar, especially with regard to their aromatic substitution structures.

The characterization of the different coal samples showed that the parameters were generally significantly different for the different density fractions but did not vary significantly across the particle size ranges.

It was also found that significant shattering occurred at heating rates of 50 °C/min, while very little shattering was observed at 15 °C/min. The low density particles formed porous ash

residues, while the high density particles formed very hard and solid ash residues that could contain unreacted carbon in the core. Combustion studies showed that particle density and size had a significant influence on the time required for complete conversion of the chars. The low density particles required less time for full conversion than the high density particles and the smaller particles reacted faster than the larger particles. Modelling of the experimental data showed that the shrinking unreacted core model can be used to describe the combustion characteristics of both the size and density separated particles. The controlling mechanism was found to be a combination of internal and external diffusion. From the modelling results it was found that effective ash layer diffusion became more prominent as the density increased and that the obtained mass transfer coefficients correlated well with values found in literature.

TABLE OF CONTENTS

LIST OF FIGURES

LIST OF TABLES

LIST OF SYMBOLS

General symbols

Symbol	Description	Units
A	Gas reagent	-
$A_{ash\ layer}$	Ash layer surface area	m^2
b	Solid reagent stoichiometric coefficient	-
B	Solid reagent	-
C	Gaseous reaction product	-
c	Gaseous product stoichiometric coefficient	-
C_{Ag}	Concentration of reactant gas	$mol.m^{-3}$
C_{As}	Concentration of reactant gas at the particle surface	$mol.m^{-3}$
C_{CO2}	Carbon dioxide concentration	%
D	Solid reaction product	-
d	Solid product stoichiometric coefficient	-
D_{AB}	Binary diffusion coefficient	$m^2.s^{-1}$
D_e	Effective ash layer diffusion coefficient	$m^2.s^{-1}$
$f(X)_i$	Conversion function for linearised characteristic equations	-
F_{Air}	Air flow rate	$Nl.min^{-1}$
F_B	Buoyancy force	N
F_{pl}	Buoyancy force due to plunger immersion	
g	Gravity constant	$m.s^{-2}$
h_D	Mass transfer coefficient	$m.s^{-1}$
k''	First order rate constant	$m.s^{-1}$
k_g	Mass transfer coefficient	$m.s^{-1}$
L	Characteristic dimension (particle diameter)	m
M_{AB}	Mean molecular weight of diffusing species	$g.mol^{-1}$
M_B	Molar weight of solid reactant B	$g.mol^{-1}$
m_B	Mass of solid reactant	kg
m_{B0}	Initial mass of solid reactant	kg
m_F	Mass reading due to force needed to counter buoyancy	g
m_p	Particle mass	g
m_{pl}	mass due to the plunger submersion	g
N_A	Amount of gas reagent A	mol
N_B	Amount of solid reagent B	mol

N_{Re}	Reynolds number	-
N_{Sc}	Schmidt number	-
N_{Sh}	Sherwood number	-
P_T	Total reaction pressure	Pa or bar
Q_A	Molar flux of reactant gas A	$mol.m^{-2}.s^{-1}$
$r_{ash\ layer}$	Ash layer radius	m
r''''_B	Reaction rate based on the volume of the reactor	$mol.m^{-3}.s^{-1}$
r'''_B	Reaction rate based on volume of reacting solid	$mol.m^{-3}.s^{-1}$
r''_B	Reaction rate based on the external surface area of solid	$mol.m^{-2}.s^{-1}$
r'_B	Reaction rate based on mass of solid particle	$mol.kg^{-1}.s^{-1}$
r_B	Reaction rate based on volume of reacting fluid	$mol.m^{-3}.s^{-1}$
r_c	Current particle radius	m
R_p	Particle radius	m
R_{pore}	Pore radius	nm
S_{ex}	External surface area of reacting solid	m^2
t	Time	s
T	Temperature	°C or K
U	Linear gas velocity	$m.s^{-1}$
V	Displaced volume	m^3
ν	Kinematic viscosity	$m^2.s^{-1}$
$\tilde{v}$	Diffusion volumes for simple molecules	$cm^3.mol^{-1}$
V_B	Volume of solid reactant	m^3
V_F	Volume of reacting fluid	m^3
V_p	Particle volume	m^3
V_r	Volume of reactor	m^3
W_F	Force needed to keep the particle immersed	N
W_p	Particle weight	N
W_{pl}	Downward force to keep plunger immersed	N
X_B	Conversion of solid reactant B	-
ρ_B	Molar density of solid reactant B	$kg.m^{-3}$
ρ_f	Fluid density	$kg.m^{-3}$
ρ_p	Particle density	$kg.m^{-3}$

Abbreviations

Abbreviation	Description
^{13}C-NMR	Carbon 13 nuclear magnetic resonance
Afrox	African oxygen limited
ASTM	American society for testing and materials
ATR	Attenuated total reflectance
CBA	Coal burning additives
CTL	Coal to liquids
DME	Department of minerals and energy
DRIFT	Diffuse reflectance infrared fourier transform
FTIR	Fourier transform infrared
HRTEM	High resolution transmission electron microscope
IDGCC	Integrated drying gasification combined cycle
IEA	International energy agency
Inerto	Inertodetrinite
IR	Infrared
IRGA	Infrared gas analyser
ISO	International organization of standards
KBr	Potassium bromide
LFES	Drycol and lignite fuel enhancement systems
MIR	Mid infrared region
MLR	Multi linear regression
PCR	Principle component regression
PLS	Partial least square
ROM	Run of mine
SABS	South African bureau of standards
SANS	South African National Standard
Sasol	South African synthetic oil liquid
SF	Semi-fusinite
ss - NMR	Solid state nuclear magnetic resonance
SUCM	Shrinking unreacted core model
TBE	Tetrabromoethane
TC	Temperature controller
TI	Temperature indicator
WCI	World coal institute
XRD	X-ray diffraction

CHAPTER 1: INTRODUCTION

1.1. Background and motivation

Energy resources and energy availability are critical to any civilization, and access to cheap fossil fuels has been the backbone of our society since the industrial revolution (Hopkins, 2006). The major fossil fuels fuelling this growing and ever more demanding society include coal, oil and natural gas.

Oil overtook coal as the world's main energy source in the 1960's (WCI, 2005) due to remarkable growth in the transportation sectors. As a result of diminishing oil reserves, however, an impending 'oil peak' (Hopkins, 2006) is expected. At the moment oil is still the primary energy source, supplying 34.4% of the world's primary energy demands, followed by natural gas and coal, which supply 20.5% and 26% respectively. The smaller contributors to the energy supply in the world include nuclear energy, contributing 6.2%, and hydro energy, contributing 2.2%. The remainder of the supply need is contributed by sources including geothermal, solar, wind and combustible waste energy, which together contribute around 10.7% (WCI, 2009)

In the global electricity sector coal is one of the most important resources, as most of the world's electricity is generated using pulverized coal combustion processes. Coal is responsible for approximately 41% of the global electricity supply, with natural gas being the second largest resource contributing 20.1%. The only major renewable resource with regards to electricity generation is hydro technology, which supplies 16% of the world's electrical demands. Nuclear energy, while being a technology with great potential, currently supplies only 14.8% to the global electricity supply (WCI, 2009).

Current estimations predict that global energy demands will increase by 60% from 2004 to 2030, and that the bulk of this growth will occur in developing countries including South Africa. It is estimated that the developing countries will account for 70% of the predicted growth, while China is estimated to contribute 30% of the predicted increase in energy demand. Predictions indicate that the increase in energy demand will mostly be supplied by the utilization of coal resources, with coal contributing as much as 80% of the required increase (WCI, 2005).

Looking at the reserves of natural resources it can be estimated that at the current production levels global coal resources will last about 122 years, whereas oil and natural gas will last approximately 42 years and 60 years respectively. Table 1.1 shows that the largest

hard coal producer in the world is the Peoples Republic of China with a production rate of 2482 Mt/year, followed by the USA with 990 Mt/year. South Africa is ranked seventh in the world with a production rate of 236 Mt/year (WCI, 2009).

Table 1.1: Leading global hard coal producers (WCI, 2009)

Country	Production (Mt/year)
PR China	2482
USA	990
India	427
Australia	309
Russia	247
Indonesia	246
South Africa	236

Despite South Africa's coal reserves amounting to between 34 000 Mt (Campbell, 2002) and 50 000 Mt (WCI, 2005), as opposed to countries like the USA and Russia having about 250 000 Mt and 160 000 Mt respectively, South Africa is still ranked seventh in terms of countries with the largest coal reserves. This makes coal a very important resource for South Africa. According to the Department of Minerals and Energy (DME, 2007), 21 % of South African coal is exported, 21 % is used locally (excluding power station coal) while the remaining 58 % of the coal produced in South Africa is mostly used for power generation, followed by synthetic fuel production. The distribution of coal use for the coal that is not export or used locally can be seen in Table 1.2.

Table 1.2: Coal uses in South Africa (DME, 2007)

Coal use	Contribution (%)
Electricity generation	62
Synthetic fuel production	23
General industry	8
Metallurgical industry	4
Sold locally or exported	3

It is estimated that 93% of South Africa's electricity demand is supplied by coal fired technologies (WCI, 2007), making it very significant for South Africa, as South Africa is experiencing a higher energy demand than can currently be supplied.

There are several coal using technologies available to meet the energy demands of a growing economy with regard to electricity generation, fuel production or industrial use. These include pulverized coal combustors, fluidized bed combustors, and several fixed bed gasifiers. The parent coal particle sizes used in these technologies range from pulverised coal (micrometer sized particles) as used in electricity generation (Hurt *et al.*, 1995) to lump coal (up to 65 mm) as used in fixed bed gasifiers (Bunt and Waanders, 2008). These technologies are continuously being studied and modified to improve parameters like conversion efficiencies, emission reductions, power requirements etc. to meet the strong demand for greener technologies (Beer, 2000).

Along with the increasing use of coal as major fuel stock, public policy is aiming to create, develop and implement clean coal technologies to achieve higher efficiency power generation and coal conversion (Beer, 2000). The main increase in public demand for clean coal technologies and more efficient processes is due to the fact that the use of fossil fuels has some negative effect on the environment. These effects include acid rain, the green house effect, and the release of trace elements into the environment (Rubiera *et al*., 2003). The energy supply processes can be improved by way of both the more efficient use of coal in existing technology, and the designing of new systems that use coal as optimally as possible. New power generation technologies, offering advances in efficiency and reduced greenhouse emissions, include processes like the integrated drying gasification combined cycle (IDGCC), the Drycol and the lignite fuel enhancement systems (LFES) (IEA, 2010).

Whether designing new processes or optimising current technologies, it is important to understand the chemical processes involved during coal utilisation. To design better technologies or to make current processes more efficient it is necessary to understand the influence of parameters like particles size (Wang and Wen, 1972), particle density (Koekemoer, 2009), temperature (Oberholzer, 2009), pressure (Niska *et al*., 2003) and coal composition (Mendez *et al*., 2003) as these parameters greatly influence performance characteristics like conversion rate, product quality and unwanted emissions. Given that as coal resources diminish the utilisation of low grade coal will become unavoidable, making it essential that the performance of low grade coal be understood in order to make suggestions regarding system upgrades.

Another important property that has a significant influence on the combustion behaviour of a coal particle is coal particle density. Coal particles of the same origin can be separated by sink-float techniques to yield particles with various mineral matter contents (Matjie and Van Alphen, 2008), while different maceral constituents of coal also have different densities (Borrego *et al*., 1997). As particles from the same origin can have different mineral matter

contents it follows that if there is catalytic activity from the mineral content, then the various density fractions will behave differently, thus affecting the reaction behaviour of these fractions. Due to the fact that particles of differing density will have different mineral contents, the ash layer formation behaviour will also be affected. This in turn may influence particle temperature behaviours (Chen and Kojima, 1996). Different densities can also affect parameters like pore diffusion during reaction, heat transfer mechanisms, and diffusion parameters (Szekely *et al*., 1976).

As mentioned earlier, the particle sizes used in coal utilization technology can range from a few micrometers up to the centimetre range. Particle size variations affect devolatilization and heating times, which then affect the reaction time required for each particle size. This in turn further affects parameters like burnout times and reactivities (Hanson *et al*., 2002). Size differences can also have a significant effect on the controlling mechanisms encountered during the combustion of coal particles (Niska *et al*., 2003) (Liu, 1999) (Wells and Smoot, 1985). As the particle size of the coal affects both the time required for full conversion, and the controlling mechanism involved during combustion, and as this in turn affects the residence time required for each particle size in a reactor setup, it is important to understand the properties and the influence of these properties on reaction systems. The behaviour of large particles is particularly important in understanding the operation of fixed bed gasifiers and chain grate stoker boilers (Bunt and Waanders, 2008). If the particle size properties and the influence of these properties on combustion reactions are better understood, then the maximum and the minimum particle sizes introduced into coal utilization technologies can be determined and changed so as to optimise conversion of these particles.

In order to optimise coal utilisation process conditions; develop more suitable and comprehensive models; and optimise the design and understanding of new technology, it is necessary to fully understand the combustion behaviour of coal particles. It is therefore imperative that the influence of parameters like particle density and particle size be further examined and understood.

1.1. Objectives of the investigation

Coal particles with different densities have different mineral contents that will influence the combustion properties of the different coal fractions. The combustion properties of coal are also influenced by the size of the coal particles, as the particle size will influence parameters like burn out times and diffusion. This dissertation presents results from a detailed study of

combustion characteristics of a typical Highveld coal separated according to density and size.

The focus of this work is to determine the combustion characteristics of particles with densities ranging from float 1.4 g/cm^3 to sink 2.0 g/cm^3 with 0.2 g/cm^3 intervals, along with particles sizes of 20, 30 and 40 mm. All of the combustion work was conducted at 1000 °C.

The objectives for this research project are the following

- Determine the chemical, and structural properties of the several density cuts and sizes of the parent coal samples
- Characterize selected samples in terms of FT-IR analysis
- Assess if either density separation or size differences influence the characterization results
- Evaluate the combustion reaction rate of the coal samples as a function of coal density and particle size
- Determine whether the obtained combustion characteristics can be explained by the characterization results, with special attention to easily obtained conventional characterization i.e. proximate and ultimate analysis.
- Evaluate the combustion parameters and fit an appropriate reaction model to the experimental data for both particle density and particle size

1.2. Scope of the study

The scope of the study has been constructed to answer the respective research questions outlined in the objectives of the investigation. The scope used is schematically illustrated in Figure 1.1.

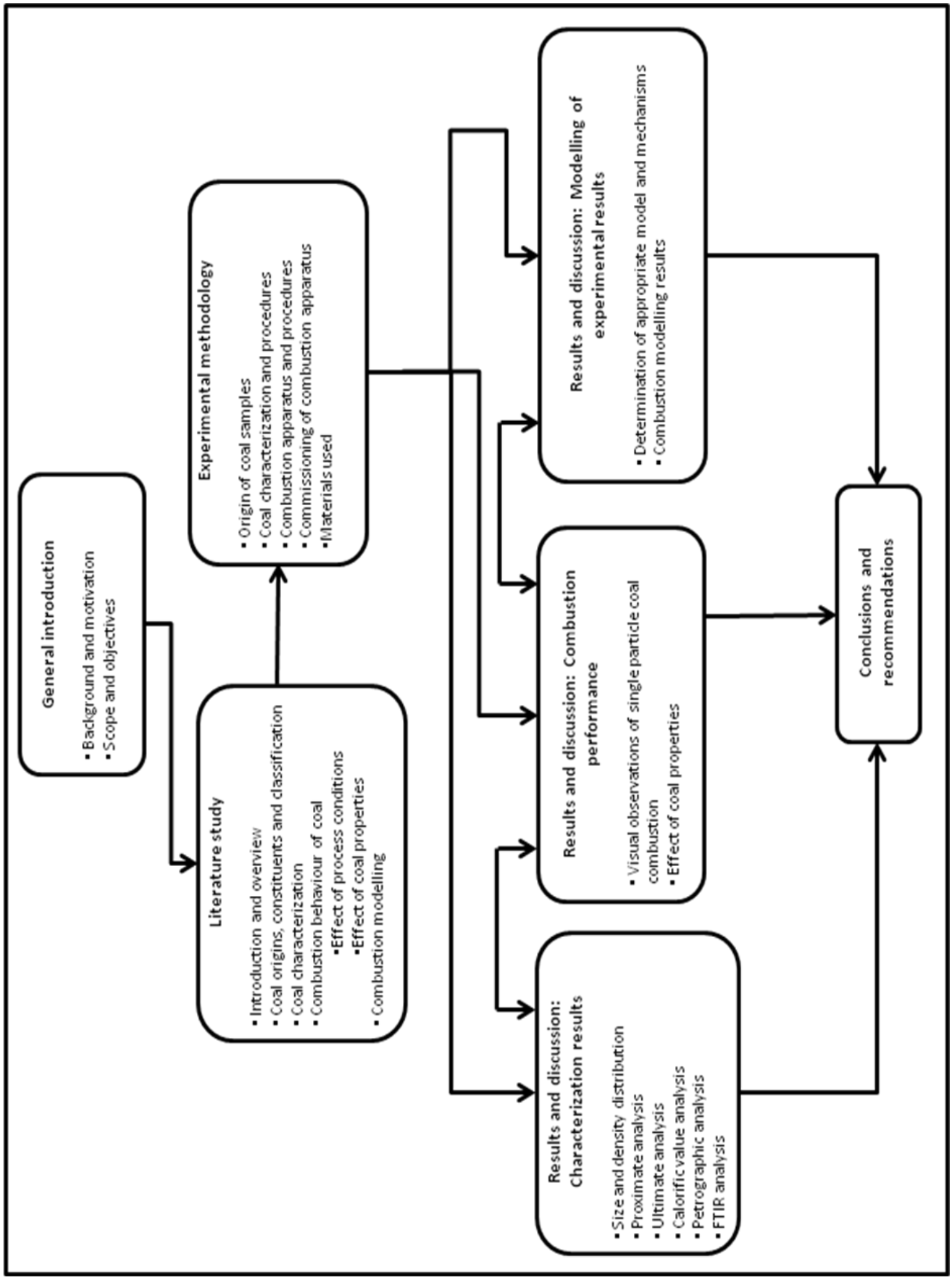

Figure 1.1: Scope of study

Chapter 1 presents a general discussion that gives background information relating to the study and that motivates arguments in support of the study of density and size separated coal particle combustion. This is followed by a section detailing the aims and objectives of the study, to ensure that the proper information can be obtained from the study. Chapter 2 presents the literature study conducted in order to better understand the origins of coal, and the techniques used to characterise these different coal particles. The literature study also reviews the characteristics and parameters that influence coal combustion processes, and briefly discusses the relevant models that can be used to describe the combustion of coal particles. Chapter 3 gives the experimental methodology along with a description of the origin of the samples studied during this investigation. It further describes the characterization done on the relevant samples; the experimental equipment; and the procedures used during the study. The experimental chapter also provides details regarding the performance of the commissioned furnace, and the verification of the results obtained from the experimental method. Chapter 4 reports the characterization results obtained and discusses the information and the conclusions that can be drawn from these results. Chapter 5 examines some of the visual observations made from the combustion experiments, and discusses aspects such as the resulting ash characteristics. This chapter also presents the combustion results based on a discussion of the influence of parameters like particle density and particle size. The modelling results are given in Chapter 6, which shows how an appropriate model was chosen for the modelling of the experimental results. A representation of the obtained modelling results, as well as a discussion of the implications of these results is also given. Information from Chapter 4 will be used to try and explain the obtained experimental results shown in Chapter 5, showing an interchangeable relationship between Chapter 4 and Chapter 5. Finally, the most important conclusions will be given in Chapter 7, along with recommendations for future work.

CHAPTER 2: LITERATURE REVIEW

2.1. Introduction and overview

This chapter covers the literature needed to fully understand the recent and relevant research done in this field of coal research. The objective of the survey is to understand the results of relevant coal research, as well as to determine the effects of parameters like density, particle size, oxygen concentration and temperature on the combustion behaviour of coal. This chapter also covers the literature needed to understand the detailed characterization of coal.

2.2. Coal origin, constituents and classification

It is widely known that coal is made of a mixture of metamorphosed plant material. It therefore has variable chemical and physical properties and is not chemically uniform (Falcon, 1978). From this non-uniformity of coal it can be concluded that no two coals are the same, and that no two coals will exhibit the same behaviour during industrial processes. Even coal coming from the same seam can vary significantly in terms of composition, properties and behaviour. Due to these variations it is necessary to model coal combustion processes, taking into account the effects of these variations.

2.2.1. Coal formation (Coalification process)

Coal is formed when plant material decays, usually under anaerobic conditions. The formation of coal thus requires aqueous environments with a lot of vegetation and enough water to prevent the decay of the organic material by preventing the oxygen required by decay processes from reaching the dead plant material. Micro-organisms present in the water induce a chemical reaction forming peat. As the peat is buried deeper during the drainage of water, there is an increase in pressure and temperature signifying the start of the coal formation process. During this process low grade coals like lignite are transformed to higher grade coals like bituminous coal and anthracite. The lower rank coal i.e. the peat and lignite are more hydrophilic, giving these coals a relatively high moisture content. The transformation from peat to bituminous coal through lignite reduces the amount of polar

groups (hydroxyl and carboxylic acids) as well as the hydrophylicity, thereby reducing the inherent moisture content. This reduction in polar groups occurs between the ranges of 81-89% carbon, having a maximum hydrophobicity at a carbon content of about 89% (Brown, 1962).

Coalification is the process through which peat is consecutively transformed to lignite, sub-bituminous coal, bituminous coal, anthracite and graphite. The major changes occurring in this process are given in Table 2.1 (Falcon, 1977), where the loss in oxygen is related to the increase in carbon content.

Table 2.1: The main changes in coalification (Falcon, 1977)

Rank	C (%)	H (%)	O (%)	N (%)
Wood	50	6	43	0.5
Peat	59	5	33	2.5
Lignite	70	5.5	23	1
Bituminous	82	5	10	2
Anthracite	93	3	2.5	1
Graphite	100	0	0	0

Apart from the steps required to form coal, (as described above) the coalification process can also be divided into three separate stages (Falcon, 1977). The sedimentation stage describes the depositions of decaying plant material in a body of water. During this stage certain minerals can be deposited along with this layer. The quantity of mineral matter deposited relative to the amount of organic material will ultimately determine the grade of the coal. Secondly, in the diagenetic stage, the primary decaying debris (in the form of banded layers) is bio-chemically changed and undergoes pressure changes due to compaction. The chemical composition and the proportion of these organic materials form the precursors of the macerals found in the fossilised coal, and are very important in rank and behaviour. Finally, in the metamorphic stage, geochemical changes like temperature, pressure and time, play a vital role in the formation of the final coal. These changes determine the degree of coalification, and therefore also the rank of the coal (Brown, 1962). This can chemically be seen as the enrichment of carbon content at the expense of oxygen and hydrogen content.

2.2.2. Coal constituents

The components that make up coal can microscopically be divided into the organic part (macerals) and the inorganic (mineral) part. The maceral or organic groups are made up of the various plant materials from which the coal was formed (Falcon and Falcon, 1987). The three main maceral groups and the inorganic material occurring in coal are discussed in the following sections.

2.2.2.1. Vitrinite:

The vitrinite maceral is considered to be an oxygen rich, high volatile organic matter that originally formed from plant material like bark, twigs, branches *etc*. Depending on the rank, the colour of vitrinite can vary from dark grey (High volatile bituminous coal) to white (anthracite), with the percentage reflected light varying accordingly from 0.5 % to 10% (Falcon and Falcon, 1987).

2.2.2.2. Liptinite (exinite):

The liptinite maceral contains hydrogen rich organic material, and was originally formed from spores, resin bodies and algae. The colour of liptinite can vary from black-brown (High volatile bituminous coal) to pale grey/white (anthracite), depending on rank, with the reflectance varying accordingly from 0.0 % to 10% (Falcon and Falcon, 1987).

2.2.2.3. Inertinite:

The inertinite maceral is the carbon-rich maceral originally formed from oxidized organic humus. The colour can vary from medium grey (high volatile bituminous) to yellow white (anthracite), with the reflectance varying from 0.7% to 10%. Inertinite has the lowest combustion rate when compared to the other macerals, and has a relatively inert behaviour towards coking, hydrogenation and devolatilization (Falcon and Falcon, 1987).

2.2.2.4. Inorganic content

While the organic parts of coal are classified under the three main maceral types, minerals can be found in various forms in coal. These include (Falcon and Falcon, 1987):

Sedimentary rock

- These include siltstones, shales and sandstones occurring between coal seams.

Mineral grains

- These grains are mixed with the organic matrix of the coal particles, from which the most abundant minerals are in the form of quartz, clays, carbonates (calcite and dolomite) and pyrite.

When these minerals and macerals occur in various combinations and proportions, they are known as microlithotypes (microscopic bands), with series of the microscopic bands forming macroscopic bands called lithotypes. Coal can be assessed by observing the various lithotypes with the use of a microscope. The microlithotype distribution plays an important role in the processing and utilization of coal (Falcon and Falcon, 1987). Some of the factors contributed by the different microlithotypes (macerals) include the variation in grindability, which will affect the distribution of microlithotypes and or macerals in various particle size ranges. Another factor that will be affected is the microlithotype (maceral) distribution variation that will occur in different particle densities due to the variation in densities of the individual macerals.

2.2.3. Coal classification

The rank of a specific coal is an indication of the maturity of the seam from which the sample was obtained. This maturity is commonly affected by factors like geological time, pressure, and temperature. How these parameters influence the mechanical properties of coal has not been quantified in South Africa. For European and North American coals, rank is determined by the amount of volatile matter and carbon content, this is however not that well established for South African coals. The rank of South African coals is determined by petrographically determining the vitrinite reflectance under oil immersion (Falcon and Falcon, 1987).

2.3. Coal characterization: Conventional analysis

This section covers some of the most relevant properties, as well as the analysis done to determine these properties, and the way in which these properties relate to the characterization of coal. The conventional analysis of coal includes proximate and ultimate analysis, calorific value analysis and petrographic analysis.

2.3.1. Proximate and ultimate analysis

During the proximate analysis of coal, four parameters are determined: moisture; ash; volatile matter; and fixed carbon content. The moisture content is the moisture contained in the pores of the coal, whereas the ash represents the remains after combustion, which is normally associated with the initial mineral matter in coal. The volatile matter is the part of the coal that can be driven off as gases at elevated temperatures in the absence of reactive gases. The fixed carbon is the organic matter left after the determination of the volatile, moisture and ash content. For this analysis moisture, volatile matter, and ash are determined analytically, and the amount of fixed carbon is determined by difference. Ultimate analysis experiments are conducted to determine the principal elements in coal; these include the carbon, hydrogen, nitrogen, oxygen and sulphur contents (SANS, 2006).

2.3.2. Calorific value analysis

The chemical energy in coal is measured by a calorific value determination, and is indicative of the value of the coal as a fuel stock. The calorific value of coal can be expressed in two forms, the gross calorific value and the net calorific value. The net calorific value is determine from the gross calorific value by subtracting 40 kJ/g of water derived per unit quantity of fuel where the water includes the original water present as well as the water produced from the combustion reaction (Montgomery, 1978).

To determine the gross calorific value the heat released from the burning of a certain amount of coal in a closed vessel in oxygen is measured. Factors that affect the measurement of the calorific value include the difficulty of acquiring a representative sample, human error in variation of analytical technique as well as incomplete combustion of the coal sample (Montgomery, 1978).

2.3.3. Petrographic analysis

Petrographic analysis of coal involves the estimation and evaluation of the composition and physical properties of coal by means of microscopic examination. Petrography is important due to the fact that the chemical and physical properties are not only affected by the classical ranking parameters, but also by parameters such as maceral components and mineral matter. For a complete parameter profile, rank parameters as well petrographic parameters need to be determined (Falcon, 1978).

Work done by Koekemoer (2009) on a typical Highveld coal, with particle size in the region of 1mm, showed that the microscopic structure of these coals varied considerably when washed at different densities. From this analysis it was found that all the fractions were medium rank C coals, or high volatile bituminous coals. It was also found that the composition of different coal samples varied considerably (Koekemoer, 2009), making petrographic analysis very important when searching and calculating correlations between compositions and physical behaviour of coal.

2.4. Coal characterization: Advanced analysis

The advanced analysis of coal can be considered as non-standard coal analysis methods or recently pioneered analysis methods for the characterization of coal. These methods include: FTIR (used in this investigation), ss-NMR, HRTEM and XRD analysis of mineral as well as amorphous coal fractions. These analysis techniques are discussed briefly in the following sections, followed by a more detailed discussion on FTIR analysis.

2.4.1. Ss-NMR

Solid state carbon - 13 nuclear magnetic resonance (^{13}C-NMR) spectroscopy has been used for coal research from as early as 1976 (Van der Hart and Retcofsky, 1976) and is a rapid non-destructive technique for acquiring the chemical structure of organic matter (Suggate and Dickinson, 2004). Some of the parameters that can be obtained from ss-NMR include: fractions of aromatic carbon, aliphatic carbon, protonated aromatic carbon, non-protonated aromatic carbon, methylene carbon and methane carbon, methyl carbon, phenolic carbon, substituted aromatic carbon and bridgehead aromatic carbon (Solum *et al*., 1989).

2.4.2. HRTEM

The changes occurring in coal during combustion as well as gasification has been studied using microscopy techniques such as high resolution transmission electron microscopy (HRTEM). HRTEM was found to be among the most effective techniques (Sharma *et al*., 1999) for interpreting the atomic structure of chars using lattice fringe imaging (Oberlin, 1989). Amongst others Furuta *et al*. (1989) developed techniques to show structural changes occurring during gasification at 900 °C, and Zielinska-Blajet *et al.* (1997) compared the structural information obtained from both XRD and HRTEM and found a qualitative agreement between the two techniques.

2.4.3. XRD

X-ray diffraction (XRD) is very helpful in characterizing coal and in determining a structural and compositional insight into coal. XRD is used to determine the mineral characteristics of coal, as well as some of the characteristics of the amorphous fractions (Saikia *et al*., 2007). Specific information that can be obtained from XRD analysis includes the average aromatic cluster size and the stacking height of the aromatic clusters (Jones *et al*., 1999). More general trends can also be shown by XRD characterization work done on coal. These include the characterization of macerals, where the authors found that inorganic compounds, like monohydrocalcite, transform differently for the various macerals while other compounds like quartz are not transformed at all (Lin and Guet, 1990).

2.4.4. FTIR analysis

The properties of coal can be determined in real time using FTIR techniques. This real time approach can make it easier to assess the quality of coal before it enters the industrial process. This can greatly enhance the process control procedure implemented in the industry, improving emissions control and quality control (Belbot, 2000).

The interpretation and prediction of coal properties by means of FTIR analysis has been attempted by numerous researchers (Estep *et al*., 1968) (Bell *et al.*, 1991) (Solomon and Carangelo, 1988), validating the improvement and development of this technique for further application. Researchers like Painter *et al*. (1981), Fuller *et al*. (1982) and Martin and Chao

(1988) found that FTIR analysis can be used to extensively analyze coal in terms of functional groups, hydrogen bonding characterization and structural changes occurring during conversion processes.

As far as quantitative analysis is concerned, most of the research covers specific groups like hydroxyl groups (Solomon and Carangelo, 1982) or aliphatic and aromatic groups (Solomon and Carangelo, 1988) which only occur in distinct sections of the IR spectrum. To fully quantify all the properties of coal it is suggested that the entire spectrum be considered to describe the coal samples. However using the entire IR spectrum requires a combination of thousands of variables that must rapidly be determined with considerable accuracy. This led to the development of multivariate calibration methods (Bona and Andres, 2008) such as multi linear regression (MLR); principal component regression (PCR); and partial least squares regression (PLS) techniques (Alciaturi *et al.* (1996); Alciaturi *et al.* (1997)). However, before these advanced processing techniques can be applied with confidence, accurate spectra acquisition techniques have to be developed.

2.4.4.1. Comparison of FTIR spectra acquisition techniques

Bona and Andres (2008) did a study to compare the influence of different FTIR analysis techniques. The techniques they investigated were transmission spectroscopy, diffuse reflectance infrared Fourier transform (DRIFT) spectroscopy and attenuated total reflectance (ATR) spectroscopy. The properties they used to compare the techniques included: moisture, ash, volatile matter, fixed carbon, heating value, as well as the elemental distribution of carbon, hydrogen, nitrogen and sulphur.

After the spectra had been acquired, different treatments were conducted on the spectra so that the different acquisition techniques could be compared in a consistent and reliable way. The samples were first analysed by standard methods to determine proximate and ultimate analysis parameters, as well as heating values. These analyses were conducted on sample sizes in the powder range (Bona and Andres, 2008).

Bona and Andres (2008) found that the best resolution to conduct FTIR experiments occur at a resolution of 1 cm^{-1}; this increases the accuracy of predicting organic related coal properties. The transmission spectroscopy samples were prepared by mixing the coal sample with potassium bromide and pressing the pellet in a die using a pressure of 10 tonnes. The DRIFT samples were prepared by mixing the relevant coal samples with potassium bromide and then placing these in a diffuse reflectance accessory, without

pressing the coal into a pellet. Finally the ATR samples were placed on a diamond crystal (creating close contact between the crystal surface and the coal sample) after which it was scanned to obtain the necessary spectra.

The results found in this study showed that there is a significant difference in the spectra that were obtained by the different techniques. The difference can be seen in Figure 2.1 obtained from Bona and Andres (2008). The standard deviation was negligible when the effect of the apparatus was calculated, indicating that the experiments have an excellent reproducibility when considering the influence of the machine. However, parameters such as the physical placement of the pellet or the sample cup in the FTIR apparatus, preparation techniques, sample dilution *etc*. were found to have a significant influence (Bona and Andres, 2008).

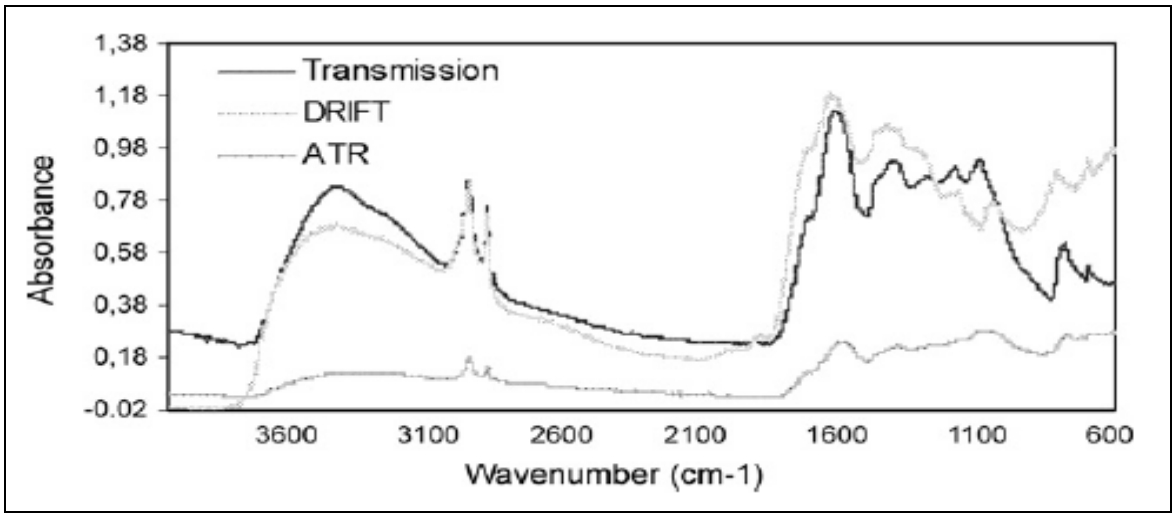

Figure 2.1: Comparison of spectra obtained from different acquisition techniques (Bona and Andres, 2008)

In general, good correlations were reported for properties concerning organic compounds (fixed carbon, heating value, carbon and hydrogen content) with the transmission technique performing slightly better. Even though the spectral positions of the different techniques differ, the error for ATR was similar to that determined for the transmission mode, with the advantage of very little sample preparation.

Diffuse reflectance infrared (IR) spectra show that transmittance intensities of hydroxyl peaks (3700-3600 cm^{-1}) are influenced by the process of pressing the kaolinite into pellets to perform the transmission infrared studies. Factors like absolute pressure, duration of pressing and the salt mixture used (if any) affect the degree of influence on the IR intensities. The use of KBr in the pellet pressing process shows a larger change in intensities

than when pressing the sample neat. By using diffuse reflectance IR in kaolinite studies the influence of pellet pressing is eliminated as this technique does not require sample pellet pressing. With the diffuse reflectance technique kaolinites can more accurately be distinguished by their hydroxyl group differences, leading to a better understanding of the hydroxyl structures of kaolinite (Bell *et al*., 1991)

From the results obtained by Bell *et al*. (1991) it is thus clear that valuable structural information can be lost when IR spectra is obtained from KBr pellets. It also showed that using the diffuse reflectance method improves the accuracy of the spectra. On the other hand a study by Martin and Chao (1988) preferred absorbance spectra rather than Kubelka-Munk units due to the fact that some of the intensities of the latter are too weak to analyse/resolve well.

2.4.4.2. Prediction of coal properties by using FTIR data.

Work done by Alciaturi *et al*. (1997) on bituminous coal demonstrated that certain coal properties can be predicted using compressed infrared spectra. The properties they tried to predict include volatile matter; fixed carbon; ash content; heating value; hydrogen content; carbon content; sulphur content; nitrogen content; and maximum vitrinite reflectance. From the studies done with compressed FTIR data it can be seen that good correlations were found for maximum vitrinite reflectance, hydrogen, fixed carbon, carbon content, ash and volatile matter, but poor correlations were found for sulphur content, nitrogen content and heating values (Alciaturi e*t al*., (1996); Alciaturi e*t al*. (1997)). Furthermore the rest of the properties can be determined with analysis appropriate for on-line systems. However, the mineral part of the determination was not so accurate, but can be improved upon if the minerals are known (Bona and Andres, 2008)

It was found that when using the osculating polynomials to obtain the reduced data, a better correlation was found to predict coal properties than using second derivatives; in addition the former method requires less computational time (Alciaturi *et al*., 1997). After the FTIR data has been reduced, techniques like multi linear regression (MLR), partial least squares (PLS) and principal components regression (PCR) are used to predict the coal properties. When using the derivative DRIFT spectroscopy technique it was found that MLR was superior to PCR in predicting the properties of coal. When using the osculating polynomial method, it was found that the superior technique to predict coal properties was PCR (Alciaturi *et al*., 1996).

2.5. Combustion behaviour of coal

2.5.1. Introduction and overview

The combustion of coal particles can be seen as “arguably the most important reaction known” (Ranish and Walker, 1993), and is involved in some of the largest industrial technologies, including combustion and gasification of coal. Due the fact that the costs of high-grade coals are continuously increasing, and considering the pressure of environmental legislation, a more effective use of coal is desired (Schobert and Song, 2002).

The processes occurring during coal conversion include drying (release of the moisture), devolatilization (release of the volatiles), immediate combustion of volatiles (due to the influence of high temperature), and then char combustion (Zajdlik *et al*., 2001). Depending on the reaction conditions these processes can occur chronologically or simultaneously (Holikova *et al*., 2005). The combustion process is one of the most important parts during coal conversion and can be seen as a non-catalysed gas-solid reaction (Zajdlik *et al*., 2001). However, in low grade coals, the influence of minerals on the conversion rate cannot be neglected. Several studies have demonstrated a catalytic effect of the minerals present in the coal (Du *et al*., 1990) (Zhang *et al*., 1997) (Mendez *et al*., 2003).

The models used to model the combustion behaviour of coal are continuously increasing in complexity, adding more and more variables to eliminate assumptions made in previous models. Some of these improvements include fluid flow, heat transfer, and homogeneous chemical reactions (Hurt and Calo, 2001). These parameters cannot easily be captured in simple oxidation models. Although the combustion of coal can be modelled from the fundamental properties of coal, semi-empirical models are normally used for the modelling of coal combustion reactions (Szekely *et al*., 1976).

2.5.2. Combustion regimes

Tu and Davis (1934) found that combustion occurs in three regimes controlled by a combination of transport processes and chemical reaction. The transfer between these regimes changes at certain temperatures and particle sizes, and is dependent on intrinsic reactivity and pore structure (Bailey *et al*., 1990). These three regimes were discussed in detail by Walker *et al.* (1959).

Regime I:

Conversions occurring in this regime are considered to be dominated by chemical reaction controlling mechanisms. This regime is characterised by: a relatively low reaction rate relative to the diffusion rate; small particles; very porous structures; and low temperatures (below 500 °C). In this regime the oxygen will penetrate the porous chars faster than it can be converted by the rate of reaction, producing a uniform oxygen concentration throughout the particle (Walker *et al*., 1959). In this regime that total internal surface area is proportional to the reactivity (Simons, 1983).

Regime II:

At higher intermediate temperatures (approximately 500 °C – 800 °C) the reactant gas is consumed by a reaction zone that does not extend to the centre of the coal particle; this results in an unreacted core inside the particle. This regime is controlled by pore diffusion mechanisms and is characterised by: fast reactions; low diffusion rates; and low porosity particles (Walker *et al*., 1959). The diffusion rates for regime II conditions include gaseous diffusion rates within the pores as well as through the char wall (Simons, 1983), which are controlled by parameters like particle wall thickness, total porosity and pore size distribution of the char.

It has been shown that reaction surface area keeps increasing over time for high temperatures due to the development of micro porosity, while the reactivity continually decreases (Simons, 1983)(Tsai and Scaroni, 1987). This results from the fact that while small pores contribute to the reaction surface area, the oxygen penetration is far less prominent for the small pores when compared to the larger pores (Bailey *et al*., 1990). This shows that macro porosity rather than micro porosity influences the char reactivity under regime II conditions (Bailey *et al*., 1990).

Regime III:

Regime III characteristics occur at temperatures exceeding 800 °C, where the reaction rate is significantly faster than the rate at which reaction gases penetrate the solid matrix. Under these conditions the reaction occurs on the external surface of the coal particle and is controlled by film diffusion effects (Walker *et al*., 1959). For large pulverized particles the reactivity can strongly be controlled by oxygen diffusion through the boundary layer to the

particle surface. This is controlled by the external dimensions and therefore indicates that the particle size has a strong influence of char reactivity (Bailey *et al*., 1990).

2.5.3. Properties influencing combustion behaviour

The following sections discuss the various properties that influence the combustion behaviour of coal. These properties include operation properties: temperature; gas mixture concentration; and particle size. The discussion will also include the influence of certain physical properties like particle density and pore size (distribution).

2.5.3.1. The effect of temperature

Previous work done on 7 – 10 mm particles indicates that the combustion reaction is reaction controlled at low temperatures and diffusion controlled at high(er) temperatures. It was found that the regime change occurred at temperatures between 530°C-550°C, but that it was also dependant on the oxygen concentration of the inlet gas stream (Holikova *et al*., 2005). Studies have also shown that diffusional control can occur at very low oxygen concentrations if the temperatures are high enough, typically in the order of 800°C (Holikova *et al*., 2004) (Remiarova *et al*., 2004). Other research also shows that for high quality graphite particles (3 -13 mm) combusted at 1110 K the conversion process is mostly controlled by oxygen diffusion to the particle surface while combustion at 985 K is controlled by intraparticle transport as well as the kinetics of the char conversion reaction (Prins and van Swaaij, 1990).

Holikova *et al*. (2005) found that if the oxygen concentration is low (<5% vol.) and the temperature below 530°C, there is not enough oxygen surrounding the particle to ignite the combustion reaction. Under these conditions there is a temperature oscillation during the combustion reaction. This phenomenon occurs due to the fact that oxygen needs to be accumulated in the pores on the surface, when enough oxygen has been accumulated the reaction can ignite, consuming all the oxygen at the surface; this is then followed by an increase in the particle temperature. After all the oxygen has been consumed new oxygen needs to be transported to the surface, because the oxygen transport is slow, the reactions slows down which is followed a decrease in the particle temperature. The increase of temperature in the particle core can also be explained by the fact that the ash layer is not

thermally conductive and thus contains the heat of combustion within the unreacted core, causing the core to overheat (Sotirchos and Amundson, 1984)

2.5.3.2. Gas mixture variations

Holikova *et al*. (2005) conducted a study to determine the influence of oxygen concentration on the combustion of 7 – 10 mm single particle coal chars. They found that the burnout times for higher oxygen concentrations (10%, 15%, 21% volume based) were shorter than for the lower oxygen concentrations (3% and 5% volume based). With higher oxygen concentrations, and temperatures above 530°C, intense overheating of the particle core was found to occur during the combustion reaction. With 21% oxygen, the core temperature rose as high as 900°C. They further proposed that under these conditions endothermic reaction between the solid carbon and carbon dioxide may occur. At the low oxygen concentrations (<5% by volume) it was also found that the combustion rate was very low, and that there was very little overheating of the unreacted core. It has also been shown that the carbon surface reaction is very dependent on oxygen partial pressures (Jelemensky *et al*., 2000).

Higher grade coal is generally depicted as having a higher carbon content and lower ash content. Even though total carbon conversion is expected (from carbon to carbon dioxide), depending on the reaction conditions, a large amount of the product gas is actually carbon monoxide. Due to this partial combustion, there is less heat released into the system. Thermodynamically, the formation of carbon monoxide is suppressed at low temperatures, typically lower than 400 °C (Pranda *et al*., 1999). The model proposed by Jelemensky *et al*. (2000) showed that the model can accurately predict CO_2 and O_2 concentrations; however the prediction of the CO concentration was unsatisfactory

2.5.3.3. The effect of particle density

Work done on coal particles ranging from 84 -135 µm by Maloney *et al*. (2005) suggests that the there is a broadening in both size and density distributions due to devolatilization as well as combustion processes. It was also suggested that the higher density particles result from particles with higher that average mineral content (Maloney *et al*., 2005), and that much of the variation was due to variations in the particle-to-particle ash content. It has been shown that high density coal fractions tend to be enriched with minerals such as pyrite and

carbonates which could either occur as minute dispersed crystals or, in some cases, as large, easily distinguishable, crystals (Mendez *et al*., 2003).

These density variations can, however, also be due to variations in maceral distribution. The density of different maceral groups varies from heaviest to lightest in the order: inertinite>vitrinite>liptinite (Borrego *et al*., 1997). The maceral distribution for different density particles can result in different char forms occurring in the different fractions. This affects particles parameters like char porosity. It has been shown that low density vitrinite rich particles form very porous chars (Strezov *et al*., 2005), whereas the inertinite rich particles tend to form much denser chars (Borrego *et al*., 1997). Gilfillan *et al*. (1999) also found that the char wall thickness tended to increase as the density of the particles increased.

The variation of bulk mineral matter content is not the only consequence of density separation. It has also been shown that there is a segregation of both minerals and macerals, along with variations in the degree of association of macerals and inorganic matter (Mendez *et al*., 2003). FTIR investigation into density separated particles revealed that the aromatic aliphatic ratio tends to increase as the density of the particles increases. This is due to the increase in the more dense macerals (Gilfillan *et al*., 1999).

2.5.3.4. The effect of particle size

It is well known that the char particle size greatly influence char combustion. This is mainly due to parameters like uneven maceral distribution (Jones *et al*., 1985); heat transfer coefficients at the particle surface; oxygen diffusion from the bulk gas stream to the particle surface; intra-particle mass transfer; and combustion rates (He *et al*., 2003) (Smith, 1982).

Work done by Niska *et al*. (2003) showed that the dimensions of coal particles have an effect on reaction controlling mechanisms and that the reaction rate (per unit surface area) becomes independent of particle size when the overall reaction is reaction controlled, and inversely proportional to particle size when the reaction is diffusion controlled. This was confirmed by Wells and Smoot (1985) who found that the reaction rate is independent of particle size at low temperatures, but is dependent on particle size at the higher temperatures due to external diffusion effects (Liu, 1999). The dependence on particle size and diffusion effects influences the transition temperatures between the different reaction regimes, which can be linked to char porosity and reactivity (Bailey *et al*., 1990). It is also believed that char reaction for particles smaller than 100 μm are chemically controlled (Essenhigh, 1976) as in the case of high temperature pulverized coal combustion boilers,

while in the case of larger particle, lower temperature fluidized bed combustors, the char reaction is controlled by diffusion mechanisms (He *et al*., 2003).

The effect of particle size on combustion can be attributed to maceral disproportionation occurring during grinding as well as to the physical structure of the particle including dimension and porosity. The size preference of macerals can be described by the difference in maceral grindability, compressibility, hardness and others factors (Falcon and Falcon, 1987). From these factors it can be proposed that smaller particles will contain a higher percentage of vitrinite, while the larger particles will tend to have a higher intertnite content. Due to different maceral content, the particles will have different devolatilization behaviour, and different reaction properties (Jones *et al*., 1985). Work done by Maloney *et al*. (2005) showed that size reduction occurs in creating chars for particles of the range 84 to 135 µm, and suggests that the reduction is due to particle shrinkage or to particle fragmentation.

2.5.3.5. Ash content and its catalytic effect

Chen and Kojima (1996) found that the ash content of a char particle can significantly influence combustion behaviour. Their work was conducted on granulated particles of between 10 – 18mm with varying ash contents. They found that the particles with a higher ash content burned with a lower peak temperature that rapidly decrease due to lower ash porosity, and had lower ash layer diffusion coefficients. It was also concluded that the high ash particle combustion was controlled by ash layer diffusion, except during the initial stages. The particles with a lower ash content showed chemical reaction control at lower temperatures, while it was observed that ash layer diffusion was the controlling mechanism at higher temperatures, with the initial stages being controlled by film diffusion. Jelemensky *et al*. (2000) went on to show that if the combustion occurs at low temperatures (350°C - 550°C) the ash layer does not form a shell on the geometrical surface of the particle.

Work done by Pranda *et al*. (1999) showed that alkali metal compounds decrease the ignition temperature of the char particle and thus have a beneficial effect on the combustion mechanism. In a related study the same authors (Pranda *et al*., 2001) showed that alkali metal carbonates decreased CO formation in favour of CO_2 formation. The mineral matter properties in coal can further be studied by adding the required component to the coal matrix, as was done by Zhang *et al*. (1997). These coal burning additives (CBA) mainly consists of metal and semi-metal oxides, including Mg, Fe, Mn, Al, Si, and B. The CBA is usually in powder form. The results showed that the energetic value of the coal samples

does not change when doping with the CBAs. It did however reveal that these additives lowered the coal ignition temperature, and that doping with the additives could change the course of the oxidation reaction due to catalytic effect. This was confirmed by an apparently decreased activation energy, and by the acceleration of the combustion reaction of graphite. These results indicate that the presence of these additives creates catalytically active centres that are beneficial to the combustion reaction.

2.5.3.6. Surface properties and pore structure

Insight into reactivity can be gained from the pore structure of the coal particle, and how this structure changes during the reaction. Studies show that the pore structure depends on the origin and the pre-treatment of the coal (Remiarova *et al*., 2004), where pre-treatment may include: drying, devolatilization, and heating of the particles (Holikova *et al*., 2005). . These studies also show that the original pore structure of the coal has a bimodal pore distribution, where nearly all the internal surface area originates from micropore (pore radius R_{pore} < 1nm) and mesopore (1nm < R_{pore} <25nm) regions and a significant amount of the total porosity is made up of the large pores (R_{pore} > 25nm) (Beveridge and Goldie, 1968) (Bhatia and Perlmutter, 1980).

The overall chemical reactivity depends on how easily the reactant gases can access the internal surface area and is thus dependent on the porous structure of the coal. The micropores might be less accessible to the gas reactants, unless the feeder pores are large enough (Jelemensky *et al*., 2000). In conclusion, it was found that the porous structure was closely linked to the process conditions.

The pore structure of coal can be studied through gas adsorption and mercury intrusion, as was done by Jelemensky *et al*. (2000). The results have shown that the specific surface area of the original coal particle is negligible. Devolatilization had a significant effect of the porous structure of the coal particle, increasing the total porosity from 5% to 10%, and thereby increasing the accessibility of the microporous region. Even though the core of the reacting particle shrinks as the combustion reaction occurs, the core surface area properties do not change significantly, however due to the consumption of solid carbon and an internal temperature above 850°C results in an increase in the surface area of the micro- and mesopore regions of the unreacted core was observed (Holikova *et al*., 2005). At low temperatures and low oxygen concentrations, the pores between 10nm to 2000nm, opened,

making the inside of the particle more accessible for reactant and product gas diffusion (Jelemensky *et al*., 2000).

When the oxygen concentration is lower than 5%, the development specific surface area was different for each temperature investigated. The results showed that at low temperatures (lower than 550°C), the specific surface area was similar to the uncombusted coal. The lack of internal structure change was attributed to the fact that the oxygen was depleted at the ash –core interface.

2.5.4. Combustion modelling

The coal char particle combustion mechanism has been extensively studied and can be very complex. The basic principle of combustion can, however, be characterized as a non-catalysed gas-solid reaction (Szekely *et al*., 1976). Different combustion models have been developed to describe the combustion of coal in the different combustion regimes. These basic models include homogeneous-diffusion models (Molina and Mondragon, 1998) and shell progressive models (Jelemensky *et al*., 2000) (Zajdlik *et al*., 2001). For homogeneous diffusion models it is assumed that the reacting solid is very porous and that the reactant gas diffusion rate is very high compared to the reaction rate. The homogeneous mode is typical for regime I combustion. On the other hand the shell progressive model assumes that the reactant gas reacts with the solid phase only on the external surface. In this case the chemical reaction rate is much higher than the rate of diffusion of reactant gas through the pores of the solid phase. The shell progressive behaviour is typically observed for regime II and III combustion conditions.

When using the homogeneous model, the coal conversion reaction can be seen as a homogenous reaction occurring in all the available space in the char, both on the external and the internal surfaces of the particle. The homogeneous model does not consider structural changes occurring during coal conversion and is one of the simplest models proposed to describe char conversion reactions. The homogeneous model has been used by various researchers to model the conversion of carbon including work done with steam gasification and with gasification using supercritical water (Ishida and Wen, 1968) (Yang and Watkinson, 1994) (Everson *et al*., 2005) (Vostrikov *et al*., 2007).

The shrinking core model is very well known and was first presented by Yagi and Kunii (1955). This model considers reactions as taking place on the surface of the unreacted centre of the particle. As the particle radius reduces during the reaction it might leave behind

an ash layer which can offer resistance to the transport of reaction and product gases. It is further assumed that there is little to no penetration or reaction within the unreacted core, and that the reaction occurs only within a thin layer on the surface of the receding particle.

The shrinking core model incorporates all three separate controlling mechanisms. The first controlling mechanism is the chemical reaction controlling mechanism where the chemical reaction is the slowest step in the process. Under chemical reaction controlling conditions the experimental conditions are such that neither the external mass transfer (high flow rates) nor ash layer diffusion (low temperatures) act as controlling mechanisms (Szekely *et al*., 1976). The characteristic equation describing the chemical reaction controlling mechanism can be given as

$$t = \left(\frac{\rho_B}{M_B b k'' C_{Ag}}\right)\left(1 - (1 - X_B)^{\frac{1}{3}}\right) \tag{2.1}$$

The above mentioned model does not account for changes in parameters like porosity and surface area that may occur during the reaction of the chars.

The second controlling mechanism is the gas film diffusion controlling mechanism. Here the transport rates of gases from the external gas stream to the particle surface area and vice versa are slow enough to limit combustion reaction (Szekely *et al*., 1976). The characteristic equation for this controlling mechanism can be given by

$$t = \left(\frac{\rho_B}{3 M_B b k_g C_{Ag} R_p^2}\right) X_B \tag{2.2}$$

The third controlling mechanism is the ash layer diffusion controlling mechanism where the transport of reactant and product gases to and from the unreacted particle core through the ash layer is controlling due to the transport resistance presented by the ash layer (Szekely *et al*., 1976). The characteristic equation describing the ash layer diffusion controlling mechanism can be given as

$$t = \left(\frac{\rho_B R_p^2}{6 D_e C_{Ag} b M_b}\right)\left(1 - 3(1 - X_B)^{\frac{2}{3}} + 2(1 - X_B)\right) \tag{2.3}$$

These controlling mechanisms can occur either independently or simultaneously. In the case of simultaneous controlling mechanisms, the total reaction time can be determined by adding the reaction times computed for the contributing controlling mechanisms (Levenspiel, 1999).

CHAPTER 3: EXPERIMENTAL METHODOLOGY

3.1. Introduction

This chapter covers a description of the origin of the studied coal samples; of the characterization techniques; and of the experimental apparatus. The chapter also contains information on the methods and techniques used to accomplish the experimental results. Section 3.2 gives a short description of the origin of the coal samples, while Section 3.3 explains the sample preparation. Section 3.4 describes the equipment used to prepare and characterise the coal samples, and Section 3.5 contains details of the combustion apparatuses and a process description of the entire setup. Section 3.6 explains the combustion investigation methods and techniques in detail.

3.2. Origin of coal samples

South African coal is predominantly obtained from coalfields located in Mpumalanga, KwaZulu-Natal, Limpopo, and the Free State. The three most important coalfields are the Witbank, Highveld and Waterberg coalfields as these contain most of the country's coal reserves (Jeffrey, 2005). The Highveld coalfield is the second largest coalfield in South Africa, and the coal from this field is either used by Sasol for the coal to liquids (CTL) process to produce liquid fuels and other industrial chemicals (Barker, 1999), or for power generation by the Matla and Kriel power stations. The original 250 kg sample used in this study originated from the Highveld coal field.

3.3. Sample preparation

The ROM (Run of mine) coal obtained from the Highveld region was sent for preparation to the laboratories at the South African Bureau of Standards (SABS). Prior to density separation the entire 250 kg sample was sieved to remove the – 0.5 mm size fraction, as these fines would significantly increase the time for sink float separation, and could affect the reference density of the separating liquid.

The remaining sample was then density separated into the density cuts listed below using sink/float techniques with TBE (tetrabromoethane).

- < 1.4 $g.cm^{-3}$
- 1.4 $g.cm^{-3}$ – 1.6 $g.cm^{-3}$
- 1.6 $g.cm^{-3}$ – 1.8 $g.cm^{-3}$
- 1.8 $g.cm^{-3}$ – 2.0 $g.cm^{-3}$
- > 2 $g.cm^{-3}$

The density separated samples were then left overnight in a convection oven at 40 °C to allow the particles to dry. The dried density cuts were then sieved according to the size ranges listed below. Sieves of appropriate sizes were stacked on top of each other, with a collection drum at the bottom to collect the smallest size.

- + 53 mm
- - 53 mm to + 25 mm
- - 25 mm to + 12.5 mm
- - 12.5 mm to + 6.3 mm
- - 6.3 mm to + 3.35 mm
- - 3.35 mm to + 1mm
- - 1mm to + 0.5 mm

This resulted in 35 samples, with each density set having the appropriate size range as presented in Table 3.1. Each sample was then assigned an arbitrary identification number ranging from A1 – E7. Individual coal particles from these samples were hand selected in order to conduct the combustion experiments in the large particle furnace.

Table 3.1: Sample identification grid

	+53mm	**-53mm +25mm**	**-25mm +12.5mm**	**-12.5mm +6.3mm**	**-6.3mm +3.35mm**	**-3.35mm +1mm**	**-1mm +0.5mm**
F 1.4	A1	A2	A3	A4	A5	A6	A7
F 1.6	B1	B2	B3	B4	B5	B6	B7
F 1.8	C1	C2	C3	C4	C5	C6	C7
F 2.0	D1	D2	D3	D4	D5	D6	D7
S 2.0	E1	E2	E3	E4	E5	E6	E7

After the sample preparation was complete, representative samples of each sample shown in Table 3.1 were obtained using rotary splitters. The representative samples were then sent

to the analytical laboratories at the South African Bureau of Standards (SABS) for characterization analyses. These representative samples were also used to determine the calorific values of the respective coals as well as to do analytical work in terms of FTIR analysis.

3.4. Sample characterization equipment and procedures

In order to relate density and size properties of coal to the combustion behaviour of coal, the characteristics of the different density and size separated coal samples had first to be determined. The samples were characterised by proximate and ultimate analysis, calorific value analysis and FTIR analysis methods. The density of the individual coal particles was determined with the help of the specially developed density measurement apparatus which is described in detail in Section 3.4.4. This characterization was done to show chemical changes occurring over different density and size ranges. These characterization results also shed some light on the variance of the constituents found in the coal samples.

3.4.1. Proximate and ultimate analysis

After the samples were density separated they were sieved to the appropriate sizes as described in Section 3.3. No crushing was done on the ROM coal as the purpose of the sieving was to determine the natural size distribution of the ROM coal. The obtained representative samples were crushed to -75 µm and left to air dry overnight before being analysed according to the standard proximate and ultimate analysis methods. The size distribution as well as the results from the proximate and ultimate analysis was thus obtained from SABS.

The proximate analysis on the coal samples was done by the South African Bureau of Standards (SABS) according to different standard methods as shown in Table 3.2.

Table 3.2: Proximate analysis methods as done by SABS

Inh. H20	SABS 925
Ash	ISO 1171
Vol.Mat	ISO 562
Fix.Carbon	By Diff.

The parameters determined by ultimate analysis are shown in Table 3.3, along with the standard methods used to determine them.

Table 3.3: Ultimate analysis methods as done by SABS

Carbon	ASTM 5373
Hydrogen	ASTM 5373
Nitrogen	ASTM 5373
Tot.Sulp	ASTM D4239
Oxygen	By Diff

3.4.2. Calorific value analysis equipment

The calorific experiments of the various coal samples were carried out in house to determine the fuel value of the various density and size separated coal samples. The calorific value work was conducted on a model MC10 bomb calorimeter supplied by Energy Instrumentation. The bomb calorimeter is equipped with a computer that is used to record the acquired calorific value data and to calibrate the bomb calorimeter.

The calorific value of the different coal samples was determined after the bomb calorimeter was calibrated. The bomb calorimeter is calibrated by combusting a benzoic acid pellet in the calorimeter and then adjusting the correction factor until the calorimeter yields the appropriate calorific value. The calorific values of the different samples were determined by measuring one (1) gram of coal sample and then combusting it inside the bomb calorimeter.

3.4.3. FTIR analysis

Selected samples were analysed and characterised using FTIR analysis techniques to determine the chemical differences across the various density and size ranges. The FTIR characterization analysis was done on a Bruker VERTEX 70 Series FT-IR Spectrometer using the mid infrared region (MIR). A picture of the infrared equipment can be seen in Figure 3.1.

Figure 3.1: Bruker Vertex 70 FT-IR spectrometer

The spectrometer was further equipped with a DRIFT spectrometer. The DRIFT add-on reduces sample preparation time and any effects that might occur during pellet preparation techniques. The FTIR spectrometer was also fitted with a KBr beam splitter. FTIR analysis was done on both the coal and char samples

The background sample was set to run for 300 scans while the sample was set to run for 400 scans with a resolution of 4 cm^{-1}. All the FTIR analysis work was done using the Diffuse Reflectance Kit.

To prepare the sample 20-25 mg of coal or char (- 75 µm) was added to 200mg of KBr. The sample was then mixed in a Wig-L-Bug automatic shaker for about 60 seconds after which the sample was stored overnight under vacuum at a temperature of 60°C. The background sample was prepared using the above-mentioned procedure, but without the addition of the coal samples. Before analysis the coal/char samples and the background sample were stored in different desiccators and the atmosphere in the desiccators was left to stabilise for about 30 minutes.

3.4.4. Mercury density measurement

Due to the fact that conventional density measurement techniques like mercury intrusion porosimetry are only capable of using small particle sizes, an apparatus that able to measure the density of large coal particles without destroying or damaging the particles was

developed. This apparatus can handle samples up to 60 mm in diameter. A diagram of the apparatus can be seen in Figure 3.2.

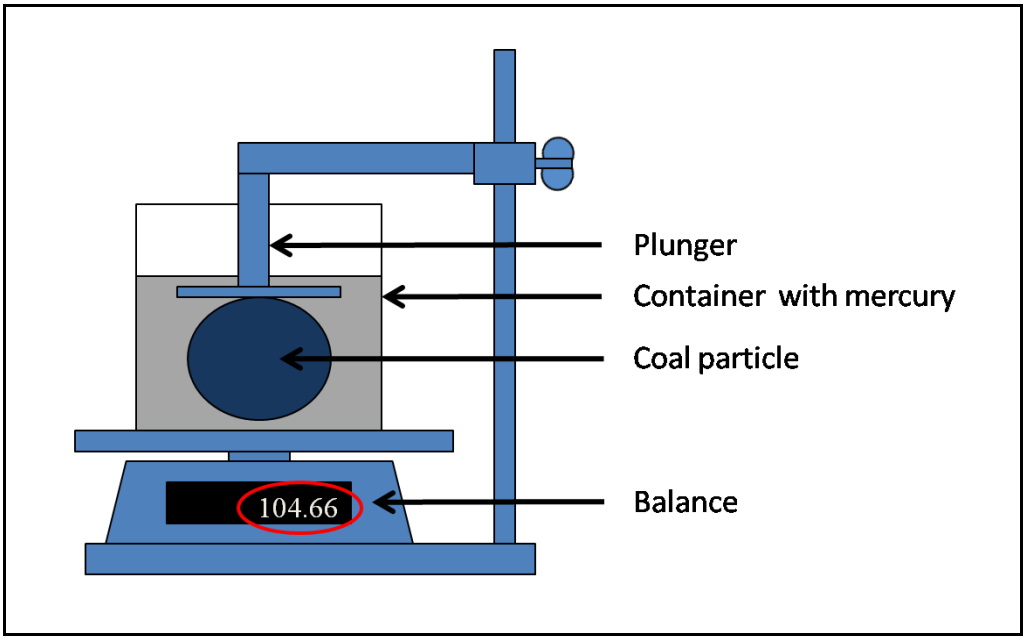

Figure 3.2: Diagrammatic representation of density measurement apparatus

In this method, the particle is submerged in the mercury using the constructed plunger arm as the particle will float due to the high density of mercury. As the particle is submerged in the mercury, the reading on the balance will increase, and this increase in mass reading will be used to calculate the density of the coal particle.

The mercury density measurement apparatus was used to measure the density of each individual coal particle respectively. The information needed to calculate the density of the coal particle can be obtained by measuring the mass of the coal particle, recording the mass reading on the balance when the coal particle is submerged and recording the mass reading when only the plunger arm is submerged. The density of the particle is then calculated using the following equation.

$$\rho_p = \left(\frac{m_p}{m_F - m_{Pl}}\right)\rho_f \qquad \text{(A.7)}$$

For the derivation of Equation A.7 refer to APPENDIX A. The technique was verified using both a spherical marble, as well as an aluminium rectangle with known dimensions. The verification calculations are shown in APPENDIX B.

3.5. Combustion apparatus

This section covers the combustion apparatus used to study the combustion of coal particles with different density and size ranges. The main equipment includes the high temperature horizontal tube furnace and the gas analysers used to measure the carbon dioxide and carbon monoxide concentration. The following sections give a detailed description of the setup of the experimental equipment.

3.5.1. High temperature horizontal tube furnace

A TSV15/50/180 horizontal tube furnace, supplied by Elite Thermal Systems Ltd, was used for the combustion experiments. The furnace is capable of handling particles of up to 60 mm in diameter, and can reach temperatures of up to 1500 °C at variable heating rates. A picture of the horizontal tube furnace can be seen in Figure 3.3.

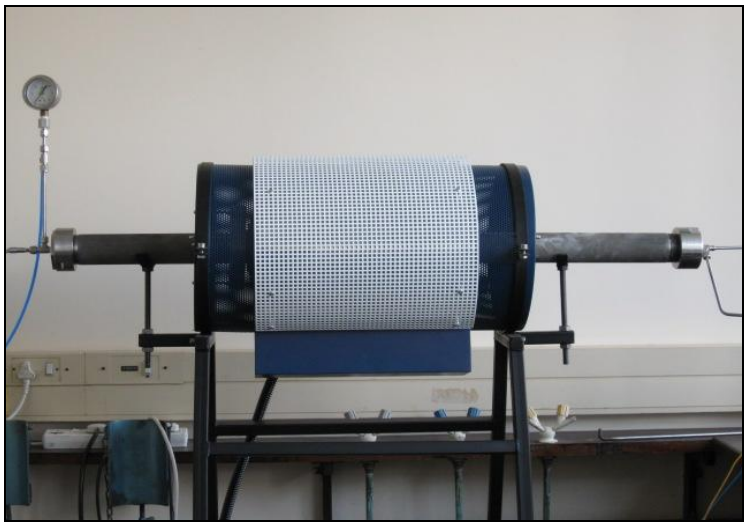

Figure 3.3: Picture of the horizontal tube furnace

To accommodate the high operating temperatures, a Kanthal pipe was inserted into the oven with the ends of the pipe customised and equipped with screw on caps that seal the ends. This directed the gas flow to the gas analysers. The inlet side was also equipped with a pressure gauge to monitor the pressure inside the furnace, and to indicate any blockage in the gas line setup. The screw on caps accommodated a thermocouple entering from the side to measure furnace temperature profiles, particle temperatures and gas feed temperatures.

The diagrammatic representation of the horizontal tube furnace setup is given in Figure 3.4, which shows the temperature controllers connected to the furnace, as well as the temperature controllers fitted to monitor particle temperatures and gas feed temperatures.

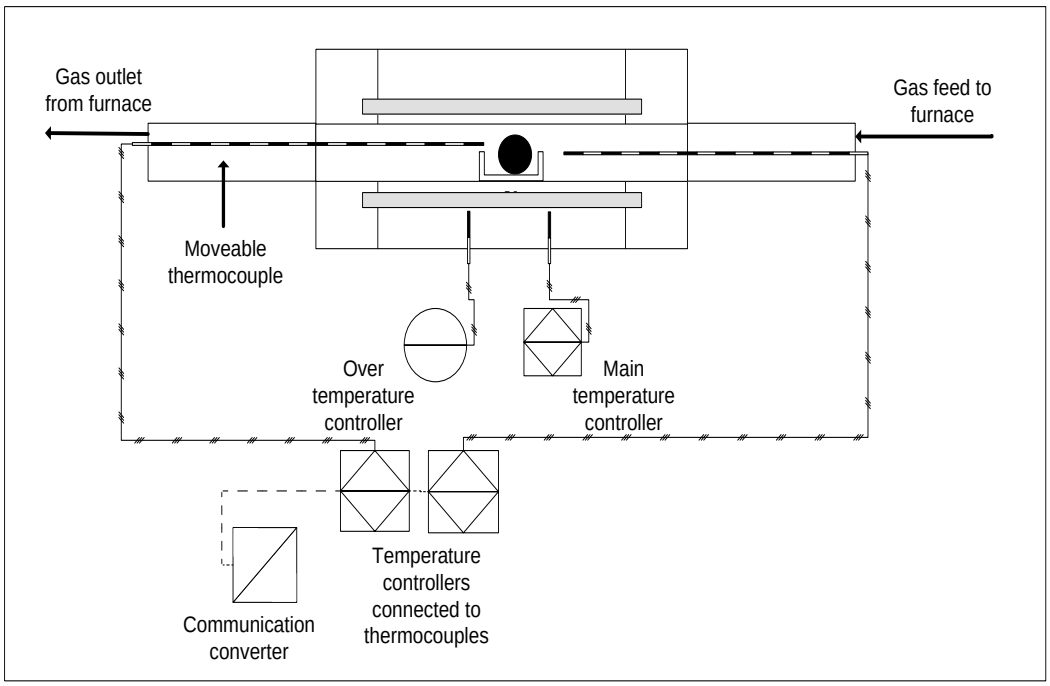

Figure 3.4: Diagrammatic representation of the horizontal high temperature tube furnace

The furnace was equipped with a model 2416 Eurotherm main temperature controller and a model 2116 Eurotherm over temperature controller. The furnace main temperature controller was equipped with a serial communication port to allow remote control of the furnace and to enable logging of the process variables. The details of the horizontal tube furnace are given in Table 3.4.

Table 3.4: Horizontal furnace ratings and settings

Model	TSV15/50/180
Maximum rated temperature (°C)	1500
Temperature controller	Eurotherm 2416
Over temperature controller	Eurotherm 2116
Supply	1PH+N+E
Voltage	230 V
Frequency	50 Hz
Maximum Power rating	3600 W
Nominal weight	22 kg

To measure the temperature close to the particle during combustion the furnace was further equipped with a K type thermocouple inserted from the side of the furnace through one of the screw on caps. This thermocouple was connected to a temperature controller so that the reading from the thermocouple could be recorded with the developed data acquisition software. Furthermore the bucket used to hold the coal particle during the combustion experiments was fitted to the thermocouple to allow the bucket to be moved inside the tube by moving the thermocouple. A picture with the bucket connected to the thermocouple can be seen in Figure 3.5.

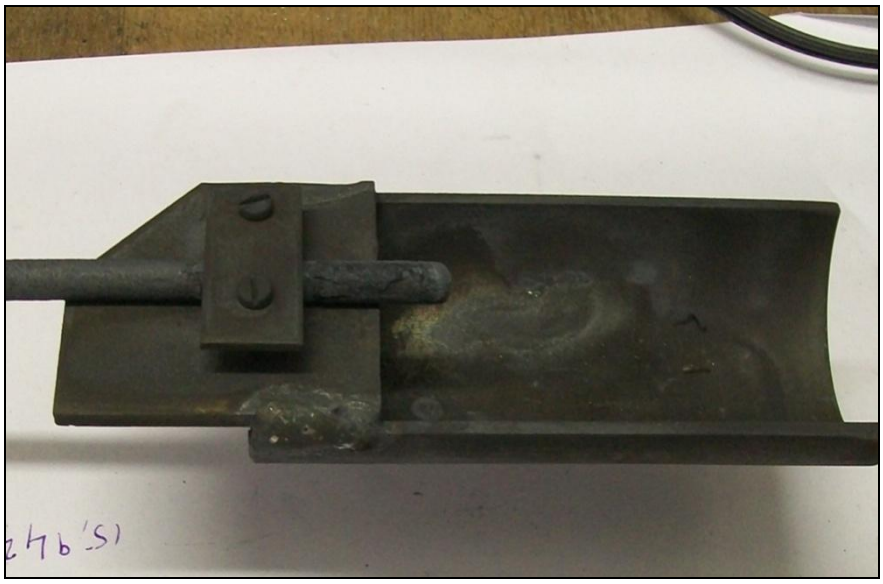

Figure 3.5: Bucket connected to the thermocouple

This thermocouple was also used to measure the temperature profile of the furnace to ensure that the particle is at the correct depth inside the tube furnace before commencing

the combustion experiments. This thermocouple was connected to a model DCL-33 Shinko controller which was then connected to a Shinko model IF 400 multi-drop RS-485 communication converter which was connected, in turn, to a computer for temperature data logging purposes.

To control the gas flow to the furnace the experimental setup was equipped with a Brooks model 0254 mass flow controller. The mass flow controller setup was capable of monitoring and controlling four different gas feeds to the furnace and was used both to measure the gas flow rates entering the tube furnace, and to switch between the different feed gases during experimentation. The horizontal tube furnace was used to char as well as to combust the various coal particles.

3.5.2. Gas analysers

To measure the gas production rate during combustion the setup was fitted with a carbon dioxide and a carbon monoxide gas analyser. An ADC model MGA 300 gas analysers using IRGA (infrared gas analyser) optical benches to measure the gas concentration was used in each case. The carbon dioxide analyser was able to detect gas concentration ranges between 0% and 6%, whereas the carbon monoxide analyser was able to detect carbon monoxide concentrations up to 7000 ppm.

To protect the gas analysers from both high pressure and the various heavy molecular tar species evolving during the devolatilization of coal particles, the gas analysers were connected to the exhaust gas stream using a depressurization bin. This was necessary due to the fact that the analysers could be damaged by pressures as low as 0.3 bar (g). The depressurization bin allows the exhaust gas to flow into an enlarged space while the internal sample pumps inside the gas analysers continuously draw samples from the moving exhaust gas stream.

During the devolatilization process the gas analysers had to be completely disconnected from the exhaust gas stream because the cold trap cannot remove all the volatiles from the gas stream; this was accomplished by removing the inlet sample lines from the depressurization bin.

3.5.3. Experimental process flow description

A horizontal tube furnace was used to create the char particles and to conduct the combustion experiments in order to determine the reactivity of the chars with respect to oxygen combustion. A diagrammatic representation of the experimental setup can be seen in Figure 3.6. The mass flow controllers were used to accurately determine the flow rate of the nitrogen gas during the heating period and the air flow rate during the combustion experiments. The mass flow controllers were also used to calibrate the two gas analysers. The gas was then fed to the furnace, where the particle was either devolatilised or combusted, via the custom screw on caps. The exhaust gas was then sent through a tar trap to cool and capture the tars that evolve during devolatilization and that might condense inside the gas analysers. The exhaust gas then passed to the depressurization bin where the two gas analysers were used to measure the carbon monoxide and carbon dioxide production rates.

The furnace temperature was controlled with the main temperature controller, while the over temperature controller was used to verify that the main temperature controller was functioning properly. The thermocouple inserted from the side of the furnace was used to ensure that the particle environment was at the required temperature.

All the necessary process variables, including the furnace temperature, the temperature close to the particle, gas feed rates and the gas concentrations as monitored by the two gas analysers, were monitored and logged using the created data logging software.

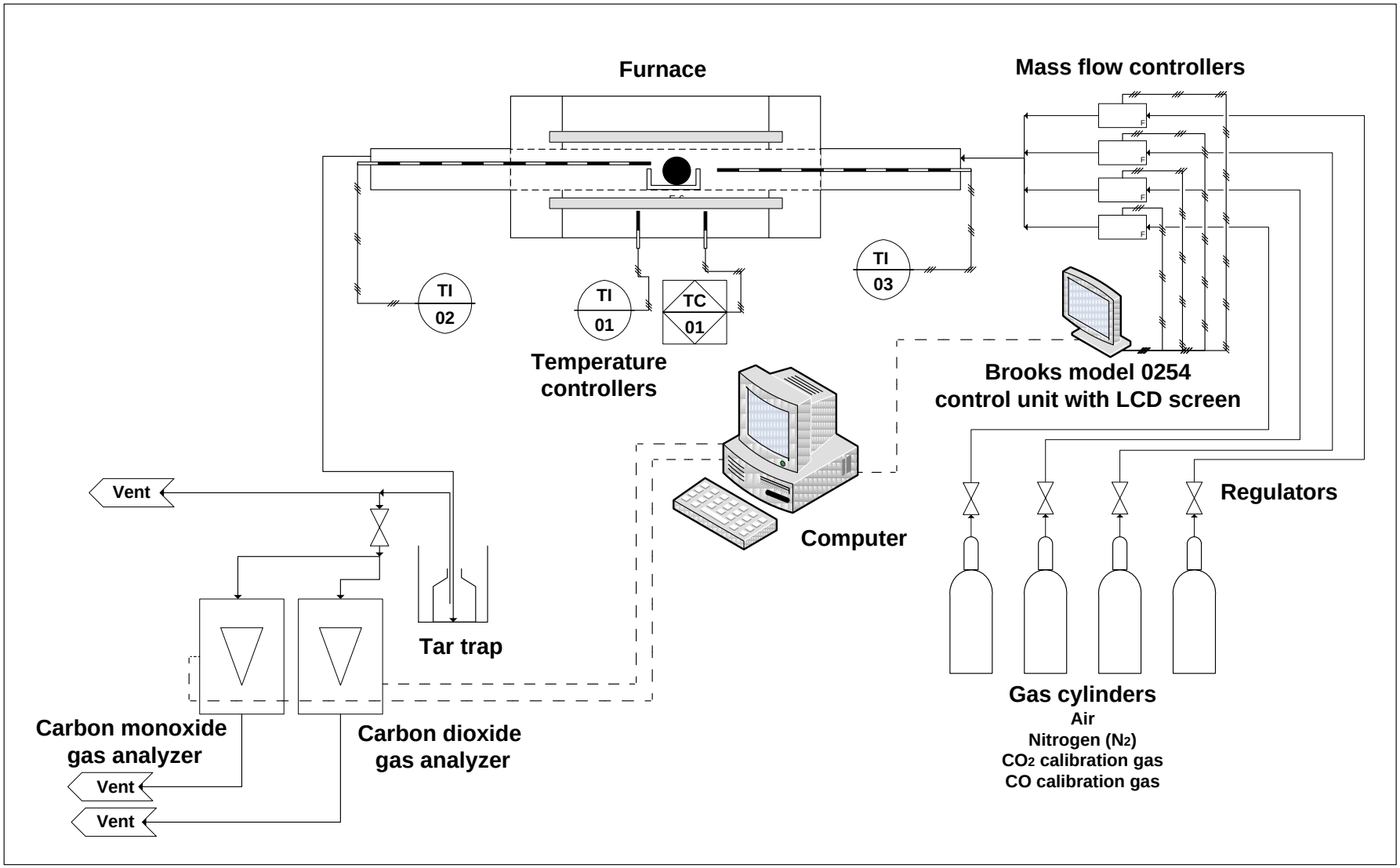

Figure 3.6: Combustion apparatus flow diagram

3.5.4. Data acquisition

In order to log the experimental data, software was created to read and log all the necessary process variables during the experimentation period. This was done with Visual Studio 2005®, incorporating Microsoft Excel® as the storage destination. All the communication was accomplished via serial port cables, utilizing USB to serial port converters to facilitate all the connections.

To combine all the elements of the experimental setup, a communication breakdown was needed to make them work together. Multithreading was used to facilitate all the elements so that the reading and writing of different parameters could work in parallel. To speed up the logging process all the variables or the process values were stored in virtual memory, and only written to excel once a complete set of values had been collected. To accommodate all the reading and writing of parameters, logging was done every ten (10) seconds. The communication breakdown can be seen in Figure 3.7.

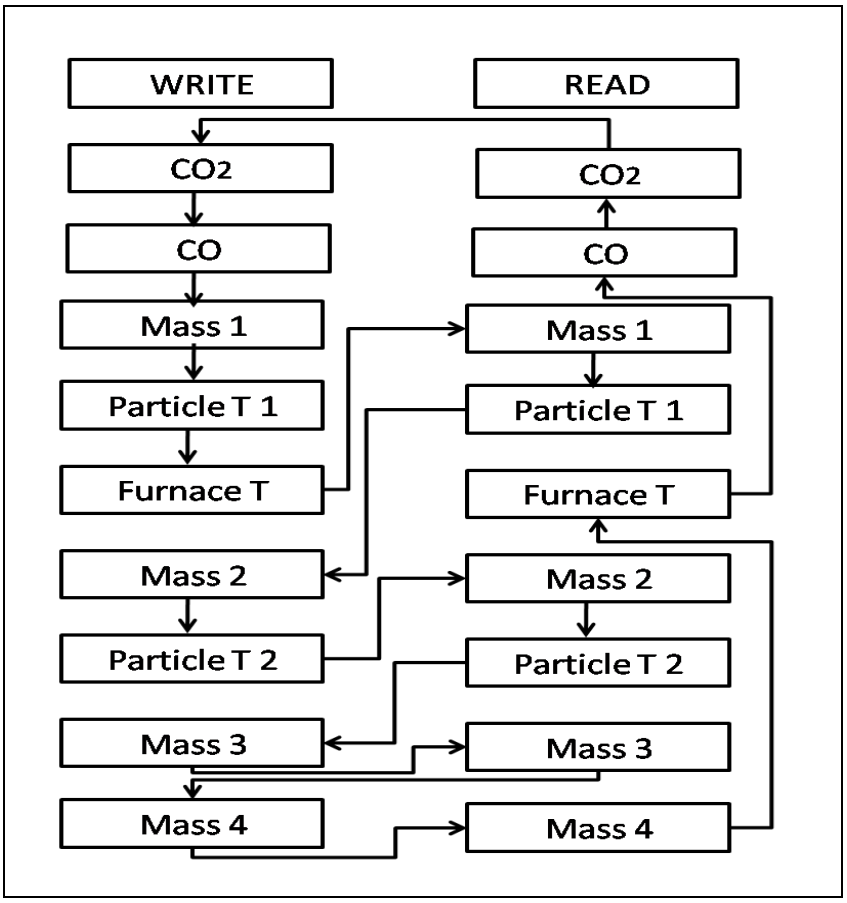

Figure 3.7: Communication breakdown for data acquisition

This communication breakdown was used to show the order in which each piece of equipment is interrogated. This was necessary because four mass flow controllers worked through a single cable, while two temperature readings were read through a separate single cable. For the mass flow controllers, one mass flow controller had to be interrogated for a process variable, and this variable had to be read from the serial port before the second mass flow controller could be interrogated. From Figure 3.7 it can be seen that each mass flow controller was interrogated and read before interrogating the next mass flow controller. Other equipment could be interrogated while waiting for the reply from one of the mass flow controllers.

The graphical user interface for the created software can be seen in Figure 3.8. This interface enabled direct communication with each piece of equipment in order to change settings or to obtain other variables or current setting values.

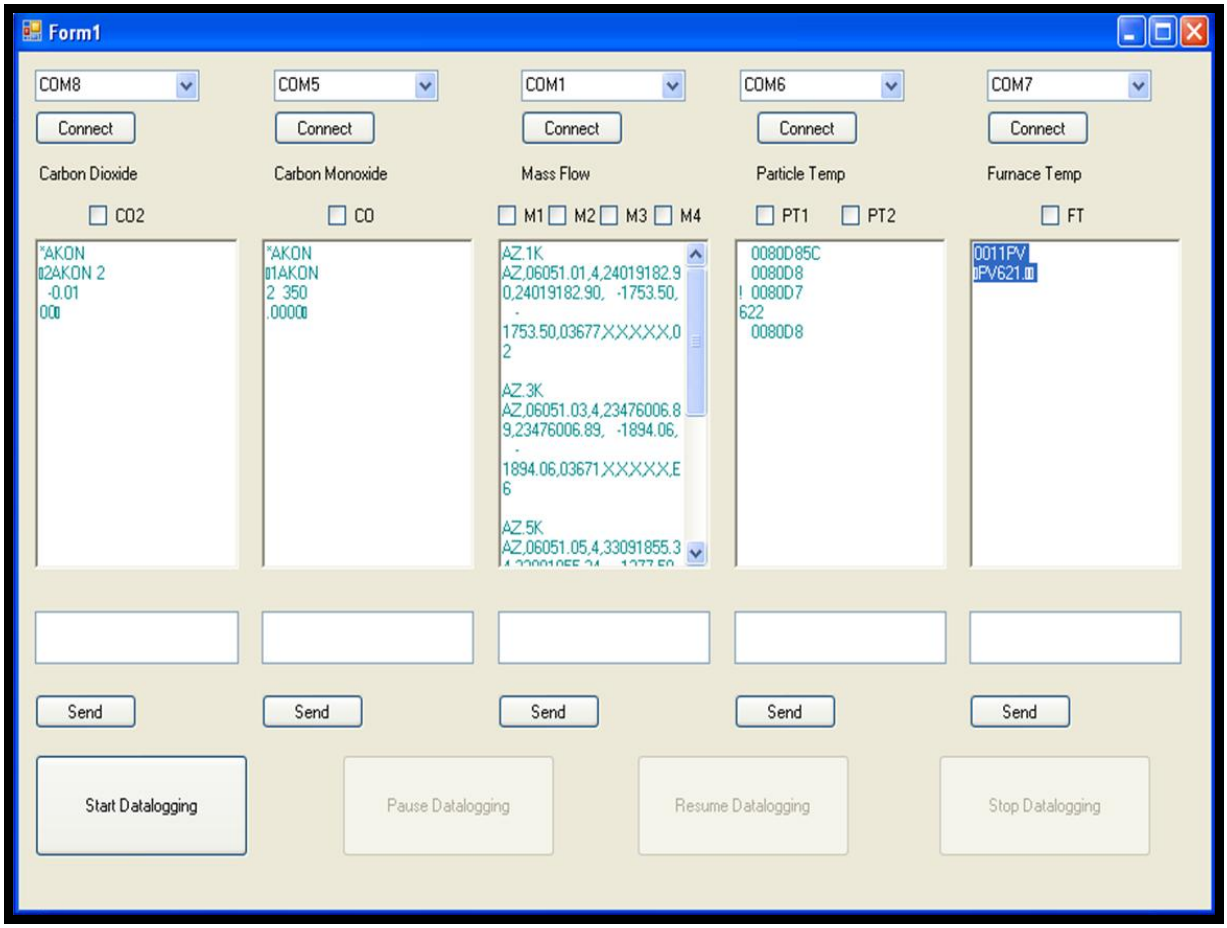

Figure 3.8: User interface for data acquisition

It can also be seen from this figure that the user was able to select which variables needed to be logged from the experimental setup. The variables selected to be logged were then collected by the software and written to Microsoft Excel® along with the date and a time stamp.

3.6. Combustion investigation procedures

3.6.1. Sample selection

In order to handpick the appropriate samples for this study the density of each individual particle had to be accurately determined. To accomplish this, random particles were chosen within the weight range for particles in the required density range. The theoretical required mass for 30 mm particles can be seen in Table 3.5. The theoretical mass of the particles was calculated using the theoretical spherical volume of the required particle size and the desired density needed for experimentation purposes.

Table 3.5: Mass calculation for 30 mm particles with different densities

Mass calculation				
Density (g/cm^3)	1.4	1.6	1.8	2.0
Mass (g)	19.79	22.62	25.45	28.27

The density of each particle was then calculated using the density measurement apparatus discussed in Section 3.4.4. The weight of each individual particle was then reduced to have an equivalent spherical diameter of 30 mm. This is done by chiselling off the protruding edges. The particles could then be charred with a known parent coal density.

The possible particles were inspected for any abnormalities, including extensive cracking, or clear rock like fragments that could influence the density. If any of these abnormalities were found to be present the particle was discarded.

3.6.2. Coal charring methods

The particles selected in Section 3.3 were then charred. To accomplish this the particles were, with the help of the bucket connected to the thermocouple, placed inside the horizontal tube furnace to a depth determined by constructing an accurate temperature profile over the length of the furnace. The particles were then charred at 1100°C under a nitrogen atmosphere. The particles were heated at 15°C/min to minimize particle breakage as a high heating rate leads to significant cracking of the larger particles. After the particles reached the required temperature, they were left for 45 minutes. The furnace was then turned off to allow the particles to cool down under a nitrogen atmosphere. As soon as the furnace temperature reaches 100°C the chars were removed and weighed. The nitrogen flow rate during charring was set to 5 Nl/min.

3.6.3. Combustion experiments

After the charring of the different particles was completed the charred particles were combusted. With the help of the bucket that is connected to the thermocouple, the charred particles were placed inside the furnace at the depth determined from the temperature profile. The particles were then heated to the required set temperature (1000 ˚C) at a heating rate of 15°C/min. When the particles reached the required temperature the particle was kept under nitrogen for an additional 20 minutes to ensure isothermal conditions in the particle. The gas feed was then changed to an air flow rate of 10 Nl/min so that the particle combustion could commence. Both the carbon dioxide and carbon monoxide production rate were recorded with the custom logging software. As soon as gas concentration reached no significant reading anymore, it is assumed that combustion was complete and the reactor was shut down and allowed to cool. As soon as the furnace temperature reached 100°C the remaining ash weight was measured.

3.7. Commissioning of experimental equipment

3.7.1. Gas production rate

For the combustion experiments, particles with different densities and sizes were heated and were then combusted in an air stream. As a means of measuring the degree of conversion of

the coal particle both the carbon dioxide and the carbon monoxide production rate were monitored. In general it was found that the carbon monoxide production rate was significantly lower than the carbon dioxide production rate. The carbon monoxide production yielded an initial concentration in the exhaust gas in the range of 80 to 120 ppm while the carbon dioxide concentration ranged from 3.5% (vol) to 6% (vol). The carbon conversion due to carbon monoxide production accounts for less than 0.01 % of the mass loss. Due to the low carbon monoxide production during combustion it was decided that the carbon monoxide production can be assumed to be negligible.

The low carbon monoxide production rate is supported by work done by Ragland and Yang (1985) who studied the oxidation behaviour of four different coals with gas temperatures ranging from 900-1200K and particle diameters ranging from 4 – 12mm. They found that carbon dioxide concentration in the effluent gas varied as the oxidation rate changed and that the observed carbon monoxide production rate was steady but also significantly lower than the production of carbon dioxide

3.7.2. Conversion of gas concentration data to mass loss data

The carbon conversion of the combusting particle was monitored throughout the investigation by measuring the concentration of carbon dioxide and carbon monoxide in the exhaust gas stream. The feed stream flow rate was controlled by the mass flow controllers to ensure that the flow rate of air passing the particle remained constant. As mentioned earlier, the carbon monoxide production rate was determined to be insignificant. Only the carbon dioxide concentration over time profile was therefore used to monitor carbon conversion. This carbon dioxide concentration over time profile was then used to calculate the mass loss due to carbon conversion. A typical carbon dioxide concentration over time graph for a 30 mm low density particle (density = 1.357 $g.cm^{-3}$) combusted at 1000 °C is shown in Figure 3.9. The graph in Figure 3.9 is constructed from the raw data collected from the gas analysers using the developed software and Microsoft Excel ®. The raw data for the individual experiments can be seen in APPENDIX C.

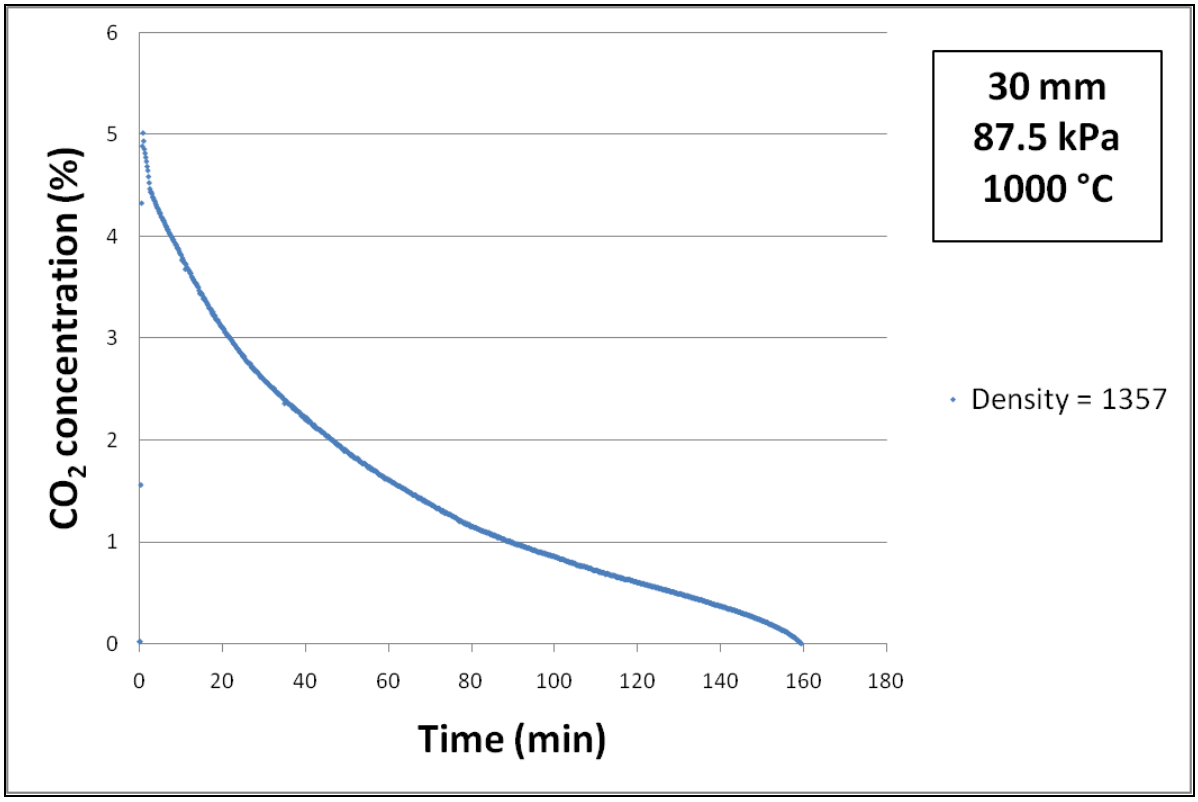

Figure 3.9: Typical carbon dioxide concentration over time profile

During the combustion experiments the air flow rate was set high enough to ensure that the carbon dioxide concentration remained within the detectable range of the carbon dioxide analyser. The gas analyser measured the concentration of the carbon dioxide as a volume percentage of the exhaust gas. Working under the assumption that one molecule of oxygen forms one molecule of carbon dioxide, the volume of gas entering the tube furnace was assumed to be the same as the volume of gas leaving the tube furnace. The developed logging software was set to measure the gas reading on the gas analyser every ten seconds. Using the carbon dioxide concentration readings, along with the known flow rate, the average volume of carbon dioxide in the exhaust stream was calculated at every ten second interval. This was done by transforming the analytic integral of the area under the concentration curve (Equation 3.1) into a numerical integration formula as can be seen in Equation 3.2.

$$ml\ CO_2 = \int_{t_0}^{tf} C_{CO_2} F_{Air}\, dt \tag{3.1}$$

$$ml\ CO_2 = \sum_{t=0}^{n} C_{CO_2} F_{Air}\, (t_2 - t_1) \tag{3.2}$$

The molar amount of carbon dioxide produced for every ten seconds was then calculated by using the ideal gas law to convert the volume of carbon dioxide produced for the ten second interval into the corresponding molar amount. By assuming that each mole of carbon dioxide produced corresponds to a mole of reacted carbon, the amount of reacted carbon was calculated by multiplying the molar amount of carbon dioxide by the molecular mass of carbon. This yields the mass of carbon that has reacted for every ten second interval. Cumulatively adding the amount of converted carbon from every ten second interval yielded the total amount of carbon converted during the combustion process.

3.8. Materials used

The coal sample used was a typical Highveld coal prepared according to the process described in Section 3.3. These samples were then charred at 1100 °C and combusted at 1000°C to determine their characteristics and combustion properties.

During the experimental methodology several gases were needed to achieve the experimental outcomes of this study as well as to setup and adequately operate the experimental equipment. These gases are shown in Table 3.6. All the required gases were supplied by Afrox (African Oxygen Limited).

Table 3.6: Gases used during the experimental methodology and their functions

Gas	Composition
Air	79 % Nitrogen, 21 % Oxygen
Carbon dioxide mixture	4 % Carbon dioxide, balance nitrogen
Carbon monoxide mixture	1 % Carbon monoxide, balance carbon dioxide
Nitrogen	Purity > 99.999 %

Several chemicals were used to perform the experimental methodology and to ensure that the experimental equipment functioned at an optimal level. These chemicals and their functions are listed in Table 3.7.

Table 3.7: The chemicals used during the experimental setup and their functions

Chemical	Function
Mercury	• Mercury was used to measure the density of the coal particles with the use of the developed density measuring equipment. Due to the hazards of working with mercury, all the experiments need to be done in a vacuum chamber.
Potassium bromide (KBr)	• Sodium bromide was used in conjunction with the FTIR analysis of the parent coal, as well as the chars. The sodium bromide was used to dilute the coal sample so that the sample doesn't fluoresce when being analyzed with the FTIR equipment
Soda lime granules	• Soda lime granules are used to remove residual carbon dioxide from the carbon dioxide analyser. These granules are initially light green and turn brown when they react with carbon dioxide

CHAPTER 4: RESULTS AND DISCUSSION: CHARACTERIZATION RESULTS

4.1. Introduction

This chapter contains the results obtained from characterization analysis done on the acquired coal samples. Section 4.2 examines the size and density distributions obtained for the prepared samples while Sections 4.3 and 4.4 discusses the results obtained from proximate and ultimate analyses respectively. Section 4.5 presents the calorific values for the various coal samples and Section 4.6 briefly presents the obtained petrographic results. Section 4.7 reports on the results obtained from sample characterization by means of FT-IR analysis. Finally, Section 4.8 summarises the findings obtained from the characterization of the coal samples.

4.2. Size and density distribution

The size and density distribution obtained from the initial sample preparation can be seen in Table 4.1. Each density fraction was separated into the various size fractions showing each size fraction as a weight percentage of that particular density fraction. From the Table it can be seen that the mass distribution concentrates between the +6.3 mm and the -53 mm particle size range as well as within the - 3.35 mm to + 0.5 mm range suggesting a type of bimodal distribution.

Table 4.1: Fractional size and density distribution of coal samples

	+53mm	-53mm +25mm	-25mm +12.5mm	-12.5mm +6.3mm	-6.3mm +3.35mm	-3.35mm +1mm	-1mm +0.5mm	Cumulative (%)
F 1.4	2.66	18.52	20.89	19.75	13.2	17.76	7.22	100
F 1.6	8.17	17.92	21.07	19.24	11.89	16.42	5.29	100
F 1.8	19.00	12.3	20.21	17.58	11.43	15.03	4.45	100
F 2.0	20.49	16.04	19.79	16.28	9.95	13.11	4.34	100
S 2.0	5.00	24.11	25.39	18.02	10.01	12.83	4.64	100

It can also be seen from Table 4.1 that, apart from the F 2.0 and F 1.8 fractions, the +53 mm content is relatively low when compared to the other size ranges. This indicates that the +53 mm size range tends toward the heavier densities. This can be due to a high mineral content in this size fraction which could make these particles more resistant to breakage. It is also interesting to note that the -6.3 mm to +3.35 mm size range is consistently lower over the whole density range. It was also observed that the S 2.0 density fractions consisted of flat shale like particles with a more greyish colour when compared to the more rounded shiny black F 1.4 density particles.

4.3. Proximate analysis

Proximate analysis results consist of the percentage of inherent moisture, ash content and volatile matter content determined according to the standard methods listed in Table 3.2. Due to the fact that the samples were both density and size separated, each individual analysis yields an array of results. The inherent moisture results can be seen in Figure 4.1. The inherent moisture is a result of the weight loss observed when the coal particles are heated to about 105 °C.

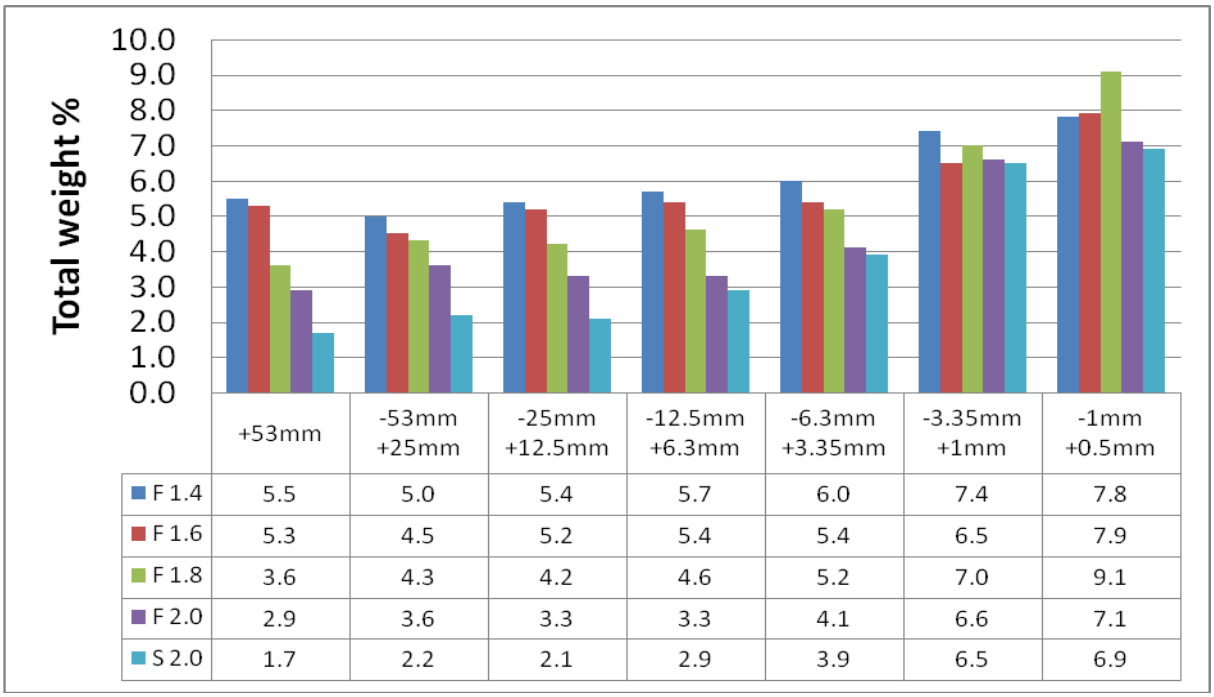

	+53mm	-53mm +25mm	-25mm +12.5mm	-12.5mm +6.3mm	-6.3mm +3.35mm	-3.35mm +1mm	-1mm +0.5mm
F 1.4	5.5	5.0	5.4	5.7	6.0	7.4	7.8
F 1.6	5.3	4.5	5.2	5.4	5.4	6.5	7.9
F 1.8	3.6	4.3	4.2	4.6	5.2	7.0	9.1
F 2.0	2.9	3.6	3.3	3.3	4.1	6.6	7.1
S 2.0	1.7	2.2	2.1	2.9	3.9	6.5	6.9

Figure 4.1: Inherent moisture analysis results (%) as received basis

From Figure 4.1 it can be seen that the lower density fractions have a higher inherent moisture content, and that the smaller particles contain more inherent moisture. It has been shown that the inherent moisture in coal can influence char yield and reactivity depending on the devolatilization conditions (Yi *et al*., 2007).

The volatile matter content analysis results can be seen in Figure 4.2. The volatile matter content also shows a decrease as the density increases. It also shows that there is no significant variation in the volatile matter content across the size range.

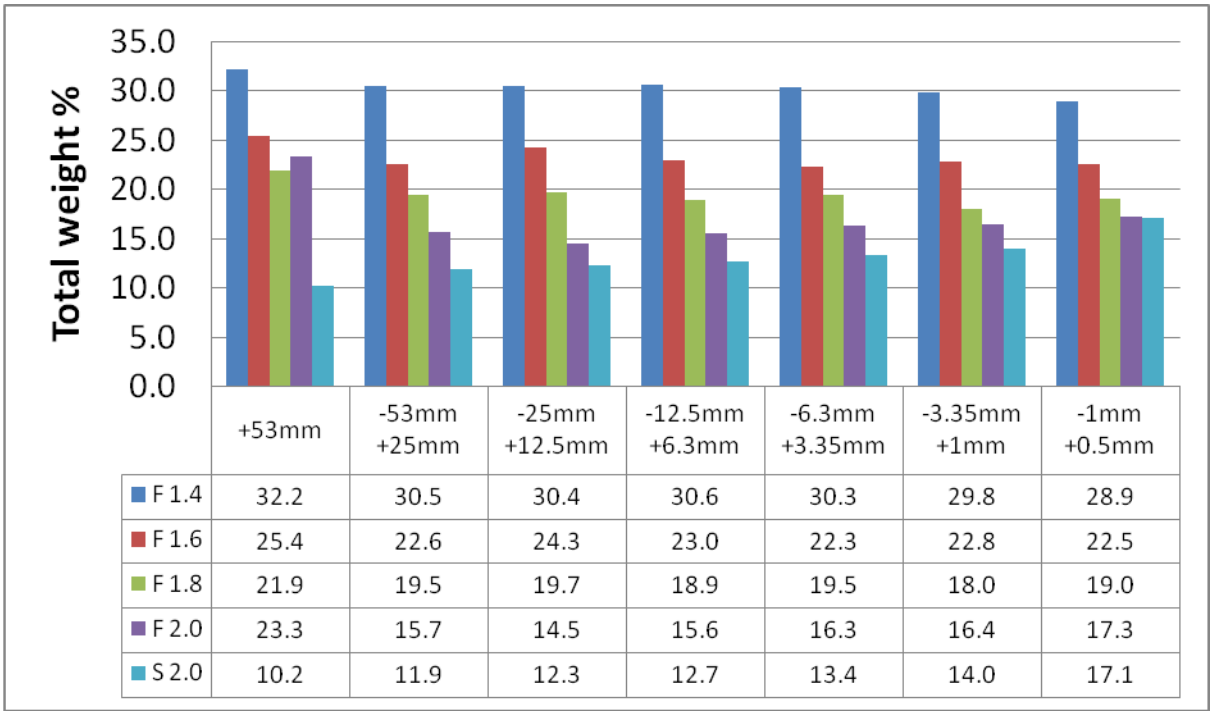

	+53mm	-53mm +25mm	-25mm +12.5mm	-12.5mm +6.3mm	-6.3mm +3.35mm	-3.35mm +1mm	-1mm +0.5mm
F 1.4	32.2	30.5	30.4	30.6	30.3	29.8	28.9
F 1.6	25.4	22.6	24.3	23.0	22.3	22.8	22.5
F 1.8	21.9	19.5	19.7	18.9	19.5	18.0	19.0
F 2.0	23.3	15.7	14.5	15.6	16.3	16.4	17.3
S 2.0	10.2	11.9	12.3	12.7	13.4	14.0	17.1

Figure 4.2: Volatile matter content analysis results (%) as received basis

The volatile matter content in coal is a collection of gases that evolve when the particle is heated to about 900 °C in an inert atmosphere. The individual components of volatile matter are hard to separate and quantify and are therefore all combined under the term ‘volatile matter’ (Schobert, 1990). Previous research has shown that the volatile matter decreases as the density increases (Strezov *et al*., 2005).

The ash content analysis results can be seen in Figure 4.3. The ash content of coal is indicative of the amount of minerals present in the parent coal.

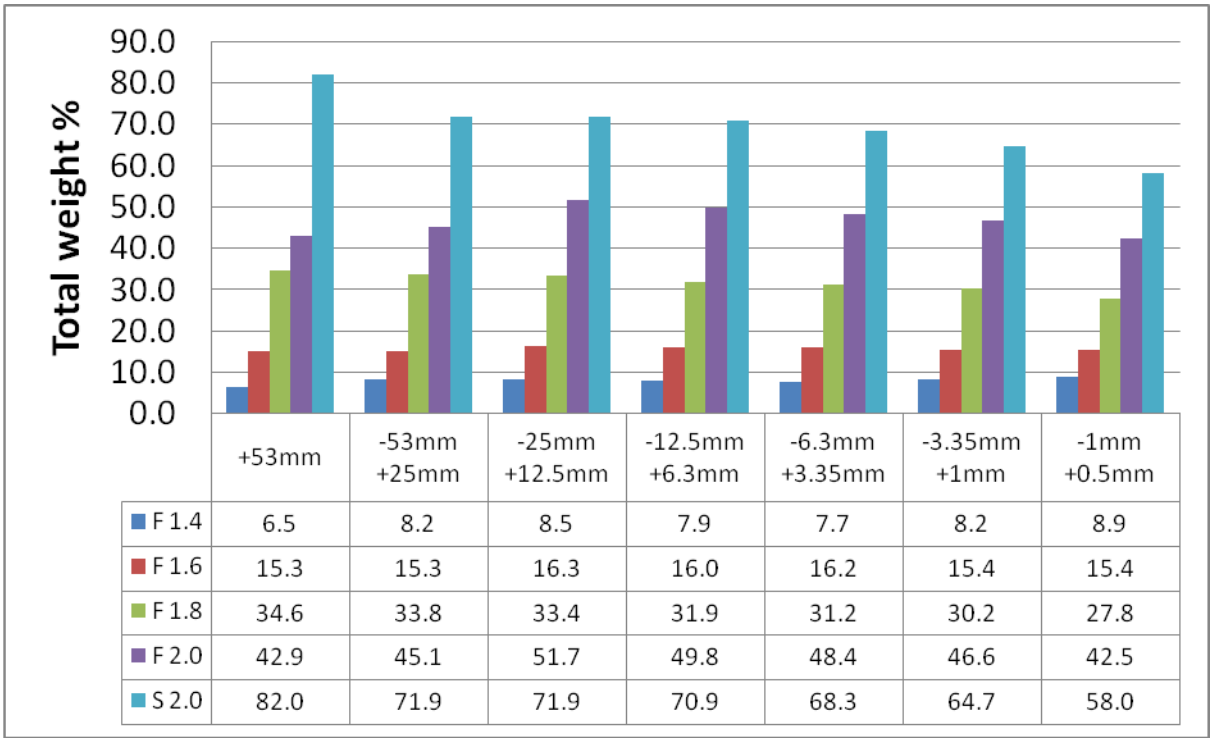

	+53mm	-53mm +25mm	-25mm +12.5mm	-12.5mm +6.3mm	-6.3mm +3.35mm	-3.35mm +1mm	-1mm +0.5mm
F 1.4	6.5	8.2	8.5	7.9	7.7	8.2	8.9
F 1.6	15.3	15.3	16.3	16.0	16.2	15.4	15.4
F 1.8	34.6	33.8	33.4	31.9	31.2	30.2	27.8
F 2.0	42.9	45.1	51.7	49.8	48.4	46.6	42.5
S 2.0	82.0	71.9	71.9	70.9	68.3	64.7	58.0

Figure 4.3: Ash content analysis results (%) as received basis

From Figure 4.3 it can be seen that the ash content increases significantly as the particle density fractions increase from -1.4 g.cm^{-3} to +2.0 g.cm^{-3} but that the ash content of the different size fractions remains relatively constant with the exception of the highest density fraction. The observed increase in ash content as the density increase has been noted by Strezov *et al.* (2005) and the relative consistency of ash content over the different size ranges has also been previously observed (Shannon *et al*., 2009). The resulting amount of ash is not necessarily equal to the original amount of mineral matter, as the ash represents the products formed from the high temperature reactions of the inorganic material. These reactions include the loss of water from clay like minerals, loss of carbon dioxide from mineral carbonates, conversion of pyrite to Fe_2O_3 and other oxides of sulphur (Riley, 2007)

The fixed carbon content analysis results can be seen in Figure 4.4. The fixed carbon content can be calculated by subtracting the moisture content, volatile matter content as well as the ash content from the original mass of the parent coal sample.

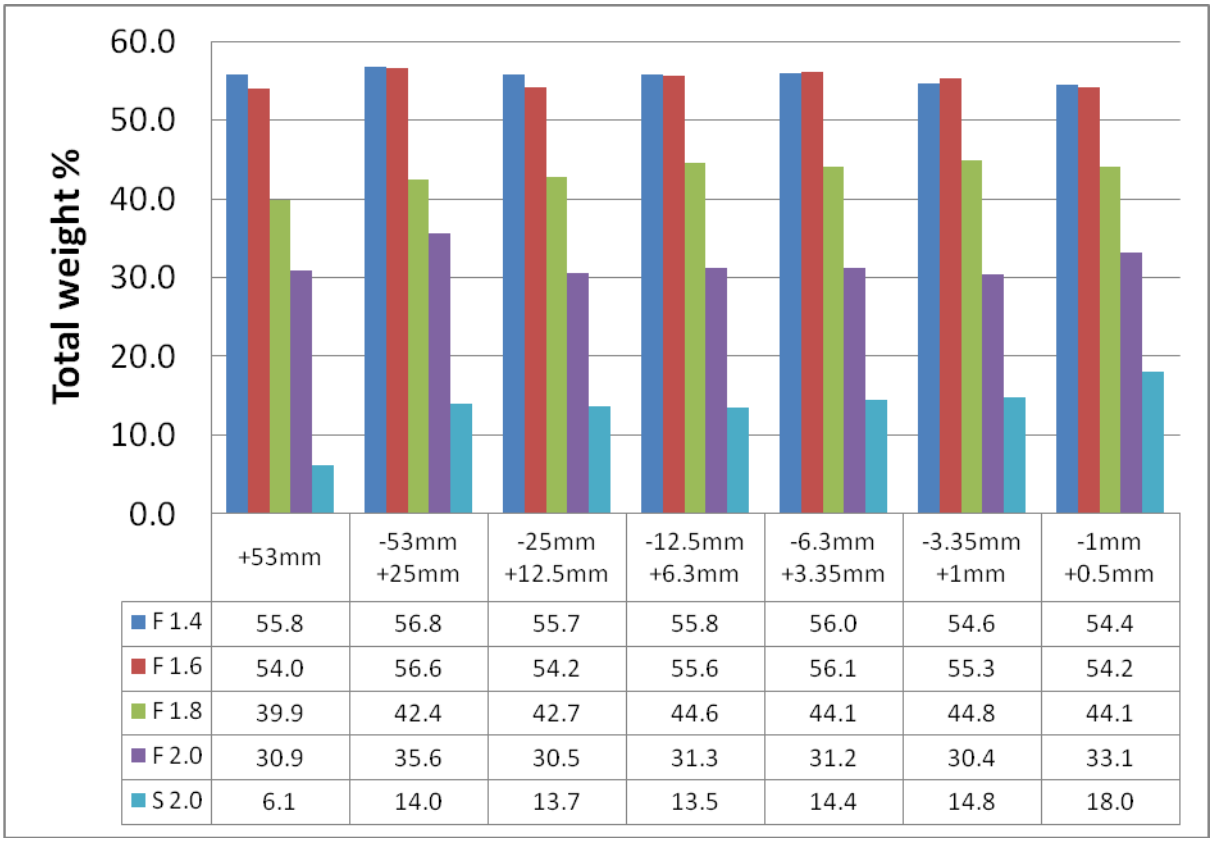

	+53mm	-53mm +25mm	-25mm +12.5mm	-12.5mm +6.3mm	-6.3mm +3.35mm	-3.35mm +1mm	-1mm +0.5mm
F 1.4	55.8	56.8	55.7	55.8	56.0	54.6	54.4
F 1.6	54.0	56.6	54.2	55.6	56.1	55.3	54.2
F 1.8	39.9	42.4	42.7	44.6	44.1	44.8	44.1
F 2.0	30.9	35.6	30.5	31.3	31.2	30.4	33.1
S 2.0	6.1	14.0	13.7	13.5	14.4	14.8	18.0

Figure 4.4: Fixed carbon content analysis results (%) as received basis

It can be seen from Figure 4.4 that the fixed carbon content decreases significantly as the density increases, and that the fixed carbon content remains relatively constant across the different size ranges. Work done by Strevoz *et al*. (2005) has also shown that the light densities have the same carbon content, but that the carbon content decreases significantly as the density increases to medium and high density fractions.

4.4. Ultimate analysis

For the ultimate analysis the percentage carbon, hydrogen, nitrogen and total sulphur were determined by the standard methods listed in Table 3.3. The ultimate analysis represents the elemental composition of the organic material in coal in terms of carbon, hydrogen, nitrogen, sulphur and oxygen (Riley, 2007)

The percentage carbon analysis results can be seen in Figure 4.5, which shows the total amount of carbon present in the parent coal sample. This includes the carbon present as

fixed carbon and the carbon present as volatile matter. All the carbon in coal occurs in combined form and can be present as very complex organic compounds or as mineral carbonates of which calcite is the most abundant component (Riley, 2007).

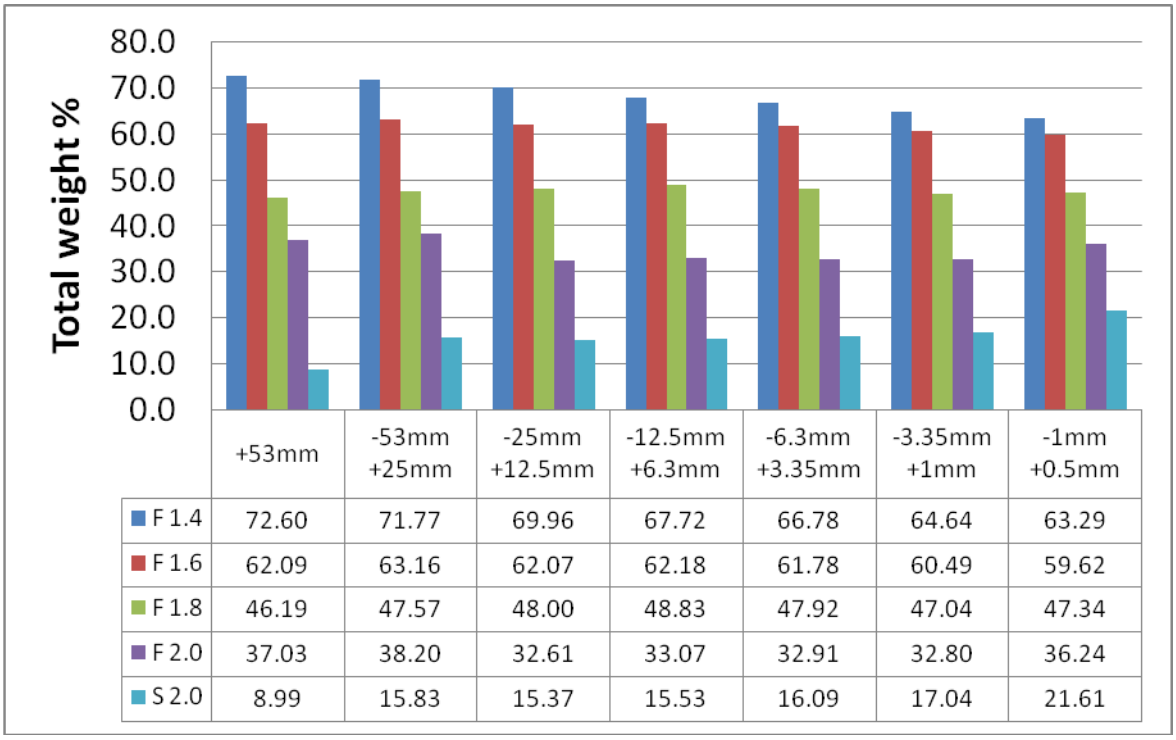

	+53mm	-53mm +25mm	-25mm +12.5mm	-12.5mm +6.3mm	-6.3mm +3.35mm	-3.35mm +1mm	-1mm +0.5mm
F 1.4	72.60	71.77	69.96	67.72	66.78	64.64	63.29
F 1.6	62.09	63.16	62.07	62.18	61.78	60.49	59.62
F 1.8	46.19	47.57	48.00	48.83	47.92	47.04	47.34
F 2.0	37.03	38.20	32.61	33.07	32.91	32.80	36.24
S 2.0	8.99	15.83	15.37	15.53	16.09	17.04	21.61

Figure 4.5: Carbon content analysis results (%) air dried basis

From Figure 4.5 it can be observed that the carbon content decreases significantly as the density increases and that the carbon content stays relatively constant over the size variation. This can be expected as the fixed carbon content and the volatile matter content showed similar trends.

The hydrogen content analysis results can be seen in Figure 4.6. All the hydrogen in coal occurs in combined form and can be part of very complex organic compounds (Riley, 2007).

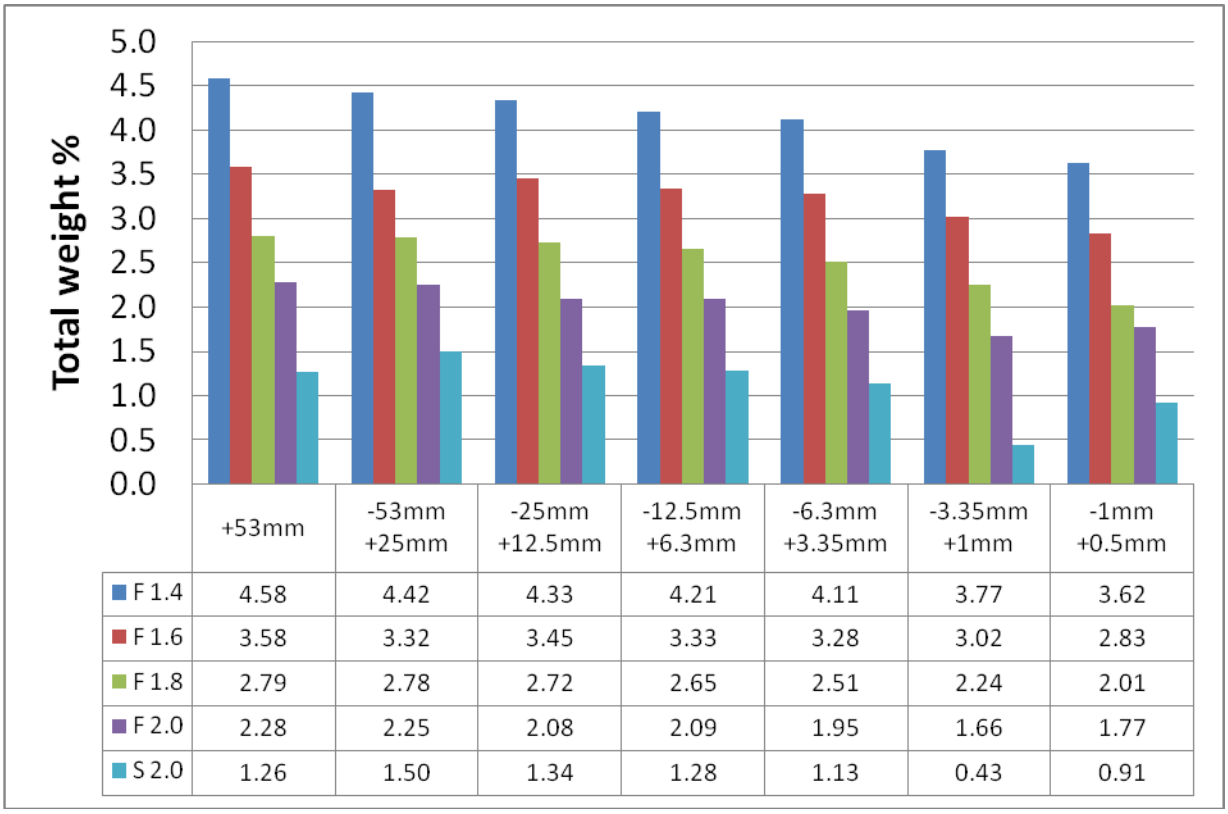

	+53mm	-53mm +25mm	-25mm +12.5mm	-12.5mm +6.3mm	-6.3mm +3.35mm	-3.35mm +1mm	-1mm +0.5mm
F 1.4	4.58	4.42	4.33	4.21	4.11	3.77	3.62
F 1.6	3.58	3.32	3.45	3.33	3.28	3.02	2.83
F 1.8	2.79	2.78	2.72	2.65	2.51	2.24	2.01
F 2.0	2.28	2.25	2.08	2.09	1.95	1.66	1.77
S 2.0	1.26	1.50	1.34	1.28	1.13	0.43	0.91

Figure 4.6: Hydrogen content analysis (%) air dried basis

As can be seen from Figure 4.6 the hydrogen content decreases as the density increases, but remains relatively constant over the size range with only slightly lower hydrogen content observed in the smaller particles.

The nitrogen content analysis results can be seen in Figure 4.7. The nitrogen content can be from either nitrogen containing volatile content (Nelson *et al*., 1991), or from nitrogen containing mineral content (Riley, 2007).

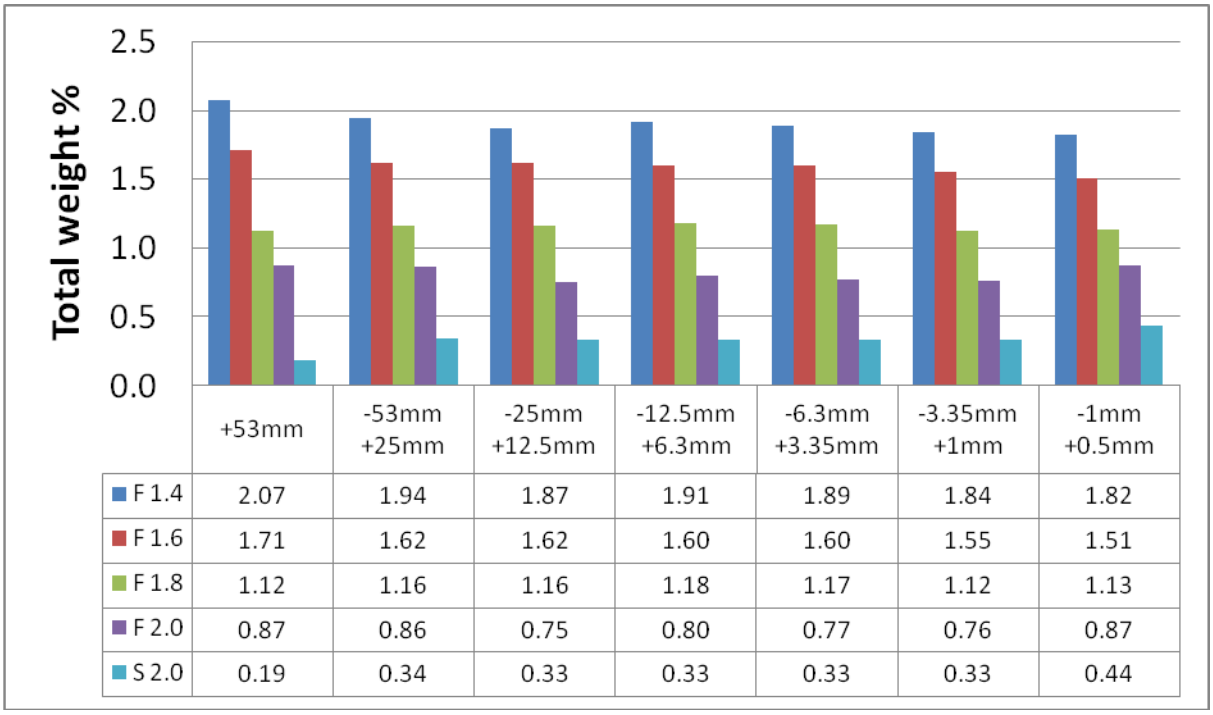

	+53mm	-53mm +25mm	-25mm +12.5mm	-12.5mm +6.3mm	-6.3mm +3.35mm	-3.35mm +1mm	-1mm +0.5mm
F 1.4	2.07	1.94	1.87	1.91	1.89	1.84	1.82
F 1.6	1.71	1.62	1.62	1.60	1.60	1.55	1.51
F 1.8	1.12	1.16	1.16	1.18	1.17	1.12	1.13
F 2.0	0.87	0.86	0.75	0.80	0.77	0.76	0.87
S 2.0	0.19	0.34	0.33	0.33	0.33	0.33	0.44

Figure 4.7: Nitrogen content analysis results (%) air dried basis

As with the hydrogen content the nitrogen content shows a significant decrease as the density increases, along with relatively little variation over the size range.

The total sulphur content analysis results can be seen in Figure 4.8. Sulphur is assumed to occur in three forms in coal: organic sulphur compounds; inorganic sulphides, which are mostly the iron sulphides, pyrite and marcasite; and as inorganic sulphates. The total sulphur value is used for ultimate analysis (Riley, 2007). The analysis done on the samples determines the total amount of sulphur making any predictions as to the origin of the sulphur inaccurate.

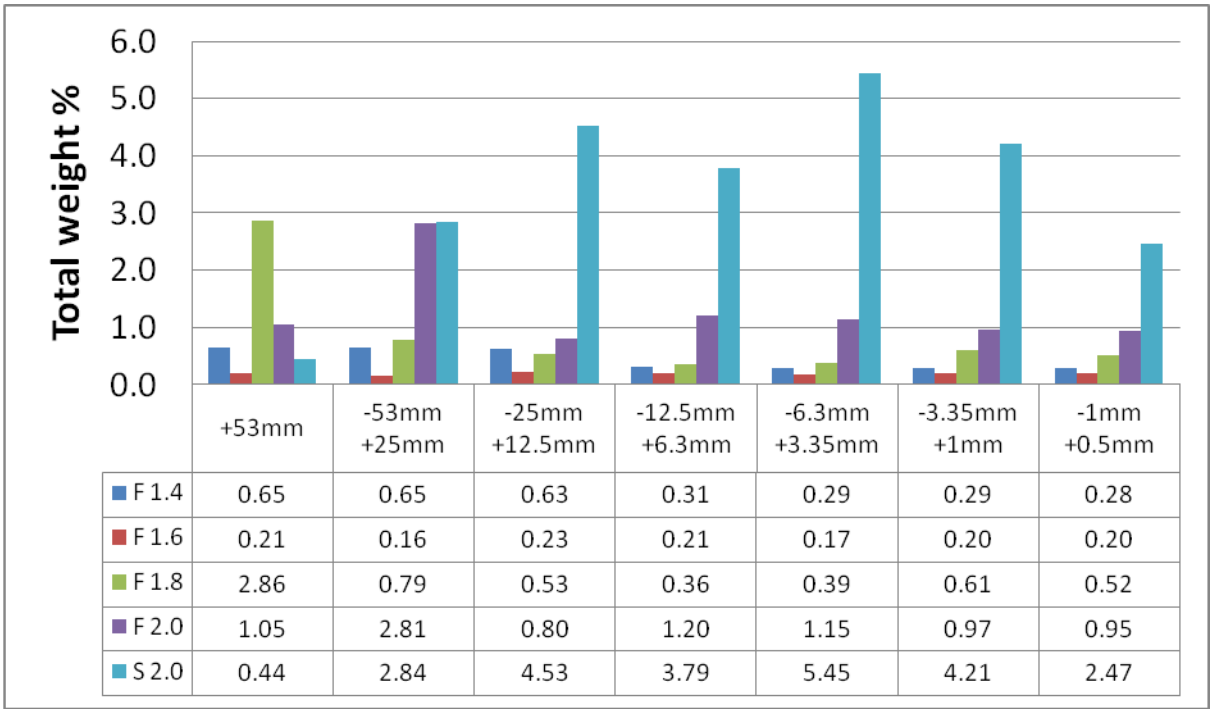

	+53mm	-53mm +25mm	-25mm +12.5mm	-12.5mm +6.3mm	-6.3mm +3.35mm	-3.35mm +1mm	-1mm +0.5mm
F 1.4	0.65	0.65	0.63	0.31	0.29	0.29	0.28
F 1.6	0.21	0.16	0.23	0.21	0.17	0.20	0.20
F 1.8	2.86	0.79	0.53	0.36	0.39	0.61	0.52
F 2.0	1.05	2.81	0.80	1.20	1.15	0.97	0.95
S 2.0	0.44	2.84	4.53	3.79	5.45	4.21	2.47

Figure 4.8: Sulphur content analysis results (%) air dried basis

Figure 4.8 shows no clear trend across the density ranges, but does however show that the sulphur content stays relatively constant across the size range. From the results it can also be seen that the high density particles contain significantly more sulphur when compared to the lower density particles. Previous work has shown that the highest density fractions in density separated samples tend to be enriched in pyrite and carbonates (Mendez *et al*., 2003). The higher pyrite concentrations in the high density fractions can be attributed as the source of the higher sulphur content in these fractions.

The oxygen content analysis results can be seen in Figure 4.9. The oxygen content includes the oxygen from oxygen-containing aliphatic groups, as well as oxygen released from the decomposition of mineral matter at the elevated temperatures of the analysis (Riley, 2007).

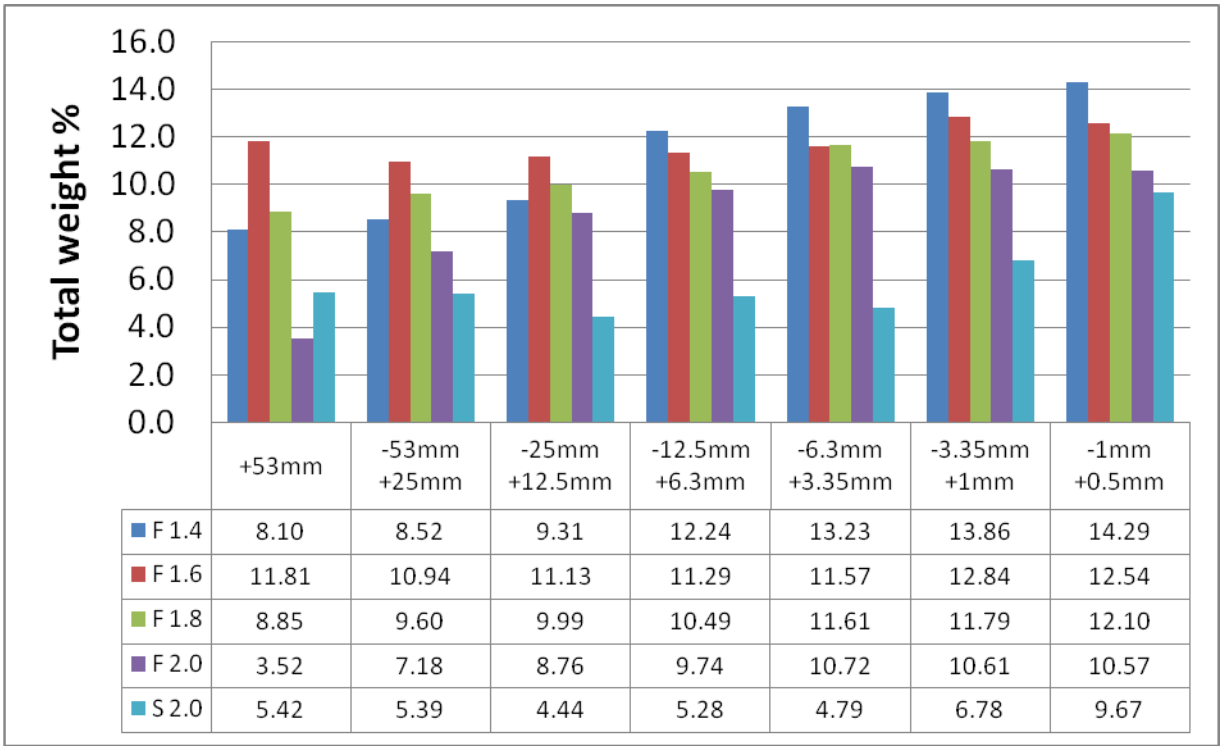

	+53mm	-53mm +25mm	-25mm +12.5mm	-12.5mm +6.3mm	-6.3mm +3.35mm	-3.35mm +1mm	-1mm +0.5mm
F 1.4	8.10	8.52	9.31	12.24	13.23	13.86	14.29
F 1.6	11.81	10.94	11.13	11.29	11.57	12.84	12.54
F 1.8	8.85	9.60	9.99	10.49	11.61	11.79	12.10
F 2.0	3.52	7.18	8.76	9.74	10.72	10.61	10.57
S 2.0	5.42	5.39	4.44	5.28	4.79	6.78	9.67

Figure 4.9: Oxygen content analysis results (%) air dried basis

From Figure 4.9 it can be seen that the lower density particles tend to have higher oxygen content when compared to the heavier densities. It was also observed that the smaller particles contain more oxygen than the larger particles. Research has shown that the smaller the particles are more prone to oxidation at room temperature. The higher oxygen content of the smaller particles may therefore be due to the fact that they oxidize more readily than the larger particles. This behaviour was explained by the particles' different surface-area-to-volume ratios. Initially the outer surface of the particle is attacked and oxidized and as the oxygen diffuses into the particle the rest of the particle can react (Tevrucht and Griffiths, 1989).

4.5. Calorific value analysis

A gross calorific value analysis was also done on the all of the samples. The calorific value analysis results can be seen in Figure 4.10. The calorific value of coal is used to define its energy content with respect to different requirements, *e.g*. defining its energy potential, determination of appropriate pricing and to properly design and operate thermal systems (Akkaya, 2009).

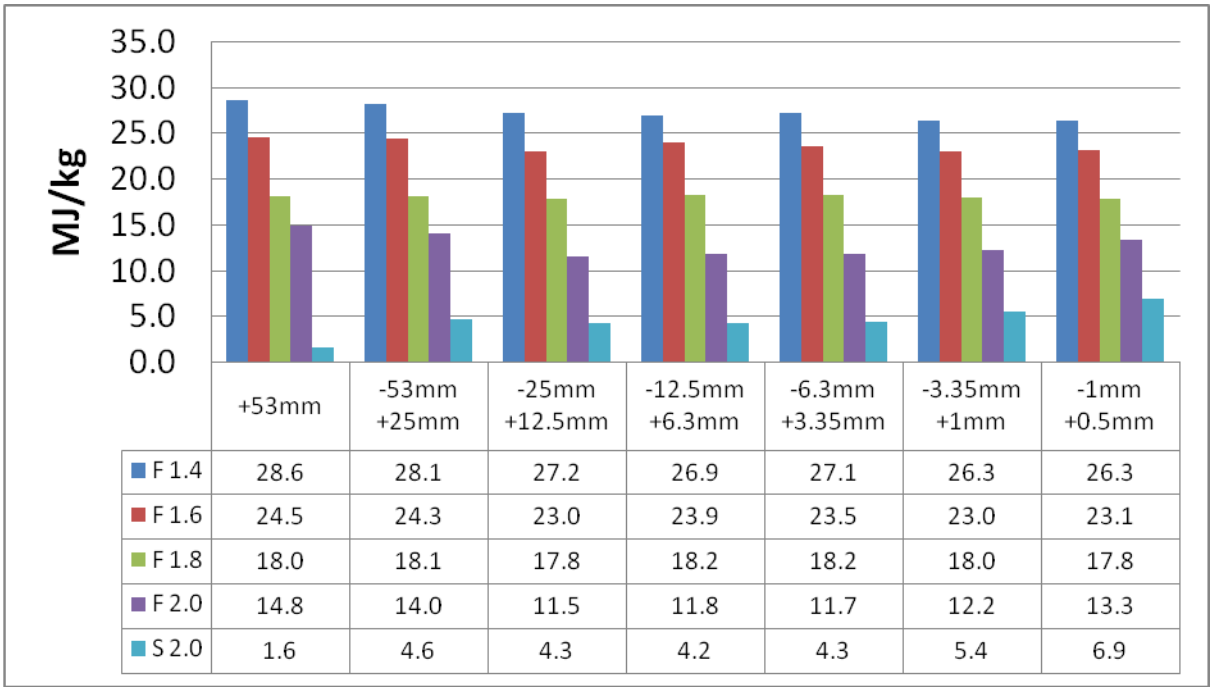

	+53mm	-53mm +25mm	-25mm +12.5mm	-12.5mm +6.3mm	-6.3mm +3.35mm	-3.35mm +1mm	-1mm +0.5mm
F 1.4	28.6	28.1	27.2	26.9	27.1	26.3	26.3
F 1.6	24.5	24.3	23.0	23.9	23.5	23.0	23.1
F 1.8	18.0	18.1	17.8	18.2	18.2	18.0	17.8
F 2.0	14.8	14.0	11.5	11.8	11.7	12.2	13.3
S 2.0	1.6	4.6	4.3	4.2	4.3	5.4	6.9

Figure 4.10: Gross calorific value analysis results (MJ/kg)

The calorific values obtained for the samples shows a similar trend to that of the carbon content analysis. This is to be expected as the caloric value is an indication of the energy of combustion of the carbon content. From the results shown in Figure 4.10 it can be observed that the calorific values of the highest density particles is significantly less when compared to the other lower density particles. This has the implication that the value of the coal can be greatly improved if the coal is beneficiated to remove the heaviest fraction, however this improvement will also increase the amount of discard.

4.6. Petrographic analysis

The petrographic analysis results of the same Highveld coal with identical density cuts are obtained from Koekemoer (2009) and are shown in Table 4.2 representing work done on 1mm particles.

Table 4.2: Maceral content of density fractions (Mineral matter free, based on volume %) (Koekemoer, 2009)

Maceral group	S 2.0	F 2.0	F 1.8	F 1.6	F 1.4
Vitrinite	18.2	8.4	5.2	9.4	34.7
Liptinite	0	2.3	4.3	7.0	6.3
Reactive SF	4.5	5.1	0.8	5.3	4.8
Inert SF	13.6	11.2	21.7	39.2	35.8
Fusinite	0	2.3	1.9	0.2	1.9
Micrinite	0	3.3	1.4	1.7	2.5
Reactive Inerto	0	1.9	0.8	1.7	0.6
Inert Inerto	63.6	65.4	63.9	35.4	13.3
Total inertinite	81.8	89.3	90.5	83.6	58.9

Inerto: Inertodetrinite, SF: Semi-fusinite

Inertinite is the most abundant maceral in all the density fractions followed by vitrinite, with very little liptinite content present in the various density fractions. The maceral content of the different density fractions shows an increase of total inertinite content from fraction S 2.0 – F1.8 which then decreases from fraction F1.6 – F 1.4. The vitrinite content for the different density fractions shows the opposite trend to that of the inertinite content, showing a decrease from fraction S 2.0 – F1.8, followed by an increase in the last two fractions. The lowest density fraction (F1.4) contains the most vitrinite, almost double the amount of the next highest vitrinite content.

4.7. FTIR analysis

Diffuse reflectance Fourier transform infrared (DRIFT) spectra were obtained for selected samples with a low, medium and high density (Figure 4.11 - Figure 4.13). The influence of each density was investigated over three different size ranges. The influence of different particle size ranges was also investigated with each size range being investigated over three different densities (Figure 4.14 - Figure 4.16). Drift spectra have a flat baseline when compared to the sloping baseline in KBr pellet spectra, and with its well-resolved bands it is the preferred spectra for qualitative analysis. Qualitative interpretation of the DRIFT spectra were based on work done by Fuller *et al*. (1982), Machnikowska *et al*. (2002) and Painter *et al*. (1981).

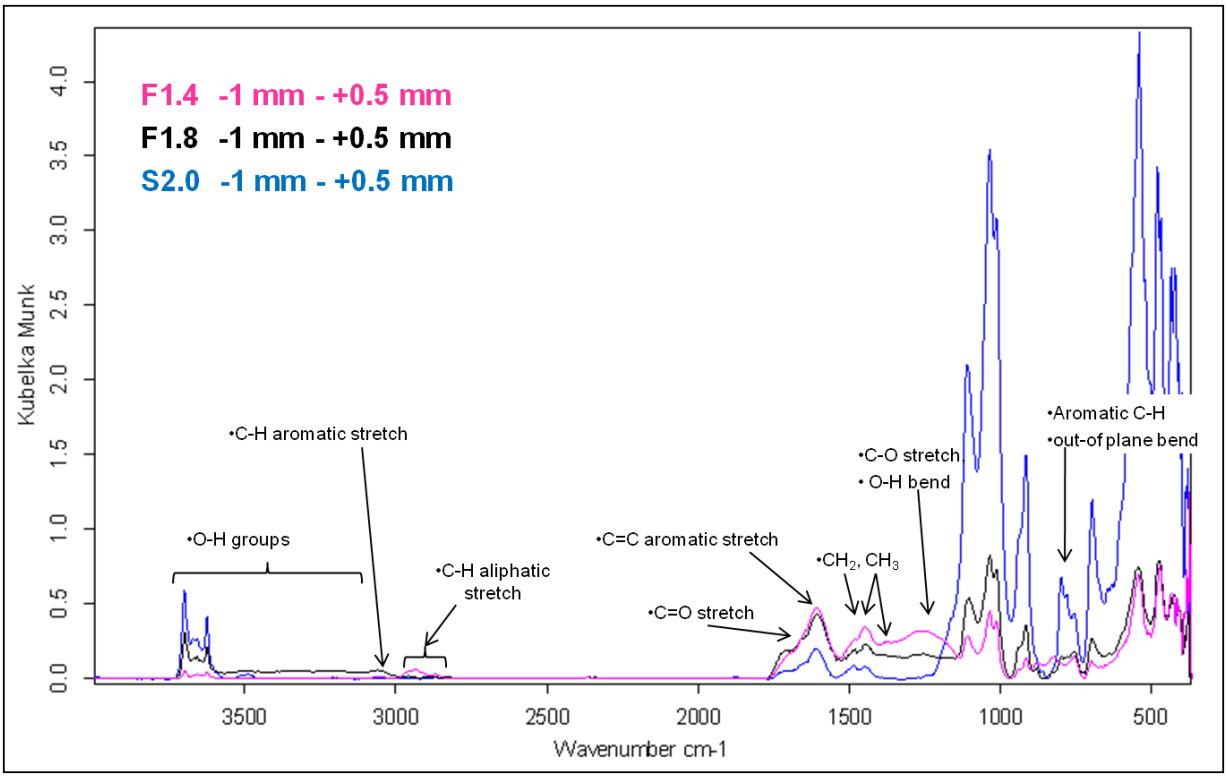

Figure 4.11: Drift spectra and peak assignments for small particles with different densities

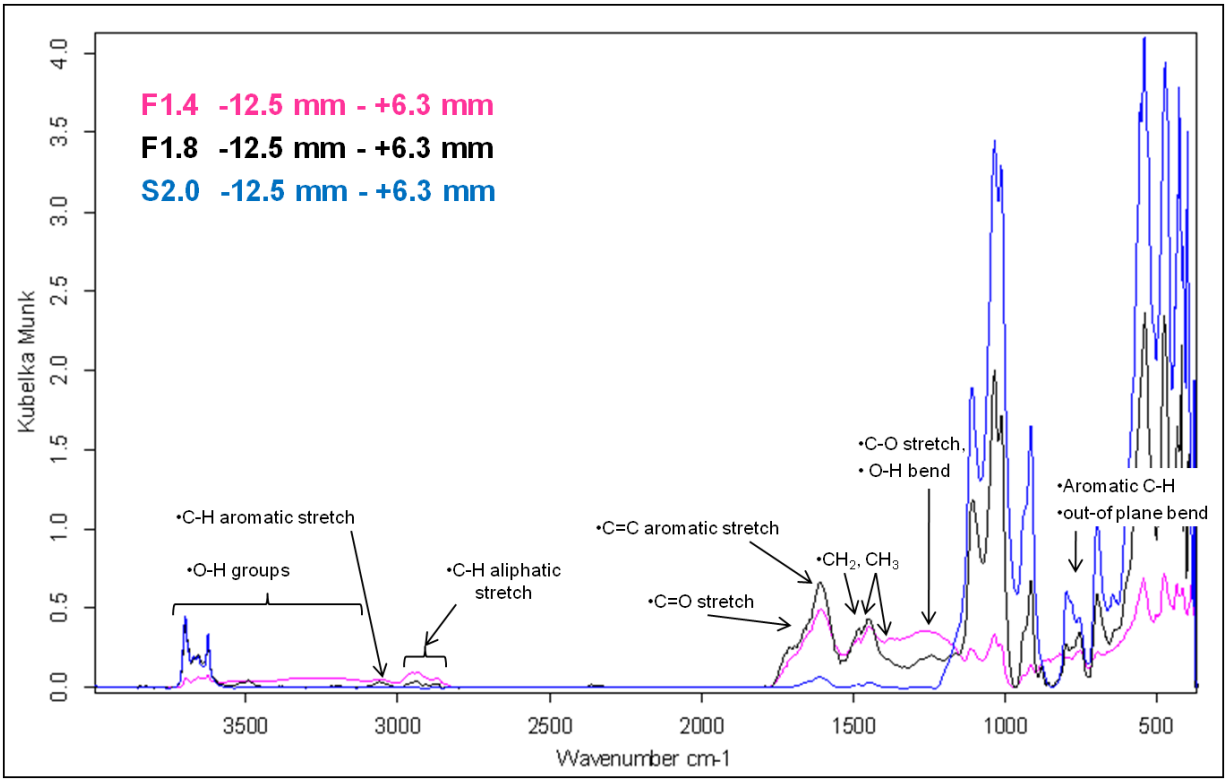

Figure 4.12: Drift spectra and peak assignments for medium particles with different densities

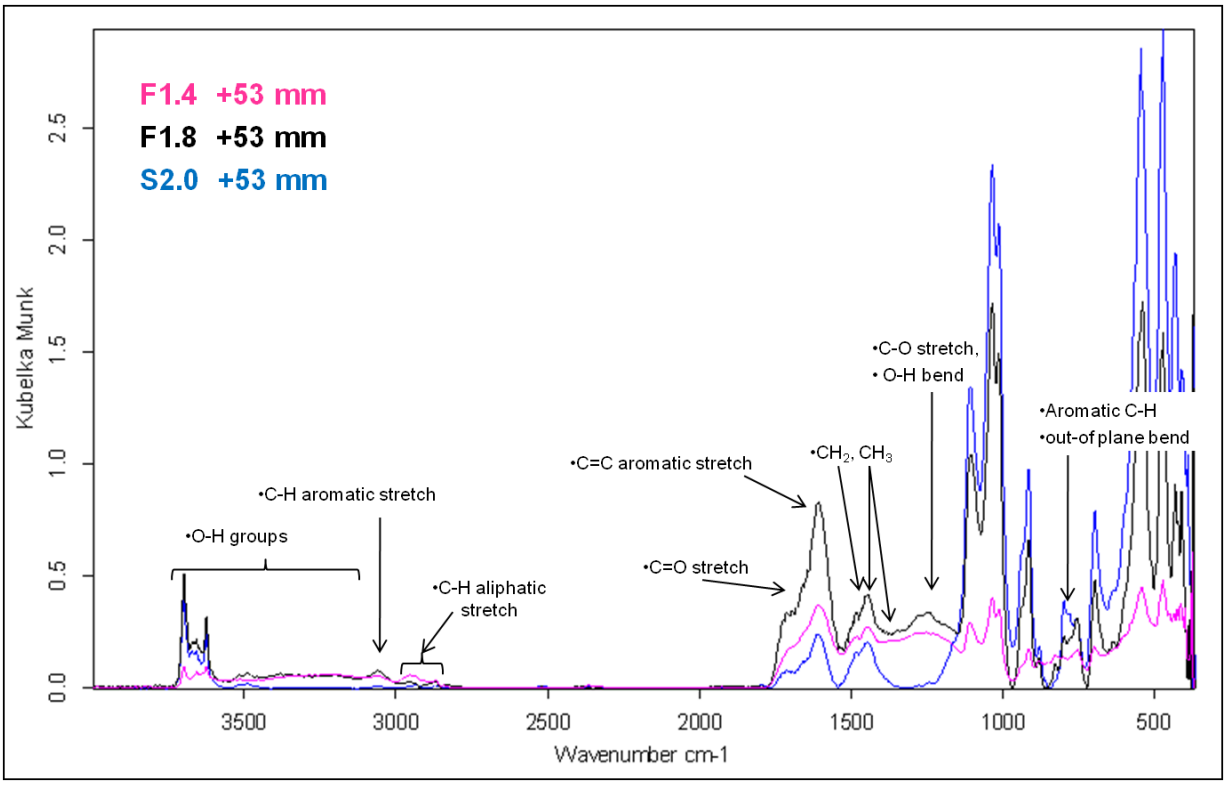

Figure 4.13: Drift spectra and peak assignments for large particles with different densities

The spectra for the different densities (Figure 4.11 - Figure 4.13) contained aliphatic (3000 to 2800 cm^{-1}) and aromatic (3100 to 3000 cm^{-1}) C-H stretching modes. The aliphatic stretching mode is more prominent in the lowest density fraction and consists of three different peaks. The 2950 cm^{-1} shoulder peak was assigned to asymmetric CH_3 vibrations, 2920 cm^{-1} to asymmetric CH_2 vibrations and 2850 cm^{-1} to symmetric CH_2 and CH_3 vibrations. The 1600 cm^{-1} band was assigned to the C=C stretching vibrations of aromatic rings (Painter *et al*., (1981), Painter *et al.* (1983)). The C=C stretch vibration peak intensity was consistently the lowest for the high density particles while the medium density particles had the most prominent C=C stretch vibration peak intensity. The shoulder peak observed on the left-hand side of the C=C stretching vibration was assigned to C=O stretching. The C=O stretch mode for the three densities was well defined and showed two C=O stretching shoulders (~1650 cm^{-1} and ~1730 cm^{-1}). This suggests that various types of C=O groups (esters, ketones, aldehyde or –COOH or a combination of these groups) may be present. A CH_2 and CH_3 band vibration (1450 cm^{-1}) was also observed in the spectra, but with weak intensities in the high density particles. Strong intensity bands were observed in the 1300 to 1110 cm^{-1} region and were assigned to ether groups, and to C-O stretch and O-H bending vibrations in phenoxy structures. It was found that this region was more prominent in the high density fractions, followed by the medium density fractions with the low density fraction having the

smallest peaks. Out-of-plane aromatic C-H vibration modes were observed in the 900 to 700 cm^{-1} region. The difference in intensity of these peaks (860 cm^{-1}, 815 cm^{-1} and 750 cm^{-1}) indicated coal particles of different densities have very different substitution patterns in their aromatic structures.

The regions between 3700 cm^{-1} and 3100 cm^{-1} were assigned to O-H stretching vibrations and are due to free OH groups and associated OH groups (hydrogen bonding due to OH). Infrared spectroscopy can provide information regarding the type of hydrogen bonding present in coal which is not possible with other spectroscopic methods (Chen *et al*., 1998).(Li *et al*., 2003). The interpretation of the O-H stretching region can be obscured by moisture and mineral matter contributions to these peaks. (Machnikowska *et al*., 2002) (Chen *et al*., 1998). The types of associated OH groups that may be present are: free OH groups (3611 cm^{-1}); OH—π hydrogen bonds (3516 cm^{-1}); self associated OH-OH bonds (3400 cm^{-1}); OH—ether hydrogen bonds (3300 cm^{-1}); cyclic OH groups (3200 cm^{-1}); and OH—N acid/base structures (3100 – 2800 cm^{-1}) (Machnikowska *et al*., 2002) (Li *et al*., 2003) (Painter *et al*., 1987). Strong peaks were observed in the 3700 cm^{-1} – 3600 cm^{-1} region which was most likely contributed by free OH groups and OH-π hydrogen bonds. The rest of the region (3500 cm^{-1} – 3100 cm^{-1}) was assigned to a combination of the various hydrogen bonds.

The spectra for the different particle size ranges with the same density are given in Figure 4.14 - Figure 4.16. Each figure shows the particle size ranges on different axes otherwise the individual spectra cannot be adequately distinguished.

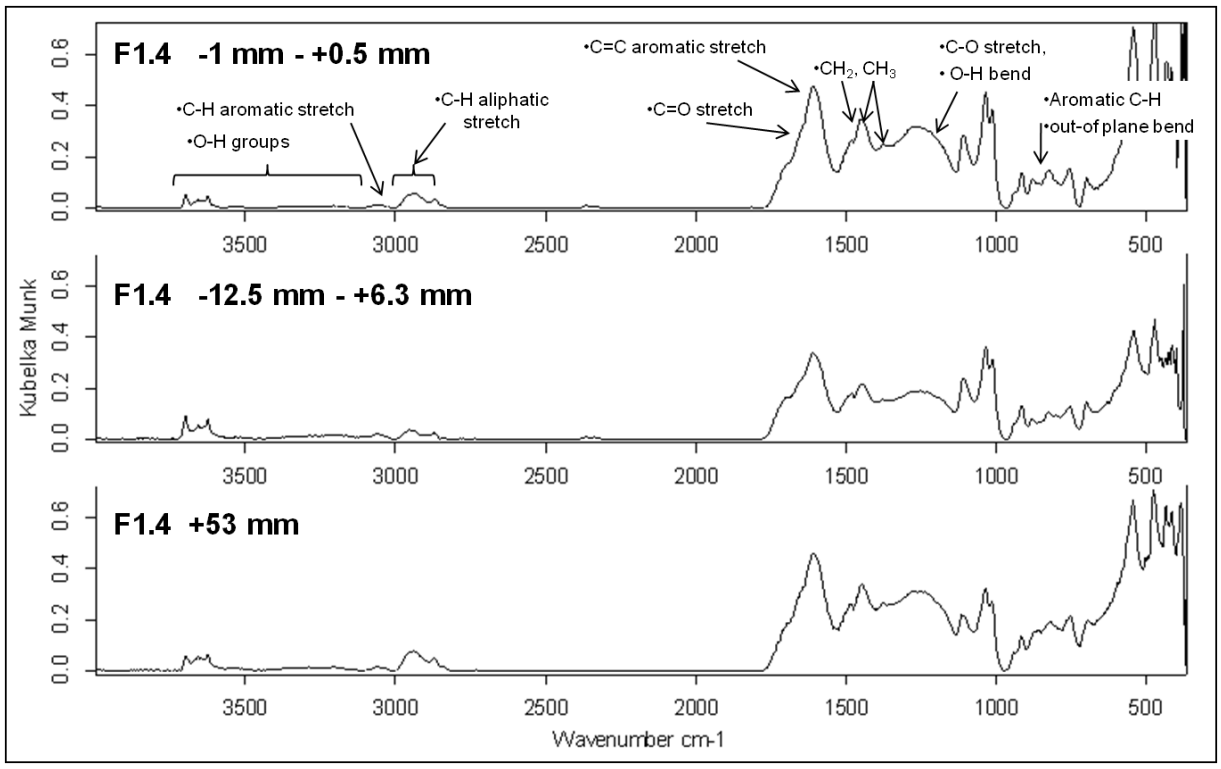

Figure 4.14: Drift spectra and peak assignments for different particle ranges with a low density

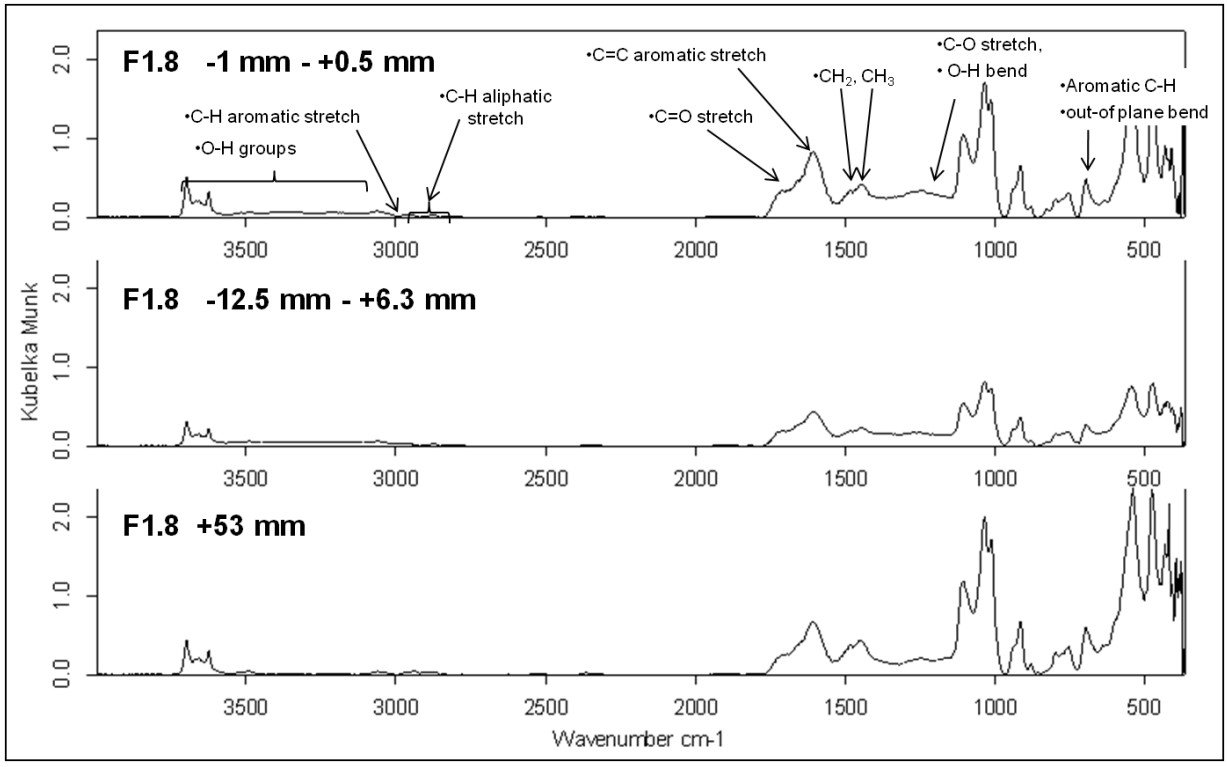

Figure 4.15: Drift spectra and peak assignments for different particle ranges with a medium density

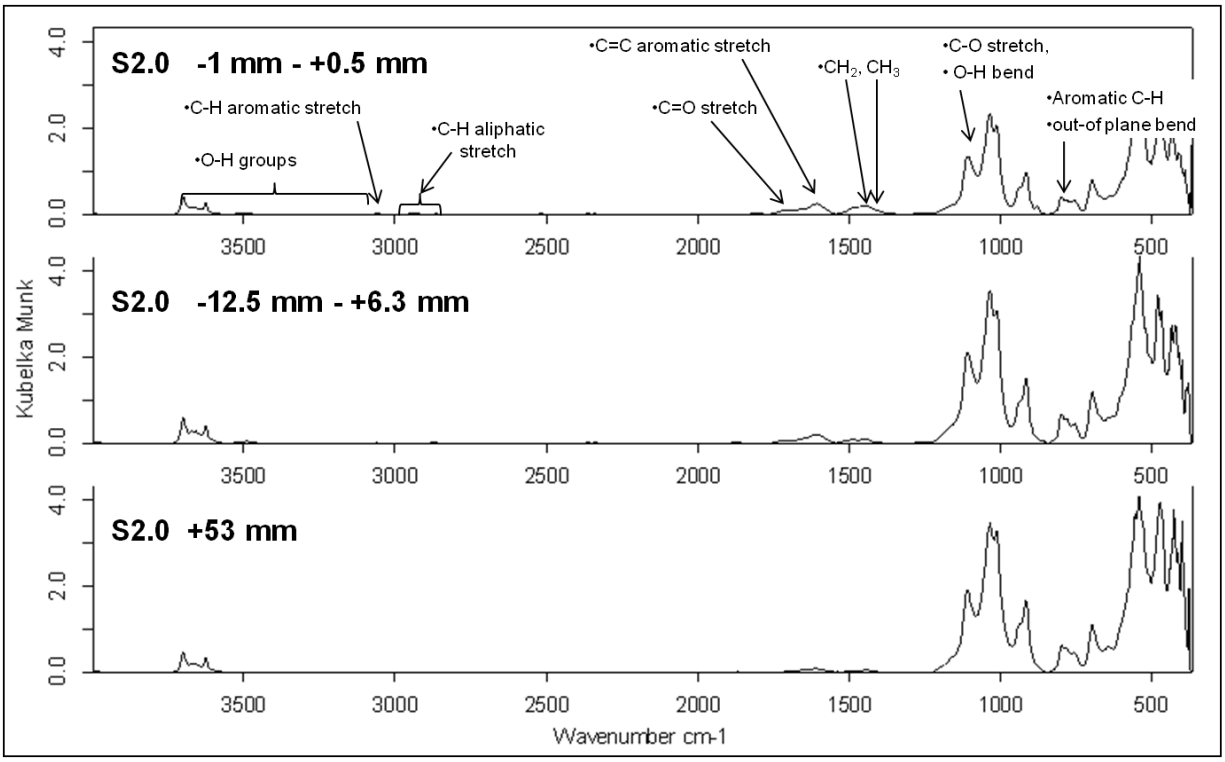

Figure 4.16: Drift spectra and peak assignments for different particle ranges with a high density

The spectra as depicted in Figure 4.14 - Figure 4.16 show the various peak assignments made for the individual peaks that were discussed previously. When the spectra for the different size ranges with a constant density are compared, it can be seen that there is no significant difference in the FTIR properties when the particle size range changes from small to medium to large particles. The most prominent feature is that the peaks and their intensities in the 900 cm $^{-1}$ to 700 cm^{-1} region do not change as the particle size range changes. This suggests that the substitution patterns of the aromatic structures are similar for all the different particle sizes.

Drift spectra were obtained for char particles with different densities created at 1100 °C and are presented in Figure 4.17. When compared to the parent coal particles the intensities of the peaks for the char particles are very weak. The weak spectra were enhanced by removing the 600 to 400 cm^{-1} region that showed very strong intensities that were mainly contributed by the mineral content present in the char particles.

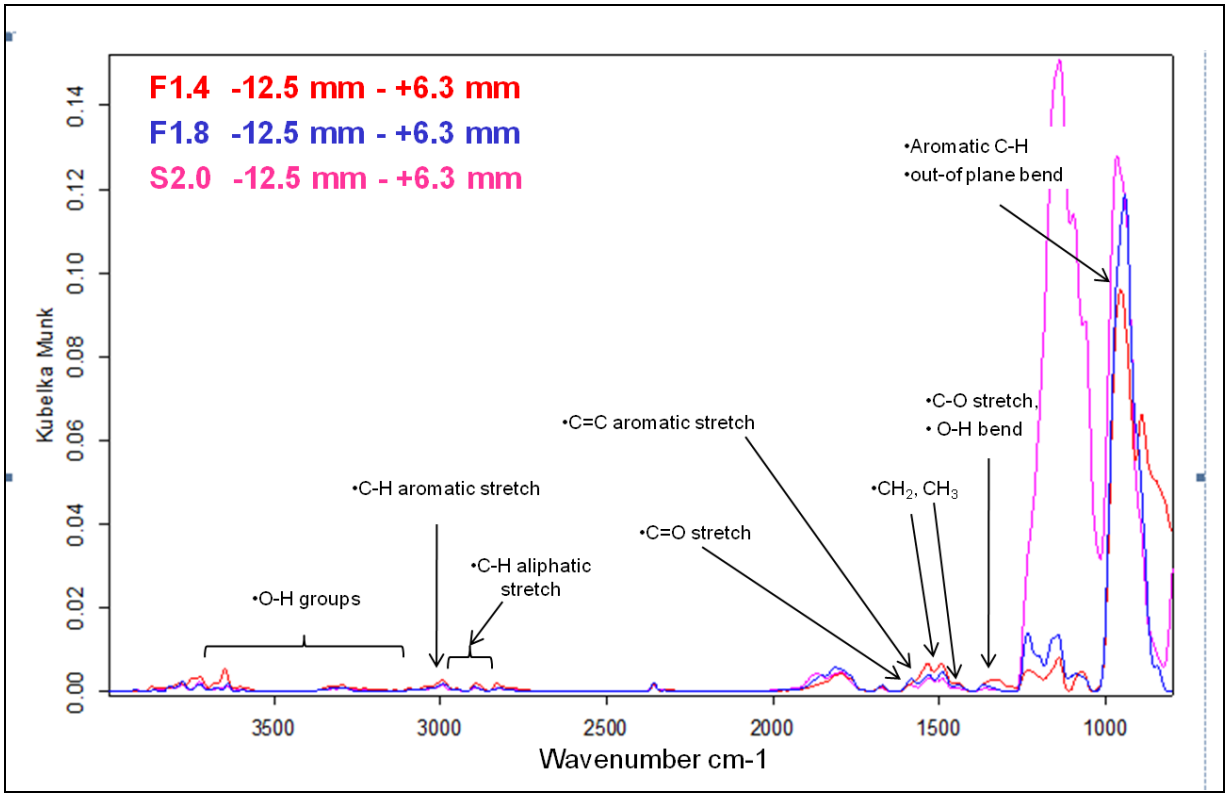

Figure 4.17: Drift spectra and peak assignments for char particles of different densities

Apart from the weak intensities it can be observed that the lowest density fraction has the strongest CH_2 and CH_3 bend vibration peak (1450 cm^{-1}), followed respectively by the medium and high density char particles. While the out-of-plane aromatic C-H vibration modes (900 cm^{-1} to 700cm^{-1}) for the parent coal samples consisted of three peaks (860 cm^{-1}, 815 cm^{-1} and 750 cm^{-1}), the lowest density char samples were observed to have only two peaks, with the medium and high density chars having only one peak. This suggests that the substitution patterns of the aromatic structures are considerably more similar than in the case of the parent coal samples. The most significant observation from the FTIR analysis conducted on the different density char particles is that the different density char particles are chemically more similar after charring than prior to charring.

4.8. Summary

The original Highveld coal sample was separated into various coal samples with different density and size ranges. These coal samples were characterized using proximate analysis, ultimate analysis, calorific value analysis and FTIR analysis to determine the characteristic

difference occurring due to different particle densities as well as different sizes. It was observed that the high density particles tended to be greyish and more shale like in nature when compared to the shinier black rounded low density particles. The inherent moisture content present in the coal particles decreased as the density increased and tended to be higher in the smaller particle ranges. The volatile matter and fixed carbon content also decreased as the density of the particles increased but showed a relatively even distribution across the different particle size ranges. As expected, the ash content present in the coal samples significantly increased as the particle densities increased. From the ultimate analysis it was found that the carbon, hydrogen and nitrogen content in the coal particles decreased as the density increased with a relatively even distribution across the size ranges. Very high sulphur content values were observed for the high density particles, while it was found that the smaller particles tended to contain a higher amount of oxygen. The main finding with regards to the calorific analysis was that the high density particles have a very low heating value, and that the overall coal sample value would be improved by removing the high density particles.

Petrographic analysis obtained from Koekemoer (2009) showed that inertinite is the most abundant maceral followed by vitrinite, and that there is very little liptinite present in the samples. It also showed that the lowest density fractions (F 1.4) contain the most vitrinite, almost twice the amount present in the sample with the next highest vitrinite content.

FTIR spectra showed that density separated coal particles differ significantly, and that these different density particles have different aromatic structure substitution patterns. It further showed that the properties of size separated coal particles tend to have similar FTIR characteristics. FTIR analysis conducted on char particles created at 1100 °C suggested that char particles created from particles with different parent coal densities tend to become chemically more similar after charring. It was also found that the aromatic structure substitution patterns become more similar due to charring of the coal particles.

The characterization of the different coal samples has shown that all the parameters were significantly different for the different density fractions, but did not vary as significantly across the particle size ranges.

CHAPTER 5: RESULTS AND DISCUSSION: COMBUSTION PERFORMANCE

5.1. Introduction

This chapter discusses the combustion performance of single coal particles with different densities and sizes. Section 5.2 presents visual observations of the combustion behaviour of large single coal particles and covers aspects such as the shattering of the single coal particles and the visual observations made regarding the resulting ash and ash characteristics when considering the influence of parameters like particle size and density. This section also presents the shrinking core behaviour that has been observed for the large particles. Section 5.3 examines the quantitative combustion conversion results as a function of particle density and particle size. Section 5.4 gives a summary of the results and observations obtained from the combustion performance of single coal particles.

5.2. Visual observations of single particle coal combustion

5.2.1. Shattering of coal particles

While heating the coal particles for devolatilization it was observed that the 30 mm particles tended to fragment at a heating rate of 50 °C/min, less shattering was observed at a heating rate of 25 °C/min, while only the medium to high density (1.6 – 2.0 g/cm^3) particles tended to shatter at the lower heating rate. At a heating rate of 15 °C/min, very little particle shattering was observed and this heating rate was consequently used for all the experimental work. It was found that the shattering of the particles was accompanied with extensive cracking. Primary fragmentation usually occurs during devolatilization, and is caused by thermal stress as the internal pressure is built up by the volatile matter in the porous network (Stubington and Moss, 1995). At the higher heating rate the pressure inside the particle will build up faster, resulting in more primary fragmentation. The higher density fractions might have a denser pore network, which might prevent the evolved gases from escaping the particle, leading to a pressure build up and primary shattering.

After the particles were heated and devolatilized the particles were cooled in a nitrogen atmosphere and then weighed to determine the mass loss that occurred due to the release

of volatiles. The particle was then placed back inside the tube furnace, and was then heated to the required combustion temperature. It was observed that none of the coal particles showed any signs of shattering upon reheating. This supports the previous finding that primary fragmentation is caused by pressure build up of devolatilization gases inside the particle.

5.2.2. Ash forms and characteristics

As the various density fractions contain different amounts of ash it can be expected that particles with different densities will behave differently during combustion. Some typical ash forms are shown in Figure 5.1, and it can be seen that different ash forms are formed.

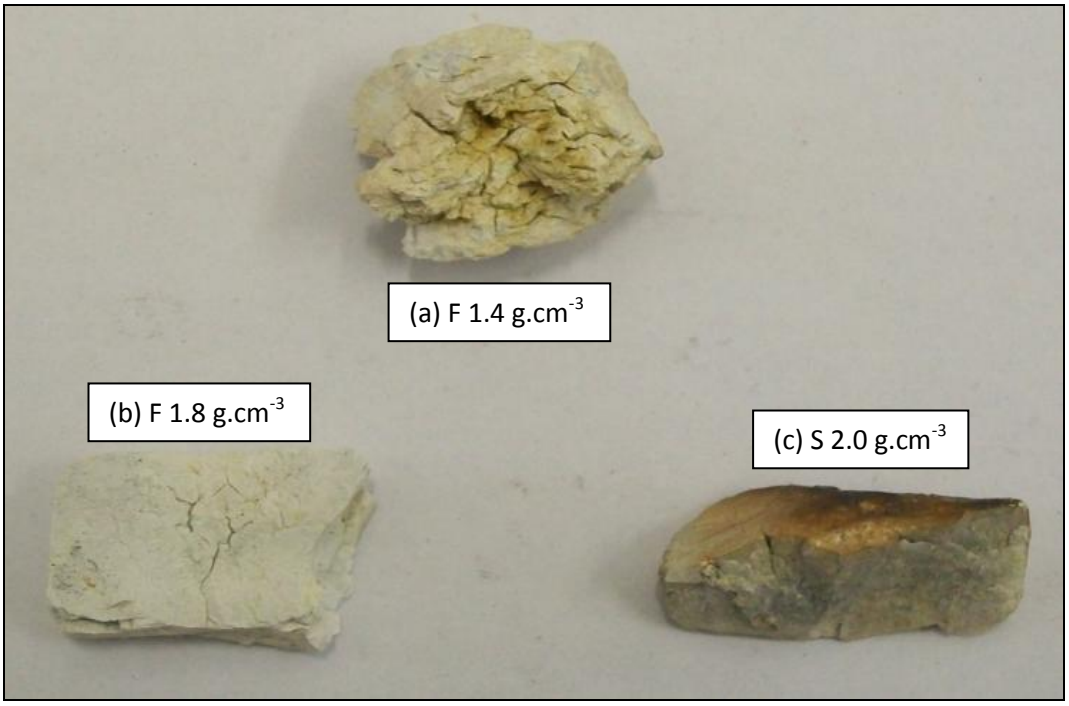

Figure 5.1: Various ash forms obtained from different densities

The first type (a) is a porous ash that easily disintegrates upon touching and is typically found for the low density coals (F 1.4). The second type (b) is also porous but has a stronger structural integrity with some cracking and is typically found for the middle density coals (*i.e*. F 1.8). The third type (c) is a solid ash with little to no cracking that needs considerable force to break, and is typically found for the most dense coals (S 2.0).

Figure 5.2: Uncombusted particle core of a 30 mm particle with a density of 2.094 g/cm^3

Combustion experiments with the densest fraction showed a particular feature: an example of a 30 mm particle is shown in Figure 5.2. This particle was left to combust until the carbon dioxide analyzer no longer detected significant levels of CO_2, indicating that the combustion reaction has finished. After removing the particle from the furnace it was found that the particle has not completely reacted. It can be seen from the figure that the centre of the particle still contains unreacted carbon. A possible reason for this phenomenon may be the large amount of minerals that encapsulate the carbon in the centre of the particle so that the oxygen cannot easily reach this part of the particle.

The sink on 2.0 g.cm^{-3} fractions yielded another interesting result which can be seen in Figure 5.3. This figure shows the part of the particle that was left after the particle reached full conversion according to the carbon dioxide analyzer and after the white ash was removed.

Figure 5.3: The melted mineral remains of a 30 mm particle with a density greater than 2.0 g/cm^3

It can be seen that some of the mineral content of the particle conglomerated to form a solid particle that is very hard. The original particle probably contained a low density carbon fraction along with the high density mineral part. Matjie and van Alphen (2008) studied the ash from lump coal gasification and also found that some of the particles formed glass-like lumps containing glass and anorthite ($CaAl_2Si_2O_8$). The glass part primarily consisted of Ca/CaMg/Fe – bearing aluminosilicate glass with varying proportions of Ca, K, Ti, Fe, P and Mg.

It was found that if the equivalent particle diameter is 60 mm, and if the particle density is 1.6 g.cm^{-3}, then the combustion reaction might not reach full conversion. The typical ash from such a particle is shown in Figure 5.4

Figure 5.4: The ash formed from combusting a 60 mm particle at 1000 °C

It can be seen from Figure 5.4 that the ash has considerable structural integrity and that the ash shows some cracking. When it was broken, the ash particle shown in Figure 5.4 revealed that the combustion reaction had in fact not reached completion. The opened ash can be seen in Figure 5.5

Figure 5.5: The unreacted core of a 60 mm particle combusted at 1000 °C

The fact that the 60 mm particle did not reach full conversion indicates that as the ash layer thickness increases, so the diffusion resistance also increases to a point where the resistance becomes too great to facilitate diffusion of reactant gas to the unreacted core. It was therefore decided to do the combustion rate experiments with 20 mm, 30 mm and 40 mm particles.

5.2.3. Shrinking unreacted core behaviour

The combustion of 30 mm particles (density = 1.6 g.cm^{-3}) at 1000 °C was stopped at various intervals into combustion. When these particles were opened it could be seen that the combustion followed shrinking unreacted core behaviour. It can be seen that the core stays unreacted as the reaction progresses and that the central unreacted core shrinks as the reaction progresses. This behaviour is shown in Figure 5.6. The time required for each interval was determined by reading the time values required for 25, 50 and 75 % conversion respectively from Figure 5.7.

Figure 5.6: Photographic representation of the shrinking unreactive core model at various stages of conversion (0-100%)

Remiarova *et al*. (2004) observed this behaviour in 5 mm particles combusted at 650 °C, and Holikova *et al.* (2005) also observed it for 10 mm particles at the same temperature. They found that the reaction immediately consumes the oxygen at the sharp ash-core interface, and concluded that combustion at 650 °C is controlled by either external diffusion, or ash layer diffusion or a combination of the two controlling mechanisms. On the basis of these findings the shell-progressive or shrinking core type models were used for modelling purposes.

5.3. Effect of coal properties

5.3.1. The effect of coal skeletal density

The influence of particle density on the combustion reaction at 1000 °C can be seen in Figure 5.7. All the runs for density variation were done on particles with an equivalent spherical radius of 30 mm. The combination of the individual experiments can be seen in APPENDIX D.

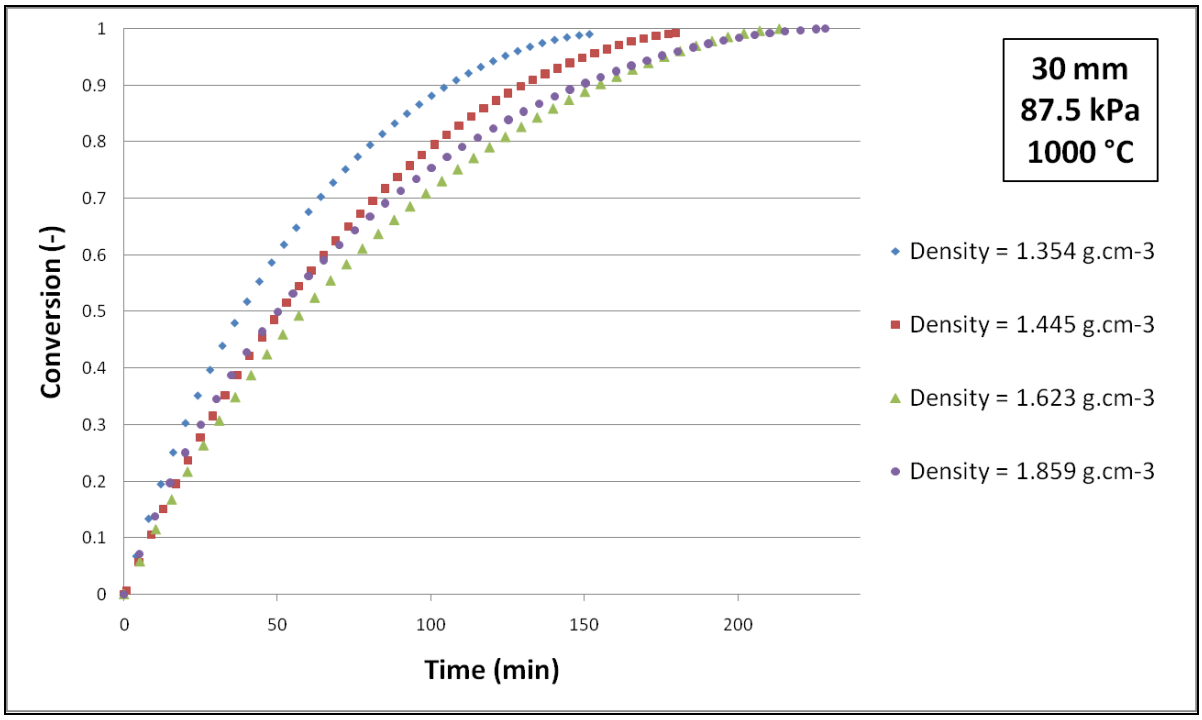

Figure 5.7: Effect of particle density on the combustion of 30 mm particles at 1000 °C

It was observed that the density of the particle has a significant influence on the combustion rate of coal. It can clearly be seen that the lower density particles (density = 1.354 g.cm^{-3}) react the fastest, while the higher density particles take longer to reach full conversion. The faster reaction of the lower density particles can be explained by their higher vitrinite content, which burns at a higher rate than inertinite (Falcon and Falcon, 1987). It can also be noted that the highest density (density = 1.859 g.cm^{-3}) does not follow the trend as would be expected. This deviation might be due to the hard ash properties of the residual combustion matter presenting high diffusion resistance; the different shape of the particles; or maceral

disproportionation occurring in the coal samples; a slower ignition due to higher heat-absorbing mineral-ash content.

5.3.2. Effect of coal particle size

The effect of particle size on the combustion reaction can be seen in Figure 5.8 which shows the effect as the particle radius is increased from 20 mm to 30 mm to 40 mm. The combination of the individual experimental work can be seen in APPENDIX D.

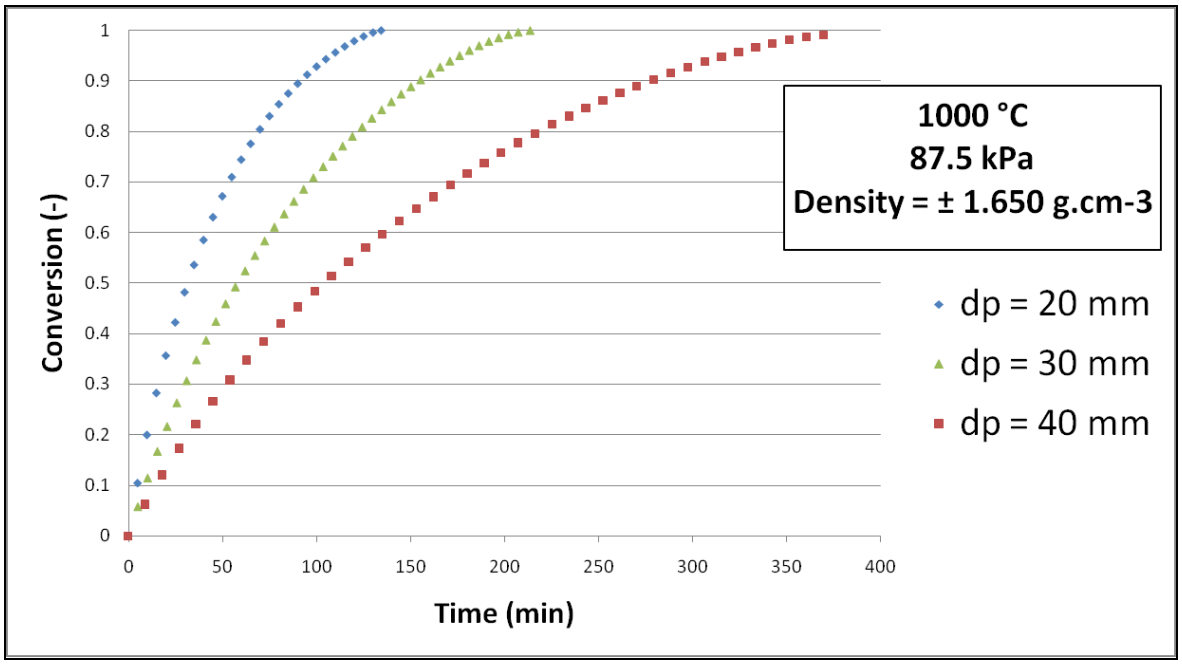

Figure 5.8: Effect of particle size on combustion at 1000 °C

From this figure it can be observed that the larger particles take longer to reach full conversion. Work done by Tevrucht and Griffiths (1989) showed a similar trend when the oxidation reaction was controlled by diffusion mechanisms rather than reaction controlling mechanisms. Diffusional effects were also observed for particles as small as 1-4 mm at 1500 K (Essenhigh, 1991) and it was shown by other researchers that air combustion of 24 mm carbonaceous particles at 800 K was ash layer diffusion controlled (Wang and Wen, 1972). It was also shown for lignite cylinder (2.5 cm diameter, 6 cm long) combustion in air that the burning rate varied inversely with ash layer thickness, and that the burning rate can be predicted by assuming effective ash layer diffusivity (Park and Edgar, 1987). During diffusion

controlled coal conversion processes smaller particles will oxidize more rapidly due to a higher surface area to volume ratio (Tevrucht and Griffiths, 1989). The variation of conversion times for the various coal sizes could also be partly due to a maceral disproportionation. The smaller particles might have a higher vitrinite content, which burns faster than the inertinite that would tend to concentrate in the larger particles (Falcon and Falcon, 1987).

5.3.3. Effect of temperature

The lower temperature experiments were conducted at 950 °C using 30 mm particles with a density of 1.650 g.cm^{-3}. The effect of temperature on the combustion of these 30 mm particles can be seen in Figure 5.9. The combination of the individual experiments can be seen in APPENDIX D.

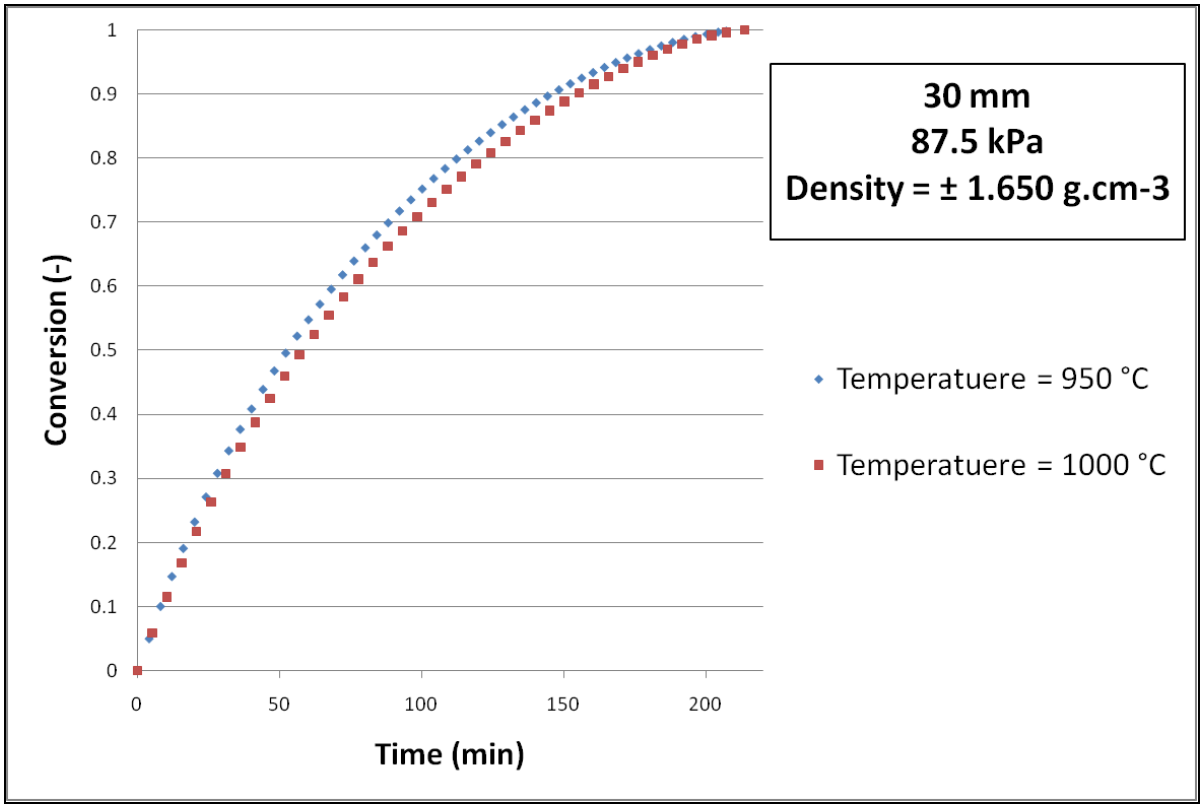

Figure 5.9: Effect of temperature on the combustion of 30 mm particles

It was observed from Figure 5.9 that the decreased temperature does not affect the reaction time for the combustion reaction of 30 mm particles with similar densities, which strongly indicates that the conversion process is not controlled by the chemical reaction, but by diffusion. It can also be proposed that the 30 mm particles have similar maceral/mineral compositions at a density of 1.6 $g.cm^{-3}$, such that they will be inertinitic with a relatively low mineral content suggesting that the controlling factor might be controlled by the difficulty to ignite the inertinite.

5.4. Summary

Qualitatively understanding the influence of different parameters on coal combustion will help to indicate which parameters require further, more detailed investigation in order to develop models or correlations that can quantitatively describe and predict the influence of the most pronounced parameters.

Extensive fragmentation of the coal particles was observed at heating rates of 50 °C/min, while only medium to high density fractions tended to shatter at a lower heating rate of 25 °C/min. Using a heating rate of 15 °C/min showed very little fragmentation and was consequently used for the experimental work. As the resulting ash from the combustion runs stayed intact, it was possible to assess whether the particles shattered upon reheating the particle to the combustion temperature. No fragmentation of the char particles was observed after the coal particles were charred, cooled and reheated to the combustion temperature.

From the visual observations it was found that the low density particles yield a very porous ash, while the high density particles yield a very dense and hard ash particle that only breaks when significant force is applied. It was also seen that high density particles can either yield ash particles that are consistently white ash that may not combust completely, leaving an unreacted core at the centre of the particle, or yield very hard glass-like solid particles. It has also been observed that large particle combustion follows the shrinking core mechanisms.

The quantitative results showed that density has an effect on conversion rate, and that the low density particles required less time for full conversion than did the high density particles. It was also found that the temperature does not affect the conversion time required for 30 mm particles indicating diffusion controlling conversion mechanisms.

CHAPTER 6: RESULTS AND DISCUSSION: MODELLING OF EXPERIMENTAL DATA

6.1. Introduction

This chapter covers the modelling done with the obtained experimental data. The shrinking unreacted core model was chosen to model the experimental data. Section 6.2 discusses the observations that led to the decision to use the shrinking unreacted core model, and Section 6.3 presents the modelling results obtained by fitting the model to the obtained experimental results. Finally Section 6.4 contains a summary of the results and conclusions obtained from the modelling of the experimental data.

6.2. Determination of appropriate model and controlling mechanisms

As mentioned earlier in Section 2.5.4, there are various models that can be used to model the combustion of coal particles. These models include, amongst others, the homogeneous model (Molina and Mondragon, 1998); the shrinking unreacted core model (Szekely *et al*., 1976); and the random pore model (Bhatia and Perlmutter, 1980).

For this study it was concluded that the most appropriate model to use in modelling the experimental results is the shrinking unreacted core model. This was determined as the combustion of several 30 mm coal particles combusted at 1000 °C visually progressed according to shrinking unreacted core behaviour (Figure 5.6). Models from the literature assume that the reaction occurs at a sharp interface at the unreacted core surface (Levenspiel, 1999) (Szekely *et al*., 1976) as can be seen in Figure 5.6. Research showing that at 985 K oxygen can penetrate a relatively pure graphite sphere up to a depth of 1.5 mm, while at the higher temperature of 1110 K oxygen only achieves penetration of about 0.25 mm (Prins and van Swaaij, 1990) confirms the sharp interface assumption. This research also indicates that for the larger 12mm particles the oxygen penetration remains relatively constant throughout combustion. Another important conclusion from this visual progression is that the unreacted core remains in the centre of the particle.

According to the shrinking unreacted core model, the rate of reaction can be controlled by either of three regimes. These controlling regimes are gas film diffusion control; ash layer diffusion control; and chemical reaction control (Szekely, 1970). The characteristic equations for the different controlling mechanisms are derived in APPENDIX E.

For gas film diffusion control the characteristic equation is given by Equation E.21.

$$t = \left(\frac{\rho_B}{3M_B b k_g C_{Ag} R_p^2}\right) X_B \qquad \text{(E.21)}$$

For ash layer diffusion control the characteristic equation is given by Equation E.31.

$$t = \left(\frac{\rho_B R_p^2}{6D_e C_{Ag} b M_b}\right)\left(1 - 3(1 - X_B)^{\frac{2}{3}} + 2(1 - X_B)\right) \qquad \text{(E.31)}$$

And finally for chemical reaction controlled mechanisms the characteristic equation is given by Equation E.35.

$$t = \left(\frac{\rho_B}{M_B b k'' C_{Ag}}\right)\left(1 - (1 - X_B)^{\frac{1}{3}}\right) \qquad \text{(E.35)}$$

The conversion functions for the three controlling regimes can be seen as the part of the equation involving the conversion of the coal particle. For the three controlling regimes, gas film diffusion control, ash layer diffusion control and chemical reaction control, the separate conversion functions can be given by the following three equations respectively.

$$f(X)_{Gas\ film\ diffusion\ control} = X_B$$

. $$f(X)_{Ash\ layer\ diffusion\ control} = \left(1 - 3(1 - X_B)^{\frac{2}{3}} + 2(1 - X_B)\right) \qquad \text{(E.36)}$$

$$f(X)_{Chemical\ reaction\ control} = \left(1 - (1 - X_B)^{\frac{1}{3}}\right)$$

As can be seen from Equations E.36, the characteristic equations can be linearised by plotting the conversion function f(X) of each controlling mechanism against time. If any of the controlling mechanisms are the only controlling factor the resulting plot for the particular controlling function should be linear. The plot of the characteristic conversion functions for the 30 mm particles with a density of 1.357 g/cm^3 can be seen in Figure 6.1.

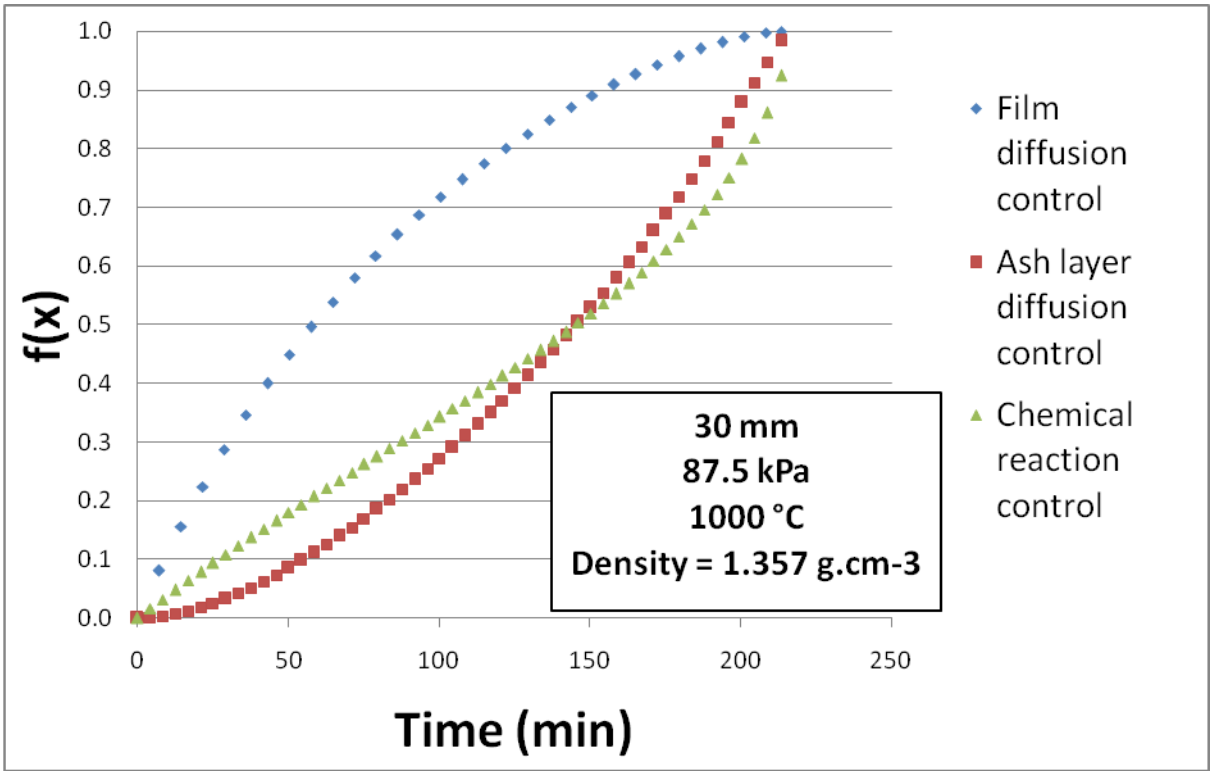

Figure 6.1: Characteristic conversion function plot for shrinking core controlling mechanisms.

Figure 6.1 shows that the conversion function for chemical reaction control yields the most linear relationship when plotted against time. This perhaps indicates that combustion at 1000 °C is chemical reaction controlled. However, research by Szekely (1970) suggests that at such high temperatures the controlling mechanism should either be gas film diffusion controlled at low flow rates, or ash layer diffusion controlled if the combustion reaction produces an ash layer. The results for varying temperatures (Figure 5.9) also fail to support a chemical reaction controlling conversion.

Due to the fact that neither the gas film diffusion nor the ash layer diffusion control conversion functions give linear correlations, it is most likely that the overall controlling mechanism is a combination of gas film and ash layer diffusion control.

6.3. Combustion modelling results

Modelling the combustion results with the shrinking unreacted core model involves solving both the external mass transfer coefficient as well as the effective ash layer diffusion coefficient by using Equation E.37.

$$t = \left(\frac{\rho_B}{3M_B b k_g C_{Ag} R_p^2}\right) X_B + \left(\frac{\rho_B R_p^2}{6D_e C_{Ag} b M_b}\right)\left(1 - 3(1 - X_B)^{\frac{2}{3}} + 2(1 - X_B)\right) \qquad \text{(E.37)}$$

Both parameters are solved by means of a least square fit by fitting the model curve to the experimental data. By solving both parameters the modelling curves shown in Figure 6.2 can be obtained.

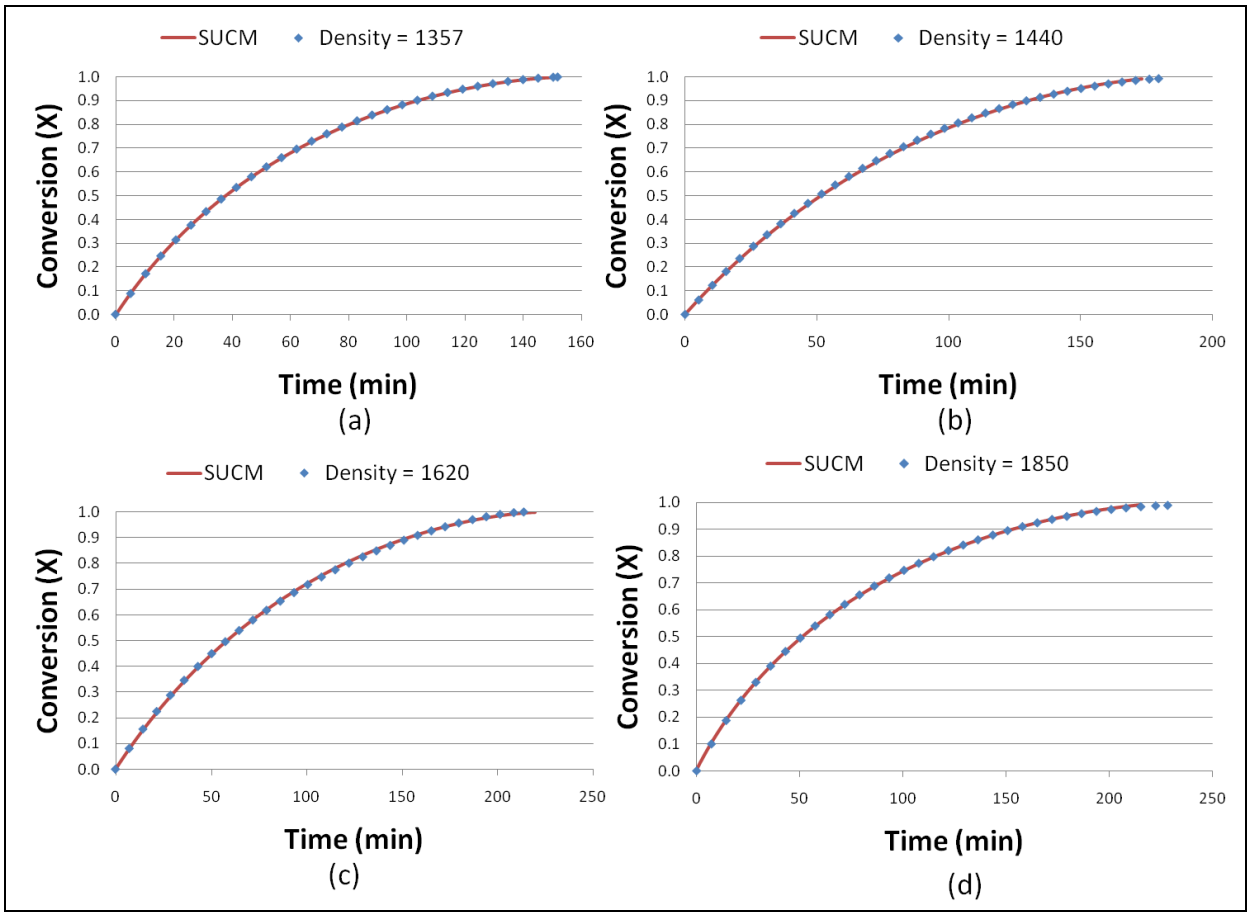

Figure 6.2: Model fits for different densities by solving both diffusion parameters

It can be seen from Figure 6.2 that by solving both external mass diffusion as well as effective ash layer diffusion the model gives a very good fit. The solved external mass transfer coefficient values are shown in Table 6.1.

Table 6.1: Fitted mass transfer coefficients for different densities of 30 mm particles

Density (g/cm^3)	k_g (m/s) x 10^{-3}
1.36	12.5
1.44	7.9
1.62	7.6
1.85	9.2

The trend observed for the solved external mass transfer coefficients clearly shows that the external mass transfer coefficients are not constant, as literature would suggest, for the different 30 mm particles. However, they are all of the same magnitude. This variation is perhaps due to the fact that the particles are not spherical, which could affect the surface area available for gas diffusion. Averaging the mass transfer coefficient for the different densities gives a mass transfer coefficient of 9.3 x 10^{-3} $m.s^{-1}$. The theoretical mass transfer coefficient can be calculated from the Sherwood number which in turn is calculated using the Reynolds number and the Schmidt number. The calculation of these values can be seen in APPENDIX F.

The mass transfer coefficient is dependent of the characteristic length of the particle, which in this case is the particle diameter. This means that each particle size will have a characteristic mass transfer coefficient. The calculated mass transfer coefficients for the various particle sizes can be seen in Table F.1, and it is observed that the fitted values are in the same order as the theoretical ones, but systematically lower. This can mainly be attributed to the non-spherical nature of the coal particles that were used.

The fitted effective ash layer diffusion coefficients for 30 mm particles with different densities can be seen in Table 6.2. The obtained effective diffusion coefficient values are in good agreement with results from literature (Froberg and Essenhigh, 1978) (Chen and Kojima, 1996) showing ash layer diffusion coefficients in the range of 8 -15 x 10^{-5} $m^2.s^{-1}$ for particles sizes ranging from 12 – 17 mm using high ash content samples.

Table 6.2: Fitted effective ash layer diffusion coefficients for 30 mm particles with different densities when solving both diffusion parameters

Density (g/cm^3)	D_e x10^{-5} (m^2/s)
1.36	5.01
1.44	4.57
1.62	3.69
1.85	2.66

The trend observed for the effective ash layer diffusion coefficient can be seen in Figure 6.3.

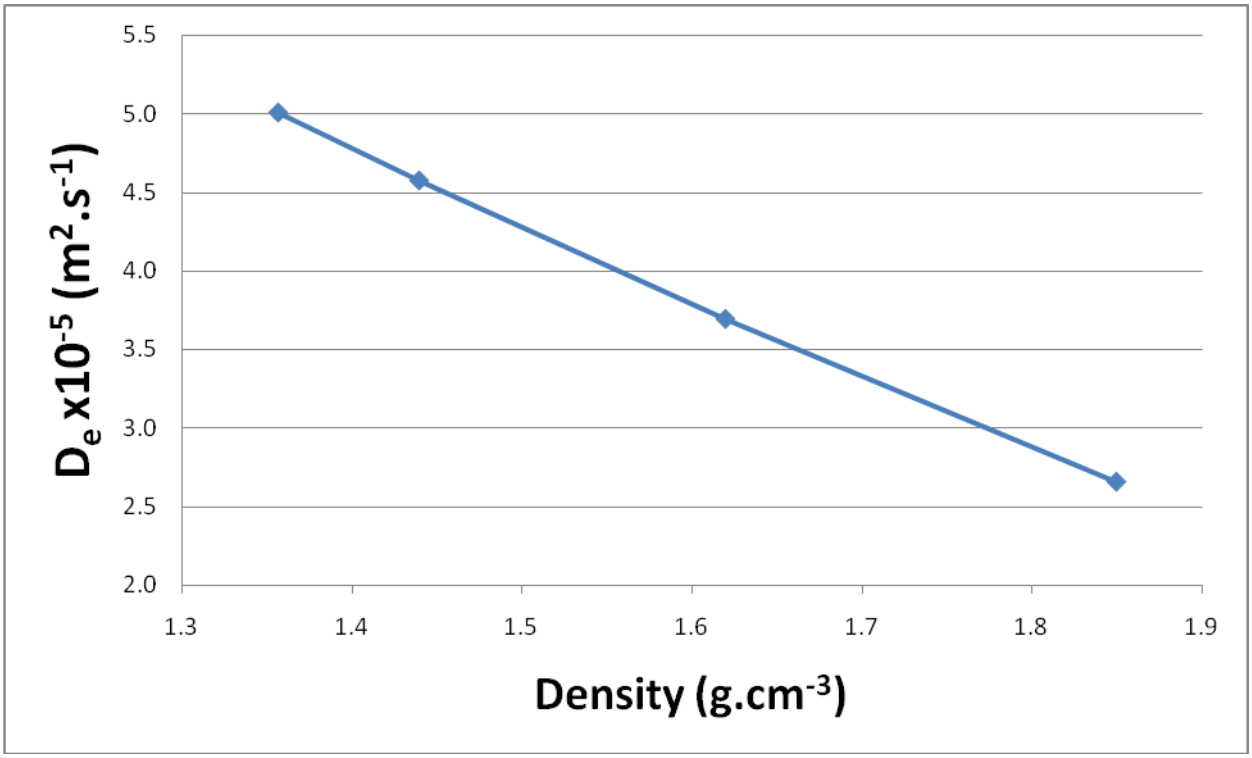

Figure 6.3: Graphical representation of the fitted effective ash layer diffusion coefficients as a function of density

Figure 6.3 shows that the effective diffusion coefficient decreases as the particle density increases, indicating that the heavier densities have larger ash layer diffusion resistances, a trend that was also observed by Chen and Kojima (1996). Work on high purity carbon spheres showed that above 1270 K the controlling mechanism was boundary layer diffusion (Froberg and Essenhigh, 1978) which supports the finding that a decreasing influence of ash layer diffusion can be seen as the particle ash content decreases. The decrease in particle

ash content results in coal particles with a higher carbon purity which in turn results in more porous ash that offers less resistance to gas diffusion.

Solving both external mass transfer as well as effective ash layer diffusion of the size ranges also gives a very good fit. The resulting fits for solving the model to fit the experimental data with a least squares fit can be seen in Figure 6.4.

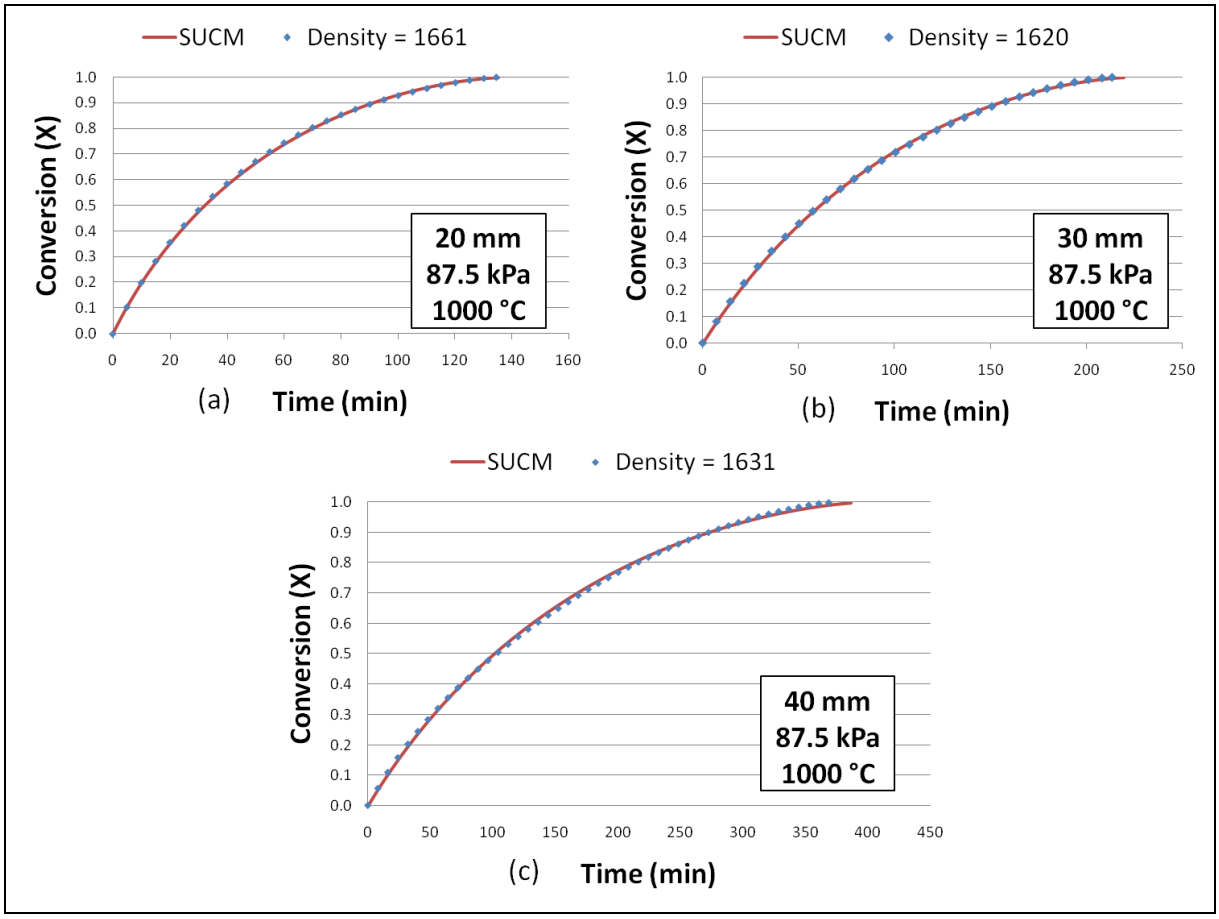

Figure 6.4: Shrinking core model fits to experimental data for particles of different sizes when solving both parameters

The values obtained from solving the external mass transfer coefficients are shown in Table 6.3. The values obtained for the external mass transfer coefficients are of the same magnitude than those obtained for the variation in density.

Table 6.3: Fitted external mass transfer coefficients obtained for different sizes when solving both parameters

Particle size (mm)	k_g (m/s) x 10^{-3} (Solved values)	k_g (m/s) x 10^{-3} (Calculated values)
20	10.4	60.2
30	7.6	45.4
40	6.1	37.3

The trend shown in Table 6.3 shows an almost linear decrease in external mass transfer coefficients as the size of the particles increase from 20 mm to 40 mm.

Values calculated from the theoretical equations shown in APPENDIX F, indicate that the external mass transfer coefficients should decrease in line with the obtained trend as the particle size increases. The solved external mass transfer coefficients were, however, found to be smaller than the calculated values, but were of the same magnitude. A decrease in mass transfer coefficients as the particle size increased has also been observed for fluidized bed combustion using particles as large as 12 mm (Prins and van Swaaij, 1990). From the fits obtained in Figure 6.4 the solved effective ash layer diffusion coefficients can be obtained, and are given in Table 6.4.

Table 6.4: Fitted effective ash layer diffusion coefficients for different sizes

Particle size (mm)	D_e x10^{-5} (m^2/s)
20	2.4
30	3.6
40	3.5

The observed trend shows that ash layer diffusion coefficients are all of the same magnitude. The smaller value obtained for the 20 mm particle is perhaps due to the inter relation between the solved mass transfer coefficient and the effective ash layer coefficient.

6.4. Summary

From the modelling results it can be shown that large coal particles exhibit shrinking unreacted core behaviour during combustion. This was found to be the case for density separated as well as sizes separated coal particles. The experiments conducted at a decreased temperature suggested that the controlling mechanism was a combination of external gas diffusion and effective ash layer diffusion. While the mass transfer coefficient for 30 mm particles calculated from literature gives a slightly higher value than when solved from the modelling of experimental data, the two values are still of the same magnitude. The effective ash layer diffusion coefficient for 30 mm particles was found to decrease linearly as the particle density increased, indicating that as the density increases the effect of ash diffusion control becomes more prominent. It was also determined that for the variation of coal particles sizes the external mass transfer coefficients decreased as predicted by literature. The solved values were, however, found to be smaller but still of the same magnitude. Finally it was observed that effective ash layer diffusion was more dominant in 20 mm particles than what it was in 30 and 40 mm particles.

CHAPTER 7: CONCLUSIONS AND RECOMMENDATIONS

7.1. Conclusions

From the characterization results is was found that the high density particles tended to be shale like and more grey when compared to the more rounded black low density particles. Moisture content of the different coal particles decreases as the densities increases, but was more likely to concentrate in smaller particles. The volatile matter and fixed carbon decreased as the coal density increased, while both had a relatively even distribution across the size ranges. It was also found that mineral content increased significantly as particle density increased.

From the ultimate analysis perspective it was determined that carbon content, hydrogen content and nitrogen content decreased as density increased with a relatively even distribution of the different size ranges. The high sulphur content observed in the high density particles was attributed to the higher pyrite concentrations in these particles. It was also observed that the smaller particles had a higher oxygen content. Calorific value analysis showed that the high density fraction had a very low heating value and that the overall sample value would be improved by removing the high density fraction.

FTIR investigations of the coal samples indicated that the properties of density separated particles differ significantly, and that the aromatic substitutions occurring on the aromatic structures also differ with density separation. This investigation also showed that the FTIR characteristics of size variations of large coal particles tend to be similar. The FTIR analysis determined that the chemical properties of char particles created from density separated particles at high temperatures tend to become more similar, and that the aromatic substitution patterns also tend to become similar.

The characterization of the different coal samples has shown that all the parameters were significantly different for the different density fractions, but did not vary as significantly across the particle size ranges.

From the qualitative observations it was determined that extensive fragmentation occurs for large particles at heating rates of 50 °C/min, and that the fragmentation behaviour was only observed for the medium to high density particles when the heating rates was reduced to 25 °C/min. When the heating rate was further reduced to 15 °C/min very little fragmentation was observed. No fragmentation was observed when the particles were reheated after charring.

It was observed that the low density coal particles produced very porous ash residues with poor structural integrity, while the high density particles produced a very dense ash residue that required significant force to break. High density particles can pose a significant resistance to ash layer diffusion effects as it was observed that some high density particles contained unreacted particle cores after several hours of combustion.

The quantitative results also showed that density has an effect on the time to full conversion of 30 mm particles, and that the lowest density particles required less time for full conversion than the higher density particles. The smaller particles react faster than the larger particles and the reaction is diffusion controlled.

It was found that temperature did not affect the conversion time required for 30 mm particles and that the shrinking unreacted core model can be used to model combustion behaviour. The mass transfer coefficients were found to be in accordance with values found in literature and the effective ash layer coefficient was, further, found to become more prominent as the particle density increased. It was also found that the fitted values for external mass transfer coefficients were following the trend predicted by literature.

7.2. Recommendations

Work on the core temperature of the particle during combustion is recommended as this work would enhance the understanding of the coal particle behaviour during combustion. This can be accomplished by inserting very thin thermocouples into the particle to evaluate the combustion temperature inside the particle as combustion progresses.

To get better resolving data from the FTIR spectra on the coal char particles, it is suggested that the char particles be demineralised to reduce the effect that mineral matter has on the peak intensity contributions. Due to the possible influence the demineralisation process can have on the properties of coal another option would be to obtain more ‘pure’ particles from the dull or bright bands in a seam as opposed to using the ROM coal. This work would show minor differences in coal char particles more clearly.

It is recommended that petrographic analysis be conducted on the different particle ranges to determine if the petrographic composition of different large sized particles varies considerably. The petrographic properties and distribution should also be determined for the different density ranges in order to determine the influence of different macerals found in

coal. This information could then be incorporated into the combustion behaviour of large coal particles.

It is also recommended combustion work be done on large particles at lower temperatures. This could show where the regime changes occur in larger coal particles. This will allow a better understanding of large scale coal utilization processes.

BIBLIOGRAPHY

Akkaya, A. V. (2009). Proximate analysis based multiple regression models for higher heating value estimation of low rank coals. *Fuel processing technology*. **90**, pp.165-170.

Alciaturi, C. E., Escobar, M. E and Vallejo, R. (1996). Prediction of coal properties by derivative DRIFT spectroscopy. *Fuel*. **75**(4), pp.491-499.

Alciaturi, C. E., Montero, T., de la Cruz, and Escobar, M. E. (1997). The prediction of coal properties using compressed infrared data from osculating polynomials. *Analytica Chimica Acta*. **340**, pp.233-240.

Bailey, J. G., Tate, A., Diessel, C. F. K. and Wall, T. F. (1990). A char morphology system with applications to coal combustion. *Fuel*. **69**, pp.225-239.

Barker, O. B. (1999). A techno-economic and historical overview of the South African coal industry in the 19th and 20th centuries. *In*: Pinheiro, H. J. (ed). *Bulletin 113*, South African Bureau of Standards, pp.1-63.

Beer, J. M. (2000). Combustion technology developments in power generation in response to environmental challenges. *Progress in Energy and Combusiton Science*. **26**, pp.301-327.

Beeston, G. (1963). Kinetics of coal combustion: The influence of oxygen concentration on the burning-out times of single particles. *The Journal of Physical Chemistry*. **67**(6), pp.1349-1355.

Belbot, M. D., Vourvopoulos, G., Womble, P. C. and Paschal, J. (2000). Proceedings of the SPIE Conference on Penetrating Radiation Systems and Applications*., 2000*., p.168.

Bell, V. A., Citro, V. R. and Hodge, G. D. (1991). Effect of pellet pressing on the infrared spectrum of kaolinite. *Clays and Clay Minerals*. **39**(3), pp.290-292.

Beveridge, G. S. and Goldie, P. J. (1968). Effectiveness factors and instability in non-catalytic gas-solid reactions: the effect of solid heat capacity. *Chemical Engineering Science*. **23**, p.913.

Bhatia, S. K. and Perlmutter, D. D. (1980). A random pore model for fluid-solid reactions: I. Isothermal, kinetic control. *AIChe Journal*. **26**(3), p.379.

Bona, M. T. and J. M. Andres. 2008. Reflection and transmission mid-infrared spectroscopy for rapid determination of coal properties by multivariate analysis. *Talanta*. **74**, pp.998-1007.

Borrego, A. G., Alvarez, D. and Menendez, R. (1997). Effects of Inertinite Content in Coal on Char Structure and Combustion. *Energy and Fuels*. **11**(3), pp.702-708.

Brown, D. (1962). Coal Flotation. *In*: *Red Froth Flotation 50th Aniverssary Volume*, New York: Aime, pp.518-538.

Bunt, J. R. and Waanders, F. B. (2008). An understanding of lump coal physical property behaviour (density and particle size effects) impacting on a commercial-scale Sasol-Lurgi FBDB gasifier. *Fuel*. **87**, pp.2856-2865.

Campbell, C. J. (2002). *Peak Oil: an outlook in crude oil depletion*. [online]. [Accessed 27 September 2010]. Available form World Wide Web: "http//www.mbendi.com/indy/oilg/p0070.htm"

Chen, C., Gao, J. and Yan, Y. (1998). Observation of the type of hydrogen bonds in coal by FTIR. *Energy and Fuels*. **12**, pp.446-449.

Chen, C. and Kojima, T. (1996). Single char particle combustion at moderate temperature: effect of ash. *Fuel Processing Technology*. **47**, pp.215-232.

DME. 2007. *South African Department of Minerals and Energy*. [online]. [Accessed 27 September 2010]. Available form World Wide Web: < HYPERLINK "http://www.dme.gov.za/energy/coal.stm" http://www.dme.gov.za/energy/coal.stm >

Du, Z., Sarofim, A. F. and Longwell, J. P. (1990). Influence of catalysts on pulverized coal combustion characteristics. *Energy and Fuels*. **37**(3), p.296.

Essenhigh, R. H. (1991). Rate equations for the carbon-oxygen reaction: an evaluation of the Langmuir adsorption isotherm at atmospheric pressure. *Energy Fuel*. **5**, pp.41-46.

Estep, P. A., Kovach, J. J. and Clarence, K. Jr. (1968). Quantitave Infrared Multicomponent Determination of Minerals Occurring in Coal. *Analytical Chemistry*. **40**(2), pp.358-363.

Everson, R. C., Neomagus, H. J., Kasaini, H. and Njapha, D. (2005). Reaction kinetics of pulverised coal-chars derived from inertinite-rich coal discards: Gasification with carbon dioxide and steam. *Fuel*. **85**, p.1076.

Falcon, R. M. (1977). Coal in South Africa, Part I: The Quality of South African Coal in Relation to its Uses and World Energy Resource. *Minerals and Science Engineering*., pp.198-217.

Falcon, R. (1978). Coal in South Africa, Part II: The Application of Petrography to the Characterization of Coal. *Minerals Science and Engineering*. **10**(1), pp.28-52.

Falcon, L. M. and Falcon, R. M. S. (1987). The petrographic composition of Southern African coals in relation to friability, hardness, and abrasive indices. *Journal of the South African Institute of Mining and Metallurgy*. **87**(10), pp.323-336.

Froberg, R. W. and Essenhigh, R. H. (1978). *In*: *17th Symposium on Combustion, 1978*. The Combustion Institute, p.179.

Fuller, M. P., Hamadeh, I. M., Griffiths, P. R. and Lowenhaupt, D. E. (1982). Diffuse reflectance infrared spectroscopy of powdered coals. *Fuel*. **61**, pp.529-536.

Furuta, T., Yamashita, Y. and Shiraishi, M. (1989). Microtextural change in carbons accompanying their reaction with carbon dioxide gas. *Tanso*. **140**, pp.241-247.

Gilfillan, A., Lester, E., Cloke, M. and Snape, C. (1999). The structure and reactivity of density separated coal fractions. *Fuel*. **78**, pp.1639-1644.

Hanson, S., Patrick, J. W. and Walker, A. (2002). The effect of particle size on pyrolysis and steam gasification. *Fuel*. **81**, pp.531-537.

He, R., Suda, T., Fujimori, T. and Sato, J. (2003). Effects of particle sizes on transport phenomena in single char combustion. *International Journal of Heat and Mass Transfer*. **46**, pp.3619-3627.

Holikova, K., Markos, J. and Jelemensky, L. (2004). Mechanism of coal char burning at a low oxygen content in the feed stream. *Journal of Thermal Analytic Calorim*. **76**(1), p.237.

Holikova, K., Zajdlik, R., Markos, J. and Jelemensky, L. (2005). Comparison of Single Coal Char Particle Combustion at Different Conditions. *Chemical Papers*. **59**(6a), pp.413-420.

Hopkins, R. (2006). *Energy Descent Pathways: evaluating potential responses to peak oil*. England.

Hurt, R. H. and Calo, J. M. (2001). Semi-Global Intrinsic Kinetics for Char Combustion Modelling. *Combustion and Flame*. **125**, pp.1138-1149.

Hurt, R. H., Davis, K. A. and Yang, N. Y. (1995). Residual carbon from pulverized-coal-fired boilers. 2. Morphology and physiochemical properties. *Fuel*. **74**, pp.1297-1306.

IEA. (2010). *Coal information 2010*. [online]. [Accessed 26 October 2010]. Available form World Wide Web: " http://www.oecd-ilibrary.org/energy/coal-information-2010_coal-2010-en

Ishida, M. and Wen, C. Y. (1968). Comparison of kinetic and diffusional models for solid-gas reactions. *American Institute for Chemical Engineering Journal*. **14**(2), p.311.

Jeffrey, L. S. (2005). Characterization of the coal resources of South Africa. *The Journal of The South African Institute of Mining and Metallurgy*., pp.95-120.

Jelemensky, L., Markos, J., Zajdlik, R. and Remiarova, B. (2000). Modelling of Nonlinear Behaviour during Combustion of Single Coal Char Particle. *Chemical Papers*. **54**, p.473.

Jones, R. B., McCourt, C. B., Morley, C. and King, K. (1985). Macerals and rank influence on the morphology of coal char. *Fuel*. **64**, p.460.

Koekemoer, A. F. (2009). *The influence of minerals content and petrographic composition on the gasification of inertinite-rich high ash coal*. *Masters thesis.* Potchefstroom: North-West University.

Levenspiel, O. (1999). *Chemical Reaction Engineering*. United States of America: Wiley.

Li, D., Li, W. and Li, B. (2003). A new hydrogen bond in coal. *Energy and Fuels*. **17**, pp.791-793.

Lin, Q. and Guet, J. M. (1990). Characterization of coals and macerals by X-ray diffraction. *Fuel*. **69**(7), pp.821-825.

Liu, G. S. (1999). *Mathematical modelling of coal char reactivity in pressurised entrained flowgasifier*. Australia.

Machnikowska, H., Krozton, A. and Machnikowski, J. (2002). The characterization of coal macerals by diffuse reflectance infrared spectroscopy. *Fuel*. **81**, pp.245-252.

Maloney, D. J., Monazam, E. R., Casleton, K. H. and Shaddix, C. R. (2005). Evaluation of char combustion models: measurement and analysis of variability in char particle size and density. *Proceedings of the Combustion Institute*. **30**, pp.2197-2204.

Martin, K. A. and Chao, S. S. (1988). *Structural group analysis of Argonne premium coals by FTIR spectroscopy*. Illinois.

Matjie, R. H. and Van Alphen, C. (2008). Mineralogical features of size and density fractions in Sasol coal gasification ash, South Africa and potential by-products. *Fuel*. **87**, pp.1439-1445.

Mendez, L. B., Martinez-Tarazona, M. R., Borrego, A. G., and Menendez, R. (2003). Influence of petrographic and mineral matter composition of coal particles on their combustion reactivity. *Fuel*. **82**, pp.1875-1882.

Molina, A. and Mondragon, F. (1998). Reactivity of coal gasification with steam and CO2. *Fuel*. **77**, p.1831.

Montgomery, W. J. (1978). *In*: Karr, C. Jr., (ed). *Analytical Methods for Coal and Coal Products Vol I*, London: Academic Press, pp.191-264.

Nelson, P. F., Kelly, M. D. and Wornat, M. J. (1991). Conversion of fuel nitrogen in coal volatiles to NOx precursors under rapid heating conditions. *Fuel*. **70**(3), pp.403-407.

Niska, S., Liu, G. S. and Hurt, R. H. (2003). Coal conversion submodels for design applications al elevated pressures. Part 1. Devolatilization and char combustion. *Progress in Energy and Combustion Science*. **29**, pp.524-477.

Oberholzer, A. (2009). Characterization and steam gasification of large, low grade coal particles using a specially designed thermo gravimetric analyser. *Masters thesis* Potchefstroom: North-West University.

Oberlin, A. (1989). *In*: THROWER, P. A. (ed). *Chemistry and physics of carbon*, New York: Marcel Dekker, p.1.

Painter, P. C., Snyder, R. W. and Starsinic, M. (1981). Concerning the application of FT-IR to the study of coal: A critical assessment of band assignments and the application of spectral analysis programs. *Applied Spectroscopy*. **35**(5), pp.475-485.

Painter, P. C., Sobkowiak, M. and Youtcheff, J. (1987). FTIR study of hydrogen bonding in coal. *Fuel*. **66**, pp.973-978.

Painter, P. C., Starsinic, M., Squires, E. and Davis, A. A. (1983). Concerning the 1600 cm-1 region in the IR spectrum of coal. *Fuel*. **62**, pp.742-743.

Park, K. Y. and Edgar, T. F. (1987). Modelling of Early Cavity Growth for Underground Coal Gasification. *Ind. Eng. Chem. Res.* **26**, pp.237-246.

Perry, R. H. and Green, D. W. (1997). *In*: *Perry's Chemical Engineer's Handbook*, McGraw Hill, pp.5-44 - 5-53.

Pranda, P., Prandova, K. and Hlavacek, V. (1999). Combustion of fly-ash carbon Part I. TG/DTA study of ignition temperature. *Fuel Processing Technology*. **61**, p.211.

Pranda, P., Prandova, K. and Hlavacek, V. (2001). Combustion of fly-ash carbon: Part II: Thermodynamic aspects and calorimetric experiment. *Fuel Processing Technology*. **72**, p.227.

Prins, W. and Van Swaaij, W. P. M. (1990). The influence of transport phenomena on the fluidized bed combustion of a single carbon particle. *Fuel Processing Technology*. **24**, pp.355-365.

Ragland, K. W. and Yang, J. T. (1985). *Combustion and Flame*. **60**, p.285.

Ranish, J. M. and Walker, P. L. (1993). High pressure studies of the carbon-oxygen reaction. *Carbon*. **31**(1), pp.135-141.

Remiarova, B., Markos, J., Zajdlik, R. and Jelemensky, L. (2004). Identification of the mechanism of coal char particle combustion by porous structure characterization. *Fuel Processing Technology*. **85**, p.303.

Riley, J. T. (2007). *Routine coal and coke analysis: Collection, interpretation and use of analytical data*. West Conshohocken: ASTM International.

Rubiera, F., Arenillas, A. and Arias, B. (2003). Combustion behaviour of ultra clean coal obtained by chemical demineralisation. *Fuel*. **82**, pp.2145-2151.

Saikia, B. K., Boruah, R. K. and Gogoi, P. K. (2007). XRD and FT-IR investigations of sub-bituminous Assam coals. *Bulletin of Materials Science*. **30**(4), pp.421-426.

SANS. 2006. *ISO 17246:2005, SANS 17246:2006, Coal - Proximate analysis*. Pretoria.

SANS. 2006. *ISO 17247:2005, SANS 17247:2006 Coal - Ultimate analysis*. Pretoria.

Schobert, H. H. (1990). *The chemistry of hydrocarbon fuels*. London: Butterworths.

Schobert, H. H. and Song, C. (2002). Chemical and materials from coal in the 21st century. *Fuel*. **81**, pp.15-32.

Shannon, G. N., Matsuura, H. and Rozelle, P. (2009). Effect of size and density on the thermodynamic predictions of coal particle phase formation during coal gasification. *Fuel Processing Technology*. **90**, pp.1114-1121.

Sharma, A., T. Kyotani, and A. Tomita. 1999. A new quantitative approach for microstructural analysis of coal char using HRTEM images. *Fuel*. **78**, pp.1203-1212.

Simons, G. A. (1983). Enhanced char reactivity via tailored pore structure. *Combustion and Flame*. **50**, p.275.

Smith, I. W. (1982). The combustion rates of coal chars: a review. *In*: *Nineteenth Symposium (International) on Combustion, 1982*. Pittsburgh: The Combustion Institute, p.1045.

Solomon, P. R. and Carangelo, R. M. (1982). FTIR analysis of coal 1- Techniques and determination of hydroxyl concentrations. *Fuel*. **61**(7), pp.663-669.

Solomon, P. R. and Carangelo, R. M. (1988). FTIR analysis of coal. 2. Aliphatic and aromatic hydrogen concentration. *Fuel*. **67**(17), pp.949-959.

Solum, M. S., Pugmire, R. J. and Grant, D. M. (1989). Carbon-13 solid state NMR of Argonnne-premium coals. *Energy Fuels*. **3**(2), pp.187-193.

Sotirchos, S. V. and Amundson, N. R. (1984). Dynamic behaviour of a porous char particle burning in an oxygen-containing environment: Part I: Constant particle radius. *AIChe Journal*. **30**(4), p.537.

Strezov, V., Lucas, J. A. and Wall, T. F. (2005). Effect of pressure on the swelling of density separated coal particles. *Fuel*. **84**, pp.1238-1245.

Stubington, J. F. and Moss, B. (1995). On the timing of primary fragmentation during bituminous coal particle devolatilization in a fluidized bed combustor. *Canadian Journal of Chemical Engineering*. **73**(4), pp.505-509.

Suggate, R. P. and Dickinson, W. W. (2004). Carbon NMR of coals: the effect of coal type and rank. *International Journal of Coal Geology*. **57**, pp.1-22.

Szekely, J. (1970). Reactions between porous solids and gases. *In*: Lapidus, L. and Amundson, N. R. (eds). *Chemical Reactor Theory*, p.856.

Szekely, J., Evans, J. W. and Sohn, H. Y. (1976). *Gas-Solid Reactions*. New York: Academic Press.

Tevrucht, M. L. and Griffiths, P. R. (1989). Activation energy of air-oxidized bituminous coals. *Energy and Fuels*. **3**, pp.522-527.

Tsai, C. Y. and Scaroni, A. W. (1987). Reactivity of bituminous coal chars during the initial stage of pulverized-coal combustion. *Fuel*. **66**(10), pp.1400-1406.

Tu, C. M., Davis, H.and Hottel, H. C. (1934). Combustion Rate of Caron. Combustion of Spheres in Flowing Gas Streams. *Industrial Engineering Chemistry*. **26**, p.749.

Van der Hart, D. and Retcofsky, H. L. (1976). Estimation of coal aromaticities by proton-decoupled carbon-13 magnetic resonance spectra of whole coals. *Fuel*. **55**, pp.202-204.

Vostrikov, A. A., Psarov, S. A. and Dubov, D. Y. (2007). Kinetics of Coal Conversion in Supercritical Water. *Energy and Fuels*. **21**, pp.2840-2845.

Walker, P. L., Rusinko, F. and Austin, L. G. (1959). Advances in catalysis and related subjects. *In*: *Gas reactions of carbon*, Academic Press, pp.133-221.

Wang, S. C. and Wen, C. Y. (1972). Experimental evaluation of nonisothermal solid-gas reaction model. *AIChE Journal*. **18**(6), pp.1231-1238.

WCI. (2007). *Coal Facts: 2007 Edition with 2006 data.* [online]. [Accessed 27 September 2010]. Available form World Wide Web: "http://www.worldcoal.org/assets_cm/files/pdf/fact_card07.pdf"

WCI. (2009). *Coal Facts: 2009 Edition with 2008 data.* [online]. [Accessed 26 October 2010]. Available form World Wide Web: http://www.worldcoal.org/bin/pdf/original_pdf_file/coal_factsnewversion09(15_09_2010).pdf"

WCI. (2005). *The coal resource: a comprehensive overview of coal*. [online]. [Accessed 26 October 2010]. Available form World Wide Web: "http://www.worldcoal.org/bin/pdf/original_pdf_file/coal_resource_overview_of_coal_report(03_06_2009).pdf"

Wells, W. F. and Smoot, L. D. (1985). Particle size dependence of coal reactivity. *Combustion and Flame*. **68**, p.481.

Yagi, S. and Kunii, D. (1955). *Proceedings, 5th Symposium (International) on Combustion*. New York: Reinhold.

Yang, Y. and Watkinson, A. P. (1994). Gasification reactivity of some Western Canadian coals. *Fuel*. **73**, p.1786.

Yip, K., Wu, H. and Zhang, D. (2007). Effect of inherent moisture in Collie coal during pyrolysis due to in-situ steam gasification. *Energy and Fuels*. **2891**(21), p.2883.

Zajdlik, R., Jelemensky, L., Remiarova, B. and Markos, J. (2001). Experimental and modelling investigations of single particle coal combustion. *Chemical Engineering Science*. **56**, p.1355.

Zajdlik, R., Markos, J., Remiarova, B. and Jelemensky, L. (2000). Kinetic modelling of single coal particle combustion. *Petroleum Coal*. **42**, p.70.

Zhang, L. M., Tan, Z. C., Wang, S. D. and Wu, D. Y. (1997). Combustion calorimetric and thermogravimetric studies of graphite and coals doped with a coal-burning additive. *Thermochimica Acta*. **299**, p.13.

Zielinska-Blajet, M., Yoshizawa, N. and (1997). *Proceedings of the International Conference on Coal Science*. Essen.

APPENDIX A : MERCURY DENSITY FORMULA DERIVATION

To calculate the bulk density of the coal particle from the apparatus the Archimedes principle is used to convert mass measurements to density measurements. The general equation for density is given as

$$\rho_p = \frac{m_p}{V_p} \tag{A.1}$$

Where

ρ_p is the density of the particle

m_p is the mass of the particle

V_p is the volume of the particle

The Archimedes principle states that 'a body immersed in a fluid will be buoyed up by a force equal to the weight of the fluid displaced'. The mathematical formulation of the principle is given as

$$F_B = g\rho_f V \tag{A.2}$$

Where

F_B is the buoyancy force

g is the gravity constant

ρ_f is the density of the fluid

V is the displaced volume

Furthermore three measurements need to be taken to accomplish the density calculation these, shown in the following diagram, are: the mass of the particle; the immersed mass of the particle and the plunger; and the immersed mass of the plunger only.

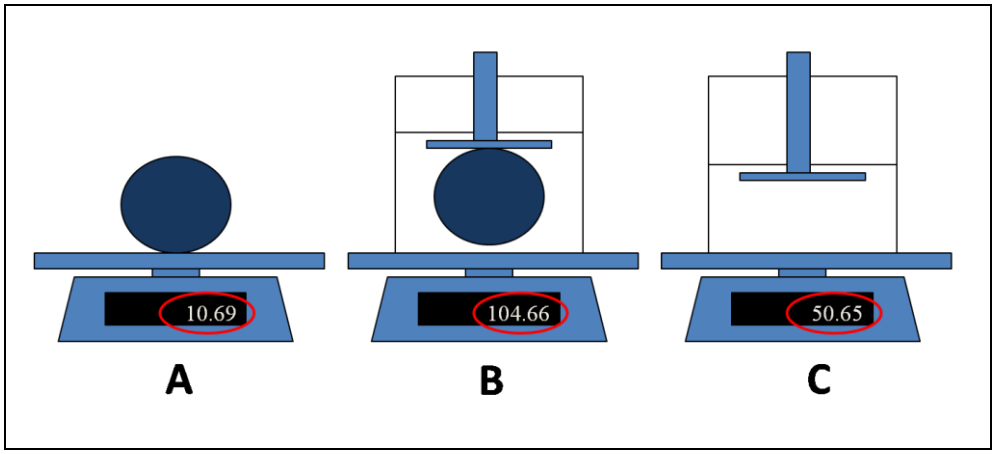

Figure A.1: Measurements needed for the density calculation

From the mass readings given in the three situations shown in Figure A.1 the three required measurements can be made.

From reading A the weight of the particle can be calculated

$$W_p = m_p g \tag{A.3}$$

Where

W_p is the weight of the particle

m_p is the mass of the particle

g is the gravity constant

From reading B the immersed weight of the particle and the plunger can be calculated

$$W_F = m_F g \tag{A.4}$$

Where

W_F is the downward force needed to keep the particle immersed

m_F is the mass reading due to the force to counter at the buoyancy

g is the gravity constant

From reading C the immersed weight of the plunger can be calculated

$$W_{pl} = m_{pl} g \tag{A.5}$$

Where

W_{Pl} is the downward force to keep the plunger immersed

m_{pl} is the mass increase due to the plunger

g is the gravity constant

From these measurements it can be shown from Archimedes principle that

$$W_F = F_B + F_{pl} \tag{A.6}$$

Combining Equations A.2 and A.6, and solving, first, the volume of the particle with Equation A.1, and second the density of the particle, it can be shown, after some simplification, that the density of the particle can be calculated as

$$\rho_p = \left(\frac{m_p}{m_F - m_{pl}}\right)\rho_f \tag{A.7}$$

APPENDIX B : MERCURY DENSITY VERIFICATION

Using Equation A.7 the density of each specific particle can be calculated. To verify this technique two samples with known densities were tested. The density of the glass marble was determined by measuring the mass and the diameter of the glass marble, while the density of aluminium is known. The calculated density values for the two samples are very close to the true density values, showing that the technique is adequate to determine the densities of the individual coal particles.

Table B.1: Verification results for the density measurement apparatus

Marble		
Diameter	34.5	mm
Mass (m_p)	53.5	g
Volume	21500.9	mm^3
True density	2486.0	kg/m^3
Calculated density (ρ_p)	2484.4	kg/m^3
Density of mercury (ρ_f)	13590	kg/m^3
Mass reading for submersion of:		
Marble (m_F)		Plunger (m_{Pl})
# 1	342.0	49.7
# 2	341.8	49.6
# 3	342.1	49.7
# 4	341.8	49.4
# 5	342.1	49.5
Avg.	342.0	49.6

Aluminium		
Mass (m_p)	10.7	g
True density	2700.0	kg/m^3
Calculated density (ρ_p)	2695.1	kg/m^3
Density of mercury (ρ_f)	13590	kg/m^3
Mass reading for submersion of:		
Aluminium (m_F)		Plunger (m_{Pl})
# 1	103.45	49.6
# 2	103.36	49.7
# 3	103.39	49.5
# 4	103.47	49.5
# 5	103.45	49.7
Avg.	103.4	49.6

APPENDIX C : EXPERIMENTAL RESULTS

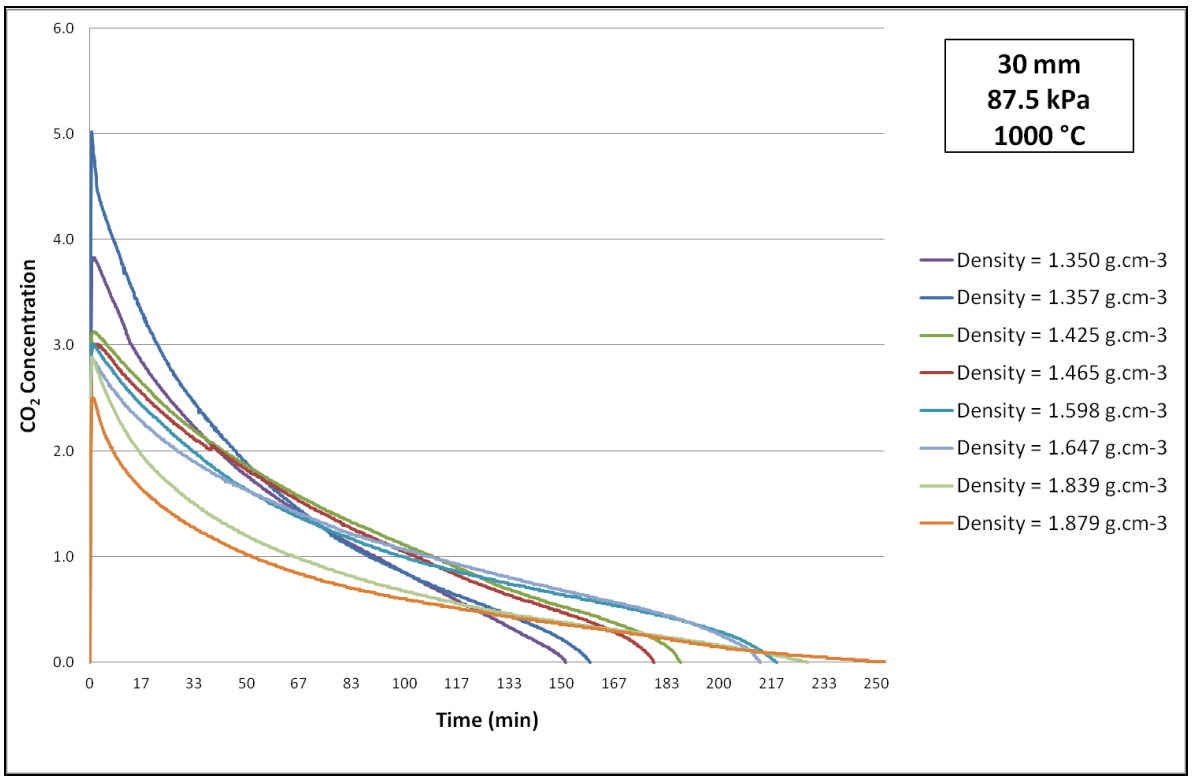

Figure C.1: Raw data of different density particles

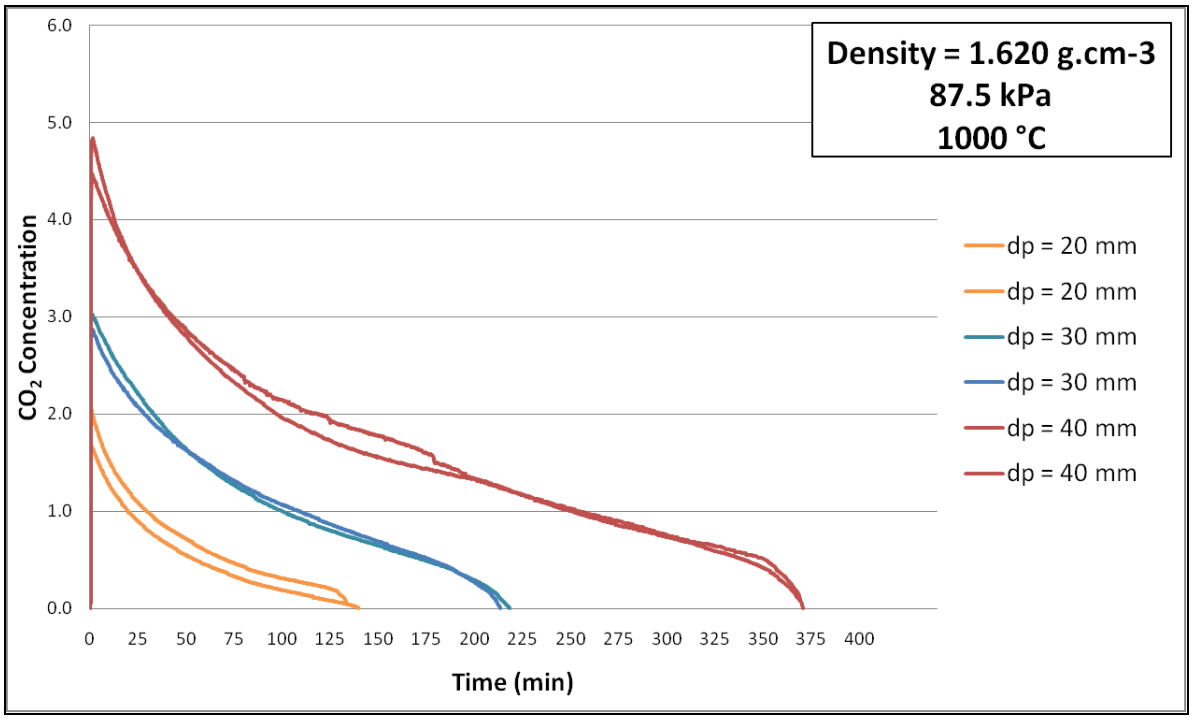

Figure C.2: Raw data of different size particles

APPENDIX D : REPEATABILITY OF EXPERIMENTAL WORK

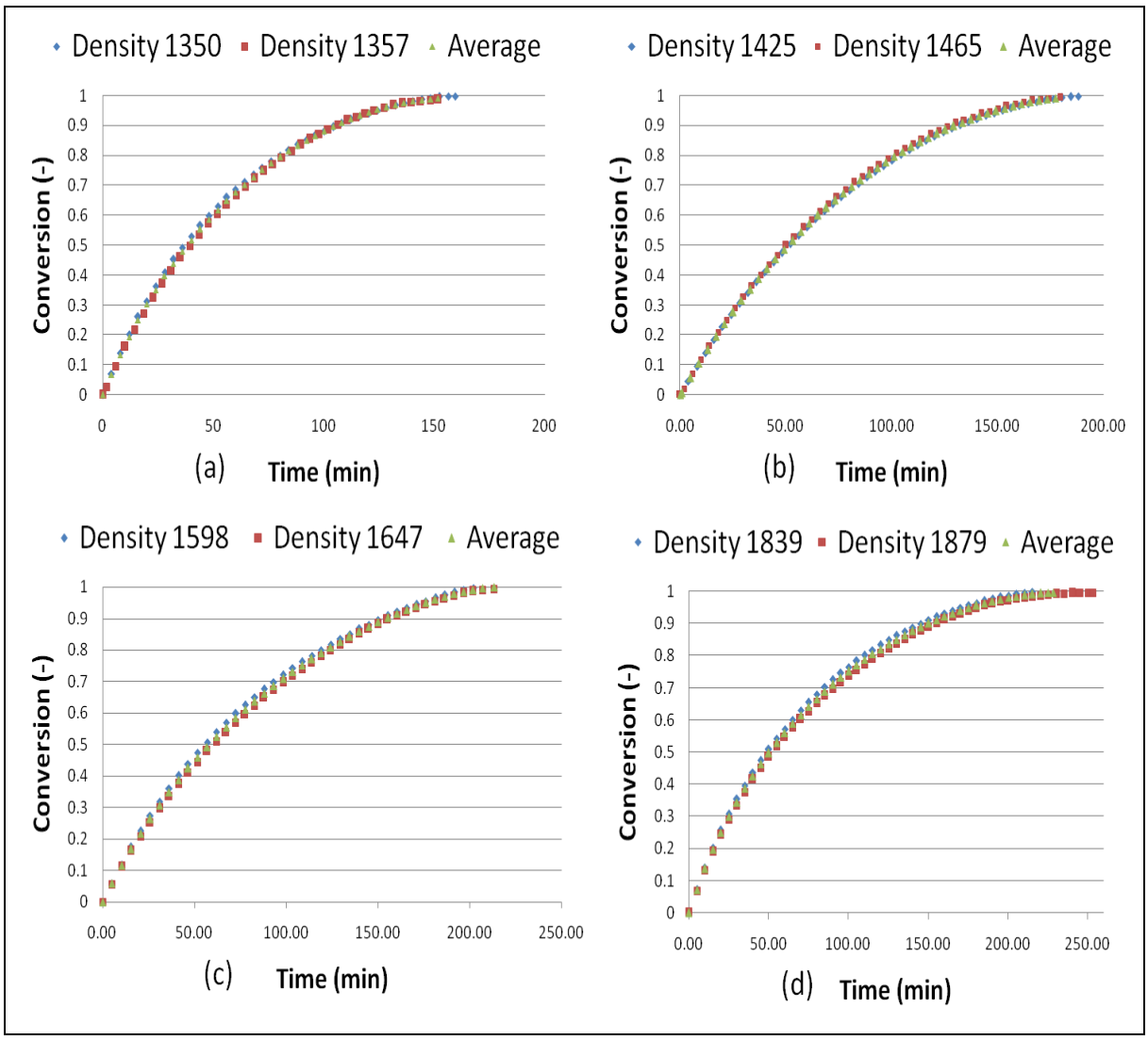

Figure D.1: Repeatability of density variation work

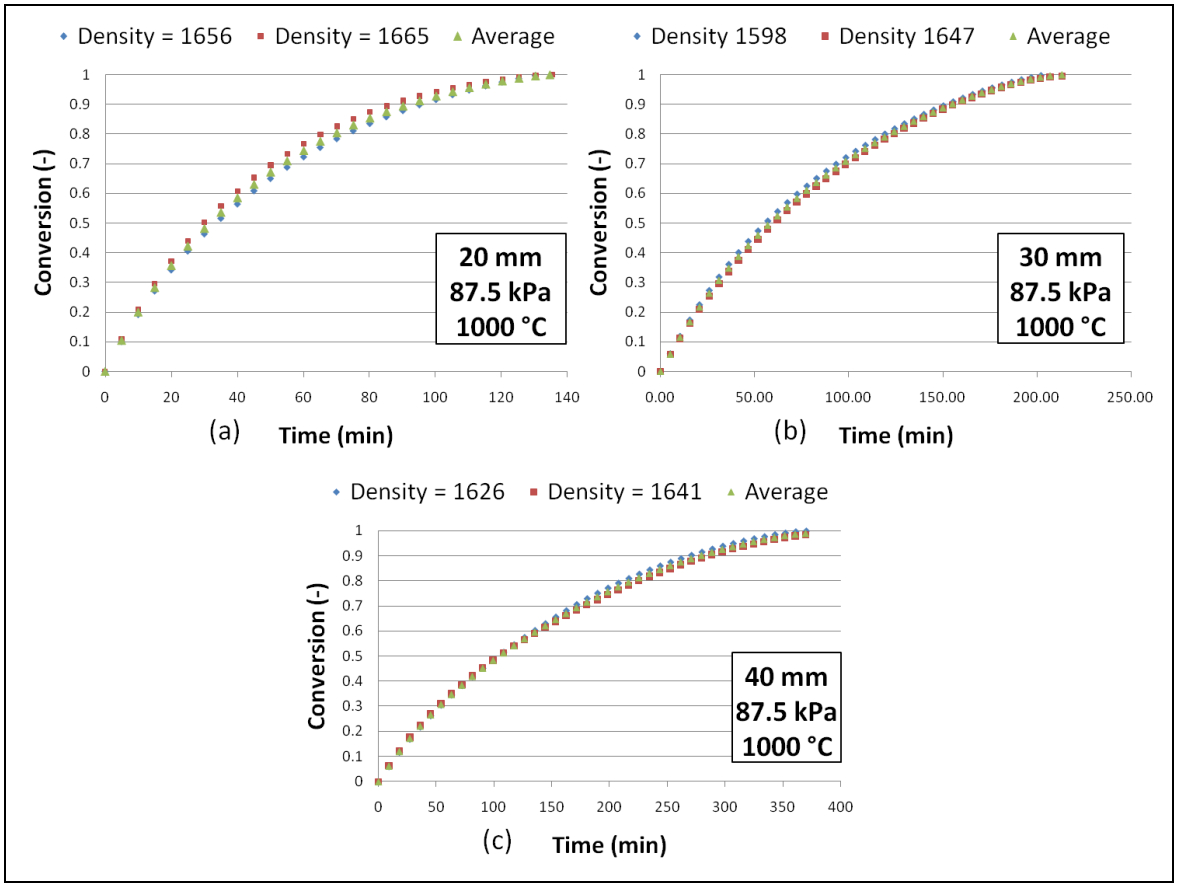

Figure D.2: Repeatability of size variation work

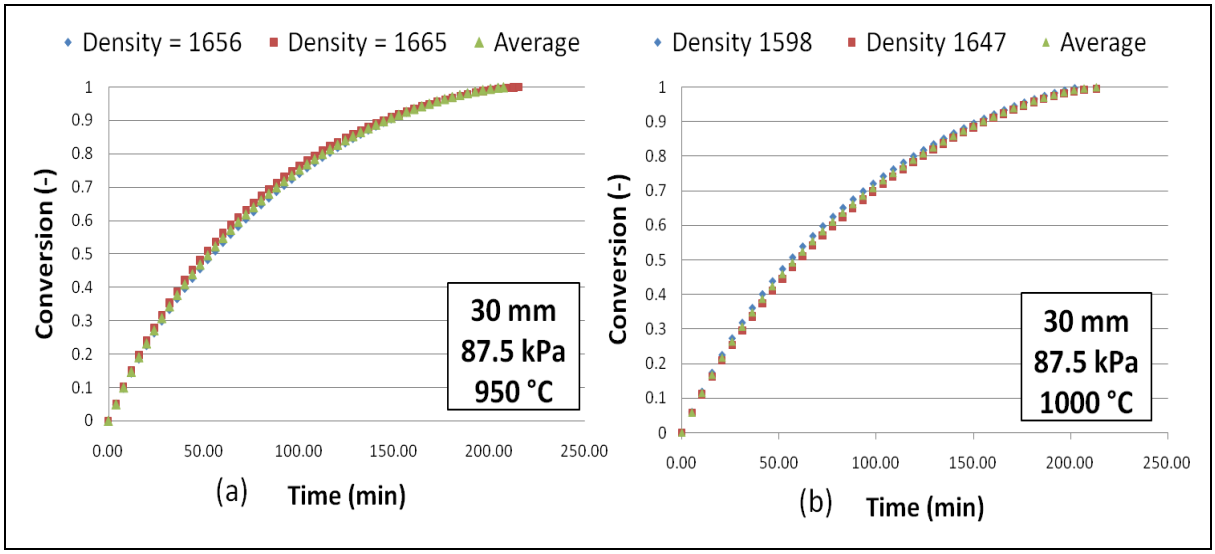

Figure D.3: Repeatability of temperature variation work

APPENDIX E : DERIVATION OF THE SHRINKING UNREACTED CORE MODEL

The shrinking unreacted core model is an isothermal model used to describe a process where a solid particle reacts with a gas to form a gas product while leaving an ash layer on the surface of the unreacted core. The diagrammatic representation of the reaction scheme can be seen in Figure E.1.

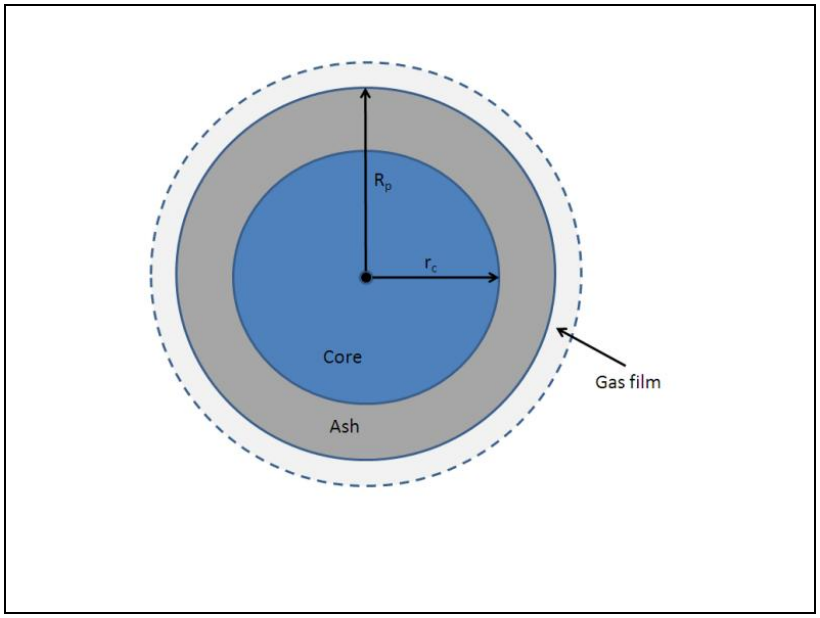

Figure E.1: Diagrammatic representation of the shrinking unreacted core model

The reaction mechanism can be described by the following chemical equation

$$A_{(g)} + bB_{(s)} \rightarrow cC_{(g)} + dD_{(s)} \tag{E.1}$$

The volume of the solid particle, V_B can be given as

$$V_B = \frac{4}{3}\pi r_c^3 \tag{E.2}$$

The amount (mole) of solid reactant B present in the particle can be calculated as

$$N_B = \frac{\rho_B V_B}{M_B} \tag{E.3}$$

With M_B being the molecular weight of solid reactant B

The conversion of reactant B can be represented as

$$X_B = \frac{m_{B0} - m_B}{m_{B0}}$$

$$= 1 - \frac{\frac{4}{3}\pi\rho_B r_c^3}{\frac{4}{3}\pi\rho_B R_p^3} \quad \text{(E.4)}$$

By elimination of the common variables the conversion of solid reactant B can be given in the form of

$$X_B = 1 - \left(\frac{r_c}{R_p}\right)^3 \quad \text{(E.5)}$$

According to Szekely (1970), the shrinking core particle model can have three main rate controlling steps. These are: ash layer diffusion control; chemical reaction control; and gas film diffusion control. The derivation of the model to include these controlling steps will be discussed in the following steps (Szekely, 1970).

Gas film diffusion control

According to stoichiometry of the chemical reaction the amount of reacted solid B can be given by

$$dN_B = bdN_A \quad \text{(E.6)}$$

The rate at which the solid B reacts can be given on the basis of different physical characteristics (Levenspiel, 1999), these can be represented by

$$-r_B = \frac{-1}{V_F}\frac{dN_B}{dt} \quad \text{(E.7)}$$

$$-r_B' = \frac{-1}{m_B}\frac{dN_B}{dt} \quad \text{(E.8)}$$

$$-r_B'' = \frac{-1}{S_{ex}}\frac{dN_B}{dt} \quad \text{(E.9)}$$

$$-r_B''' = \frac{-1}{V_B}\frac{dN_B}{dt} \quad \text{(E.10)}$$

$$-r_B'''' = \frac{-1}{V_r}\frac{dN_B}{dt} \quad \text{(E.11)}$$

Where Equation E.7 is based on the volume of the reacting fluid, Equation E.8 is based on the mass of the solid particle. Equation E.9 is based on the external surface area of the reactant solid while Equation E.10 is based on the volume of the solid reactant and Equation E.11 is based on the volume of the reactor.

For the derivation of the model the external surface area of the solid particle will be used. For this the external surface area will be given as

$$S_{ex} = 4\pi R_p^2 \quad \text{(E.12)}$$

This external surface area is for a spherical particle.

From Equation E.3 dN_B/dt can be given as

$$\frac{-dN_B}{dt} = \frac{d4\pi\rho_B r_c^3}{3M_B dt} \quad \text{(E.13)}$$

As r_c is the only changing variable this equation can be written as

$$\frac{-dN_B}{dt} = \frac{-4\pi\rho_B r_c^2}{M_B}\frac{dr_c}{dt} \quad \text{(E.14)}$$

But $-r_B'''$ is the mass transfer across the gas film layer and can be described as Fick's law (Levenspiel, 1999)

$$-r_B''' = bk_g(C_{Ag} - C_{As}) \quad \text{(E.15)}$$

Where

b = stoichiometric coefficient

k_g = mass transfer coefficient

C_{Ag} = concentration of reactant gas in the bulk stream

C_{As} = concentration of reactant gas at the particle surface

If it is assumed that film layer diffusion is the controlling mechanism, the chemical reaction at the surface will instantaneously use the reactant gas as it reaches the particle surface. If this

is the case the reactant gas concentration at the particle surface will be negligible; resulting in Equation E.16.

$$-\bar{r_B} = bk_g C_{Ag} \tag{E.16}$$

Combining Equations E.9, E.12, E.14 and E.16 the gas film layer diffusion equation can be written as

$$-\left(\frac{4\pi\rho_B r_c^2}{4\pi M_B R_p^2}\right)\frac{dr_c}{dt} = bk_g C_{Ag} \tag{E.17}$$

After simplification and rearranging the following equation in obtained

$$-\left(\frac{\rho_B r_c^2}{M_B R_p^2}\right)dr_c = bk_g C_{Ag}dt \tag{E.18}$$

This equation can then be integrated with the following boundary conditions

At t = 0 $r_c = R_p$ and

At t = t $r_c = r_c$

After integration and some manipulation the following equation is obtained

$$\left(\frac{\rho_B}{3M_B R_p^2}\right)\left(R_p^3 - r_c^3\right) = bk_g C_{Ag}t \tag{E.19}$$

If Equation E.19 is then solved for time t the equation can be written as

$$t = \left(\frac{\rho_B}{3M_B bk_g C_{Ag} R_p^2}\right)\left(R_p^3 - r_c^3\right) \tag{E.20}$$

To write Equation E.20 in terms of conversion X_B it is multiplied with R_p^3/R_p^3, and in combination of Equation E.5 it can be written as

$$t = \left(\frac{\rho_B}{3M_B bk_g C_{Ag} R_p^2}\right)X_B \tag{E.21}$$

Equation E.21 then gives the equation for gas film diffusion control reactions in terms of the conversion of solid reactant B.

Ash layer diffusion control

From Equation E.6 it can be shown that

$$\frac{-dN_B}{dt} = \frac{-bdN_A}{dt} \tag{E.22}$$

Further from Equation E.14 it is known that

$$\frac{-dN_B}{dt} = -\left(\frac{4\pi\rho_B}{M_B}\right) r_c^2 \frac{dr_c}{dt} \tag{E.23}$$

It can also be shown that the rate of reaction of A at any instant is given by its rate of diffusion to the reaction surface (Levenspiel, 1999) , or in equation form

$$\frac{-dN_A}{dt} = A_{ash\ layer} Q_A \tag{E.24}$$

Where

$A_{ash\ layer}$ = area of ash layer surface through which diffusion has to occur

Q_A = molar flux of reactant gas A to the reaction core

If the assumption of equimolar counter diffusion is made it can be shown that (Levenspiel, 1999)

$$Q_A = \frac{D_e dC_A}{dr} \tag{E.25}$$

Where

D_e = the effective diffusion coefficient of gaseous reactant in the ash layer

And the area of the ash layer can be given as

$$A_{ash\ layer} = 4\pi r_{ash\ layer}^2 \tag{E.26}$$

Equation E.26 can now be written as

$$-\left(\frac{dN_A}{dt}\right) r_{ash\ layer}^2 dr = 4\pi D_e dC_A \tag{E.27}$$

Equation E.27 can then be integrated from R_p to r_c and C_{As} (concentration of reactant gas at the particle surface) to C_{Ac} (concentration of reactant at the core surface). It is also assumed

that the reaction is significantly fast; making the concentration of reactant gas at the core surface negligible, and the concentration of reactant gas at the particle surface is the same as the concentration of reactant gas in the bulk stream. After integration and some rearranging the resulting equation is given as

$$\frac{-dN_A}{dt} = \frac{4\pi D_e C_{Ag}}{\left(\frac{1}{r_c} - \frac{1}{R_p}\right)} \tag{E.28}$$

Combining and rearranging Equation E.23 and E.28 with the help of Equation E.6 it can be shown that

$$D_e C_{Ag} b M_B dt = -\rho_B r_c^2 \left(\frac{1}{r_c} - \frac{1}{R_p}\right) dr_c \tag{E.29}$$

Equation E.29 can then be integrated with the following conditions

dt from 0 to t

dr_c from R_p to r_c

Thus the result can be written as

$$D_e C_{Ag} b M_B t = -\rho_B \left(\frac{r_c^2}{2} - \frac{r_c^3}{3R_p} - \frac{R_p^2}{6}\right) \tag{E.30}$$

To convert Equation E.30 in terms of conversion and solving for time t, it is multiplied with R_p^2/R_p^2, and with $1\text{-}x = r_c^3/R_p^3$ it can be written as

$$t = \left(\frac{\rho_B R_p^2}{6 D_e C_{Ag} b M_b}\right)\left(1 - 3(1 - X_B)^{\frac{2}{3}} + 2(1 - X_B)\right) \tag{E.31}$$

Equation E.31 represents the characteristic equation for ash layer diffusion control in terms of conversion X_B.

Chemical reaction control

Using the surface of unreacted core (Equation E.9) in terms of r_c, the rate of reaction for Equation E.1 can be written as (Levenspiel, 1999)

$$-\left(\frac{\rho_B 4\pi r_c^2}{M_B 4\pi r_c^2}\right)\frac{dr_c}{dt} = k^{''} C_{Ag}^{n} b \tag{E.32}$$

Assuming first order reaction order and after rearranging Equation E.32 can be written as

$$\left(\frac{\rho_B}{M_B}\right) dr_c = bk^{''} C_{Ag} dt \tag{E.33}$$

Integrating Equation E.33 for dr_c from R_p to r_c and dt from 0 to t and then solving for time t, it can be written as

$$t = \left(\frac{\rho_B}{M_B bk^{''} C_{Ag}}\right)(R_p - r_c) \tag{E.34}$$

Converting Equation E.34 in terms of the conversion of solid B, it is multiplied with Rp/R_p, and with the help of Equation E.5 the resulting equation can be written as

$$t = \left(\frac{\rho_B}{M_B bk^{''} C_{Ag}}\right)\left(1 - (1 - X_B)^{\frac{1}{3}}\right) \tag{E.35}$$

Equation E.35 represents the characteristic equation for chemical reaction controlled systems. If the characteristic equations of the three controlling mechanism are linearized in terms of conversion of solid reactant B, the following equation can be obtained.

$$f(X)_{Gas\ film\ diffusion\ control} = X_B$$

$$f(X)_{Ash\ layer\ diffusion\ control} = \left(1 - 3(1 - X_B)^{\frac{2}{3}} + 2(1 - X_B)\right) \tag{E.36}$$

.

$$f(X)_{Chemical\ reaction\ control} = \left(1 - (1 - X_B)^{\frac{1}{3}}\right)$$

The characteristic equations for the different controlling mechanism can be combined by simple addition. Equation E.37 shows the combination of film and ash layer diffusion controls.

$$t = \left(\frac{\rho_B}{3M_B bk_g C_{Ag} R_p^2}\right)X_B + \left(\frac{\rho_B R_p^2}{6D_e C_{Ag} bM_b}\right)\left(1 - 3(1 - X_B)^{\frac{2}{3}} + 2(1 - X_B)\right) \tag{E.37}$$

APPENDIX F : MASS TRANSFER COEFFICIENT CALCULATION

The external mass transfer coefficient needs to be determined as the external mass transfer can have a significant influence on the overall reaction rate of the combustion of large particles. The mass transfer coefficient is calculated from the Sherwood number, which in turn requires a binary diffusion coefficient as well as a Reynolds number.

The mass transfer coefficient can be calculated from the following correlation (Szekely *et al*., 1976)

$$N_{Sh} = \frac{h_D L}{D_{AB}} \tag{F.1}$$

Where

h_D is the mass transfer coefficient

L is the characteristic dimension which is the particle diameter

D_{AB} is the binary diffusion coefficient

The binary diffusion coefficient can be calculated from the following correlation (Perry and Green, 1997)

$$D_{AB} = \frac{0.001T^{1.75}M_{AB}^{0.5}}{P_T((\Sigma\hat{v})_A^{0.333} + (\Sigma\hat{v})_B^{0.333})^2} \tag{F.2}$$

For A: O_2 and B: N2 the diffusion volumes ($cm^3.mol^{-1}$) are respectively 16.6 and 17.9. The mean molecular mass for the gas mixture can be calculated with

$$M_{O2-N2} = \frac{1}{M_{O2}} + \frac{1}{M_{N2}} \tag{F.3}$$

The Reynolds number can be calculated using the pipe diameter of the tube furnace along with the gas flow rate past the particle using the following correlation (Szekely *et al*., 1976)

$$N_{Re} = \frac{UL}{v} \tag{F.4}$$

Where

L is the characteristic length which is the particle diameter

U is the linear gas velocity flowing past the particle measured outside the boundary layer surrounding the particle

v is the kinematic viscosity of air which can be found from literature to be 1.66×10^{-4} at 1000°C

The Schmidt number can be calculated from the following correlation

$$N_{Sc} = \frac{v}{D_{AB}} \tag{F.5}$$

Where

v is the kinematic viscosity of air

D_{AB} is the binary diffusion coefficient

Finally the Sherwood number is calculated from the following correlation

$$N_{Sh} = 2.0 + 0.6 N_{Re}^{\frac{1}{2}} N_{Sc}^{\frac{1}{3}} \tag{F.6}$$

The binary diffusion coefficient is calculated first, followed by the Sherwood and the Reynolds numbers, which are then used to calculate the Sherwood number. Finally the mass transfer coefficient is calculated from Equation F.1. All the parameters that are required to calculate the mass transfer coefficients are shown in Table F.1.

Table F.1: Mass transfer coefficient calculation parameters

Particle diameter	Reynolds	Schmidt	Sherwood	k_g (m/s) $\times 10^{-3}$
20	409.07	0.63	4.56	60.2
30	613.61	0.63	5.14	45.4
40	818.15	0.63	5.63	37.3

APPENDIX G: CALIBRATION AND VERIFICATION OF APPARATUS

Measuring the mass of the parent coal particle before and after charring should give the mass percentage of volatile matter, including the moisture content of the coal particle. For this study the charring of the coal particles was conducted at 1100 °C to ensure that there were no volatiles coming off while the particles were reheated to the combustion temperature of 1000 °C. However the mass percentage of volatile matter present in the parent coal obtained from the proximate analysis was calculated from mass loss measurements conducted at 900 °C. A comparison of the proximate analysis volatile matter content versus the charred volatile matter content can be seen in Table G.1.

Table G.1: Volatile matter comparison of proximate analysis and experimental mass differences

Density (g/cm^3)	Proximate analysis (Volatile matter + inherent moisture) (%)	Mass balance calculation (Parent coal mass – char mass) (%)
1.357	33.1	32.8
1.440	29.6	32.5
1.620	25.1	24.3
1.850	20.4	21.7

Comparing the actual volatile matter content to the values obtained from proximate analysis shows a good correlation indicating that most of the volatile matter has been removed from charring at 900 °C.

Comparing the mass loss due to fixed carbon conversion can be done by subtracting the residual ash mass from the mass of the char particle and comparing this value to the mass calculated from converting the carbon dioxide concentration data to mass loss data. The comparison between the proximate analysis (as presented in Chapter 4) fixed carbon content and the calculated fixed carbon content can be seen in Table G.2.

Table G.2: Fixed carbon content comparison between mass difference and calculated values

Density (g/cm^3)	Char mass (g)	Ash mass (g)	Fixed carbon mass (g)	Calculated fixed carbon mass (g)	Difference (%)
1.357	13.03	1.47	11.56	11.18	3.30
	12.68	1.67	11.01	10.82	1.74
	12.85	1.57	11.29	11.00	2.52
1.44	14.16	2.22	11.94	11.46	4.03
	13.38	3.20	10.19	10.06	1.26
	13.77	2.71	11.06	10.76	2.65
1.62	17.24	5.26	11.99	11.30	5.75
	17.44	5.58	11.86	11.25	5.15
	17.34	5.42	11.92	11.28	5.45
1.85	20.66	12.82	7.84	7.30	6.88
	19.95	10.70	9.25	8.20	11.32
	20.31	11.76	8.54	7.75	9.10

It can be seen from Table G.2 that the fixed carbon content calculated from the carbon dioxide production rate gives a very good correlation but was consistently lower than the fixed carbon content obtained from the mass difference between the chars and their respective ash mass values. These differences can be attributed to the fact the chars still contain nitrogen, hydrogen and oxygen containing compounds that react during combustion. It can also be seen that the mass difference increases as the density increases. The larger differences in the higher density particles can more likely be attributed to the fact that the high density particles contain more unburnt carbon in the remaining ash (as was observed in Section 5.2.2).

The calibration and verification results show a sufficient correlation to the proximate analysis, showing that the apparatus gave satisfactory results in terms of operation and carbon conversion measurement.